Spring 1-1-2011

Microstructure Characterization of Multi-Phase Composites and Utilization of Phase Change Materials and Recycled Rubbers in Cementitious Materials

Pania Meshgin
University of Colorado at Boulder, pania.meshgin@colorado.edu

MICROSTRUCTURE CHARACTERIZATION OF MULTI-PHASE COMPOSITES AND UTILIZATION OF PHASE CHANGE MATERIALS AND RECYCLED RUBBERS IN CEMENTITIOUS MATERIALS

by

Pania Meshgin

B.A., Bahai Institute for Higher Education, 2001

M.S., University of New Mexico, 2006

M.S., University of Colorado at Boulder, 2009

A thesis submitted to the

Faculty of the Graduate School of the

University of Colorado in partial fulfillment

of the requirements for the degree of

Doctor of Philosophy

Department of Civil, Environmental and Architectural Engineering

2011

This thesis entitled:
MICROSTRUCTURE CHARACTERIZATION OF MULTI-PHASE COMPOSITES AND UTILIZATION OF PHASE CHANGE MATERIALS AND RECYCLED RUBBERS IN CEMENTITIOUS MATERIALS
written by Pania Meshgin
has been approved for the Department of Civil, Environmental and Architectural Engineering

Dr. Yunping Xi

Dr. Ross B. Corotis

Dr. Richard A. Regueiro

Dr. Siva Mettupalayam

Dr. Abie Liel

Dr. Stephan Durham

Date

The final copy of this thesis has been examined by the signatories, and we find that both the content and the form meet acceptable presentation standards of scholarly work in the above mentioned discipline.

Meshgin, Pania (Ph.D., Civil Environmental, and Architectural Engineering)

MICROSTRUCTURE CHARACTERIZATION OF MULTI-PHASE COMPOSITES AND UTILIZATION OF PHASE CHANGE MATERIALS AND RECYCLED RUBBERS IN CEMENTITIOUS MATERIALS

Thesis directed by Professor Yunping Xi

This research focuses on two important subjects:

(1) Characterization of heterogeneous microstructure of multi-phase composites and the effect of microstructural features on effective properties of the material.

(2) Utilizations of phase change materials and recycled rubber particles from waste tires to improve thermal properties of insulation materials used in building envelopes.

Spatial pattern of multi-phase and multidimensional internal structures of most composite materials are highly random. Quantitative description of the spatial distribution should be developed based on proper statistical models, which characterize the morphological features. For a composite material with multi-phases, the volume fraction of the phases as well as the morphological parameters of the phases have very strong influences on the effective property of the composite. These morphological parameters depend on the microstructure of each phase. This study intends to include the effect of higher order morphological details of the microstructure in the composite models. The higher order statistics, called two-point correlation functions characterize various behaviors of the composite at any two points in a stochastic field. Specifically, correlation functions of mosaic patterns are used in the study for characterizing transport properties of composite materials.

One of the most effective methods to improve energy efficiency of buildings is to enhance thermal properties of insulation materials. The idea of using phase change materials and recycled rubber particles such as scrap tires in insulation materials for building envelopes has been studied.

Dedication

To my husband, my father, and my brother, who without their love, support and prayers, I would not be able to be here. I would also like to dedicate this to my mother, who I am confident, is resting in peace in the Abha kingdom, her spirit has been with me as well. I love you all with all my heart and I will do my best to make you proud of me.

Robert Newell

Parviz Meshgin

Simin Elahi

Payam Meshgin

Acknowledgements

I would like to express my most sincere gratitude to Professor Yunping Xi for his guidance, encouragement, his time, and his support throughout this endeavor. I am so thankful for working under his supervision. He is a great, caring, knowledgeable professor, whom I learned how to be a better person as well as better researcher.

I would also like to thank Professor Kaspar Willam, Professor Ross B. Corotis, Professor Ricahrd A. Regueiro, Professor Siva Mettupalayam, Professor Stephan Durham and Professor Abie Liel for their helpful comments on this dissertation. Their valuable comments are highly appreciated.

I am so thankful to the former chair of the Department of Civil, Environmental and Architectural Engineering- Professor JoAnn Silverstein, graduate coordinator- Medford Moorer, former office manager- Cyndi Alvarado, accounting technician- Wayne Morrison and administrative assistant- LeeAnn Stevens for all their help through my journey at the Colorado University at Boulder.

I would also like to thank Professor Ronggui Yang and his PhD student Suraj Joottu Thiagarajan from the Department of Mechanical Engineering at the University of Colorado at Boulder for providing equipments and their help for the thermal analysis throughout this research. Their sincere help is highly appreciated.

Thank you so much.

Contents

Chapter

Tables

Table

Figures

Figure

Chapter 1

INTRODUCTION

1.1 Background and objectives

This research focuses on two topics:

(1) Characterization of heterogeneous microstructure of multi-phase cementitious materials and the effect of microstructural features on transport properties of the material.

(2) Utilization of phase change materials and recycled rubber particles from waste tires to improve thermal properties of insulation materials used in building envelopes.

Characterization of heterogeneous microstructure of multi-phase cementitious materials and the effect of microstructural features on transport properties of the material.

There are many practical problems in civil engineering and structural engineering that can be mathematically characterized by transport equations of different degrees of complexity. Penetration of de-icing salts in concrete structures is a typical example. Other important examples are heat conduction in steel and concrete structures under fire, which is one of the causes for the collapse of the two towers of World Trade Center; and water penetration into the levees in New Orleans which attributed to the failure of the levees when Katrina struck.

Spatial pattern of multi-phase and multidimensional internal structures of most composite materials are highly random. Quantitative description of the spatial distribution should be developed based on proper statistical models, which characterize the morphological features of the

internal structure of composite materials. In general, two different types of models have been developed for this purpose. One uses spherical units of either mono-size or different sizes. The units can be non-penetrable or penetrable, i.e. with solid core and soft shell. These models are actually a special case of the Boolean model in stereology, which is more general and includes basic units of different shapes, not just spheres, and can be used to simulate a wide variety of spatial structures. Another kind of model is called mosaic pattern, in which a space or a plane is divided into polygons of 3D or 2D. Different dividing methods result in various spatial structures.

Mosaic patterns will be used in this research. It is one of the morphological models that can be used for characterization of internal structures of concrete. There are different types of mosaic patterns, such as S-mosaic, L-mosaic, and C-mosaic. Mosaic patterns are also referred to as random tessellation.

Much has been done in composite mechanics on how to evaluate an effective transport property of a composite material based on volume fractions and transport properties of the constituents of the material. Volume fraction is the first order statistical information of a multi-phase random composite microstructure. There have also been studies on how to include higher order statistical information of the microstructure in constitutive models for transport properties of composite materials. However, how to obtain higher order microstructure information is not an easy task. Therefore in this study, mosaic patterns are adopted to develop an analytical model of high order statistical information of the microstructure for predicting the transport properties of composites. Analytical models are developed to characterize mechanical and thermal behavior of the composite materials and the models are verified based on the present experimental data. The analytical models adopted in this research include several microstructural arrangements of the constituents such as parallel coupling, series coupling, and generalized self consistent model (concentric spherical model). Since each composite has more than two phases and each phase has different grain sizes, the multi-phase and multi-scale analysis were used to develop more accurate models. These models are used to predict thermal conductivity and drying shrinkage of cementitious materials. Furthermore, the higher order statistical information (i.e. autocorrelation functions of the stochastic field)

based on the mosaic patterns are used to develop an analytical model for predicting the effective transport properties of multi-phase composites.

Utilization of phase change materials and recycled rubber particles from waste tires to improve thermal properties of insulation materials used in building envelopes.

One of the most effective methods to improve energy efficiency of buildings is to enhance the thermal properties of insulation materials. The idea of using phase change materials and recycled rubber particles such as scrap tires in insulation materials in building envelopes has been adopted in this research. Phase change materials (PCM) have the ability to absorb and release energy at a certain temperature. Therefore, incorporating PCM in cementitious materials can improve thermal property of the material. On the other hand, disposal of waste tires is a major environmental issue for many metropolitan areas of the world. Effectively reutilizing scrap tires has become an important research topic in recent years. The main focus of this part of the thesis is based on these two concepts with an overall goal to utilize scrap tires and phase change material to make a new insulation mortar. We envisioned that the new mortar can enhance thermal resistance and capacity of exterior walls of timer and masonry structures, thus improving the energy efficiency of residential buildings. We also envisioned that the technology for the new insulation mortar can be used for concrete which satisfies the strength and stiffness requirements for structural applications and at the same time improves thermal properties of the material.

One of the focuses of this research is on experimental analysis and finding the optimal percentage of scrap tires as well as PCM in the mix design in both mortar and concrete. In order to obtain this information, various experiments such as compressive strength, flexural strength, drying shrinkage, bond strength, thermal conductivity, and microstructure features by scanning electron microscopy (SEM) are performed. Based on the results, the optimized percentage of scrap ties and PCMs within the mix design will be chosen.

1.2 Organization

This dissertation has ten chapters, including this chapter which covers the background, objectives and organization of the dissertation. The remaining chapters are organized as follows

Chapter two presents the microstructural thermal stresses in multi-phase composite. A detailed background information is provided. The mosaic pattern is adopted to link the microstructure of a multi-phase composite to the thermal stresses variation within the composites.

Chapter three describes the experimental study on the application of phase change material in building envelopes. Different percentages of sand (volumetric %) have been replaced by phase change material. Several tests were performed and the results were compared with conventional concrete.

Chapter four shows the analytical modeling of PCM-concrete. Two analytical models were developed based on the generalized self consistent model to predict the effective thermal conductivity and drying shrinkage of PCM-concrete. The analytical results were compared with the experimental data and the necessary modifications were made to the models to capture the behaviors more accurately.

Chapter five covers the experimental study on rubberized-mortar and PCM-mortar. Different percentages of the sand volume have been replaced either by phase change material or rubber particles. Some additives were added to the mix designs as well. Several tests were performed and the results were explained in detail.

Chapter six presents the analytical modeling of PCM-rubberized-mortar, rubberized-mortar and PCM-mortar. An analytical model was developed based on the generalized self consistent model to predict the effective thermal conductivity of PCM-rubberized-mortar, rubberized-mortar and PCM-mortar. The analytical results were compared with the experimental data and the necessary modifications were made to the model to capture the behaviors more accurately. The modified models were then calibrated with other mix designs as well.

Chapter seven covers the experimental study on the rubberized-concrete and PCM-concrete.

The effect of surface treatment on rubber particles; the compressive strength of rubberized-concrete with surface treatment; rubberized-concrete without surface treatment; PCM-concrete and PCM-rubberized concrete with surface treatment were studied in detail.

Chapter eight presents the hot box test on different mortar specimens. Based on the results from chapter five, four different mortar specimens were selected for the hot box test. Conventional mortar, PCM-mortar, rubberized-mortar with rubber particles (8-10 mesh) and rubberized mortar with rubber powder (200 mesh) were tested in the environmental chamber and their thermal performances were compared and analyzed.

Chapter nine covers the higher order autocorrelation function for effective thermal conductivity. First, an analytical model for effective thermal conductivity of the two-phase composite based on higher order autocorrelation functions was developed, and then the effect of each of the main parameters on the effective thermal conductivity of the composite was studied.

Chapter ten contains the recommendations for future research in this field.

Chapter 2

MICRO-STRUCTURAL THERMAL STRESSES VARIATION IN MULTI-PHASE COMPOSITE

2.1 Introduction

When a multi-phase composite material is subjected to a temperature change, the material exhibits a thermal expansion or a contraction. Even if the material can expand freely at the macroscopic level, there are significant internal stresses in the material at the microscopic level due to the mismatch in mechanical and thermal properties of the constituent phases. The variation of the internal thermal stress could be very high, resulting in cracking of the material. This is a commonly seen phenomenon when a concrete structure is subjected to extreme heat. The purpose of this study is to find the relationship between the level of the thermal stress variation and the influential material parameters, such as the volume fractions, the grain sizes, the mechanical and the thermal properties of the constituent phases.

In the last few decades, the behavior of heterogeneous materials under different environmental conditions has received considerable attention from researchers and engineers. A heterogeneous material is composed of domains of different materials or phases, such as a composite or the same material in different states, such as a poly-crystal [73]. The heterogeneity of a composite material usually occurs at the microscopic scale level, so it is a subject of micro-mechanics dealing with the mechanics related to the microstructure of materials [47]. There has been a substantial amount of work done in this field, considering the effective properties or overall properties of multi-phase composites with various types of micro-structures. However, an accurate description of the effec-

tive properties of composites is very difficult or not workable due mainly to the random orientation and random shape of the constituent phases in the composite. Therefore, in many instances, the micro-structures of the composites must be characterized only by statistical approaches [73].

Recently, there has been a considerable attention given to the use of statistical continuum theories to predict the effective properties of heterogeneous materials. For instance, with the work of Kroner [40], [39] and Beran [8], the mathematical description of heterogeneity has received some breakthroughs. In most of these formulations a good understanding of the spatial correlation functions related to the micro-structures of the heterogeneous material in the form of statistical functions is required [40], [2] and [77]. Usually, making simple assumptions about a microstructure feature (e.g. the shape of the phases) is needed for the further progress [38], [39]. Although it has been shown that, in theory, any spatial correlation function (i.e. multi-point probabilistic function) can be described by a set of corresponding probability distribution functions [34], it is actually very difficult to obtain a spatial correlation function for a specific microstructure. Therefore, most of the studies have relied on the one-point probability function, which is the volume fractions of the constituents within the microstructure and ignore the shape and geometry characteristics of the microstructure. However, it has long been noticed that to be able to measure materials' heterogeneity, it is important and necessary to incorporate the second and even higher order probability functions. Lin et al. [46] hhas shown that two-point functions can adequately predict the properties of heterogeneous materials. Torquato [73], and in his recent work with Jiao and Stillinger [35] , also showed that the two-point cluster function which gives the probability of finding two points separated by a distance r in the same cluster of the phase of interest can provide a superior descriptor of random textures. In the present study, the effect of thermal expansion coefficients and the mechanical properties of the constituents in a multi-phase composite material on the variation of thermal stresses have been investigated. First, general principles for establishing the relationship between the stresses based on the variations in both properties of each constituent phase and local heterogeneity are developed. Then, a method evaluating the variation of the thermal stress due to local heterogeneity is introduced. There exists a relationship between local heterogeneity and the morphological features

of the internal structure of composites. To this end, the mosaic pattern, which is a morphological model, has been adopted in the present study.

2.2 Field equation

The primary focus of this analysis is the characterization of the thermal stress variation in the microstructure of multi-phase composite materials such as concrete. This study begins with the formulation of the field equations governing the microscopic response of the material under a temperature variation. Assuming the mechanical behaviors of the phases are linear elastic, the stress-strain relations can be expressed based on Hooke's law as follows:

$$\sigma(x) = C(x).\epsilon(x) - \beta(x).\theta(x) \tag{2.1}$$

where $\sigma(x)$, $\epsilon(x)$ and $\theta(x)$ represent the stress, strain and temperature fields. $C(x)$ is the elastic modulus and $\beta(x)= C(x).\alpha(x)$ is the coefficient of thermal expansion (CTE), and x is the coordinate vector. It should be noted that the material is assumed to be thermally heterogeneous, and the strain and temperature fields are assumed to be constants throughout the composite, then the above equation can be simplified as:

$$\sigma(x) = C(x).\epsilon - C(x).\alpha(x).\theta \tag{2.2}$$

Based on the definition of the covariance, which is a measure of how much two variables are changing together, the stress covariance can be considered as a good measure of the fluctuation in the stress field, and it can provide a complete description of the statistical distribution of the thermally-induced thermal stress in the composite [56]. Thus, the stress covariance for two points within the composite with the ν distance apart can be written as:

$$cov(\sigma(x), \sigma(x+\nu)) = E(\sigma(x).\sigma(x+\nu)) - E(\sigma(x)).E(\sigma(x+\nu)) \tag{2.3}$$

Where E is the expected value of two random variables $\sigma(x)$ and $\sigma(x+\nu)$.
The first term on the right-hand side can be derived as:

$$E(\sigma(x).\sigma(x+\nu)) = \epsilon^2.R_C(\nu) - 2\theta.\epsilon.E(C(x).C(x+\nu).\alpha(x)) + \theta^2.R_C(\nu).R_\alpha(\nu) \tag{2.4}$$

where R_C and R_α are autocorrelation functions for modulus of elasticity and CTE, respectively. Assuming the mechanical properties and CTE are two independent random variables, the above equation can be rewritten as:

$$E(\sigma(x).\sigma(x+\nu)) = \epsilon^2.R_C(\nu) - 2\theta.\epsilon.R_C(\nu).E(\alpha(x)) + \theta^2.R_C(\nu).R_\alpha(\nu) \tag{2.5}$$

As one can see, the problem of evaluating thermally-induced stress variation is converted to a problem of finding autocorrelation functions for the modulus of elasticity and CTE in a multiphase microstructure. The autocorrelation functions for the modulus of elasticity and CTE are second order statistical information of the microstructure. General theory of higher order correlation functions of a random field has been developed for many years. In the present study, mosaic patterns are selected for characterizing the microstructure of cementitious composites, and the autocorrelation functions of mosaic patterns are used to evaluate the thermal stress variation in cementitious materials. This is because that mosaic patterns look like internal structure of cementitious materials at different scale levels such as concrete, mortar, and cement paste.

2.3 Mosaic patterns

An n-phase mosaic is a spatial arrangement of the n-phases, in which every point within the spatial domain is assigned to be a particular phase, and all the phases are presented as patches of finite extent. Therefore, there is no overlapping between various phases [58].

There exists two common mosaic patterns, one is a random set mosaic and the other is a random line mosaic. The random set mosaic pattern is called S-mosaic and the random line mosaic is called L-mosaic. Beside these two patterns, Masao [48] proposed another mosaic pattern named covering mosaic pattern, which can be called C-mosaic. Therefore, the main mosaic patterns are as follows:

(1) Random line mosaic (L-mosaic).

(2) Random set mosaic (S-mosaic).

(3) Random covering mosaic (C-mosaic).

Figure 2.1 shows these different mosaic patterns.

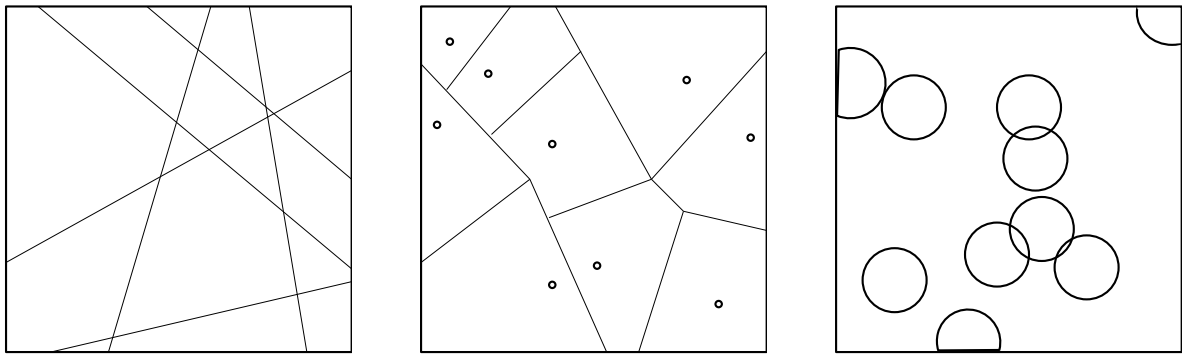

(a) L-mosaic (b) S-mosaic (c) C-mosaic

Figure 2.1: Random mosaic pattern. (Random set mosaic, Random line mosaic, Random covering mosaic)

There are various methods of constructing a random mosaic. However, it is not possible to define a mosaic as random without specifying the exact definition of randomness [58]. Below are two different ways of constructing a random mosaic pattern.

2.3.1 L-mosaic pattern model

Taking a 2D L-mosaic as an example, in the map of a 2D mosaic pattern, the patch-phase may be colored black and the gap-phase may be left white. L-mosaic is one of the ways of constructing a random mosaic, which is based on drawing random lines, subdividing an area into a network of convex polygons or cells. Then, each cell can be assigned its color with fixed probabilities. b for a black cell and w for a white cell with $b+w=1$.

When contiguous cells are colored black, they form a many-celled patch and if they are colored white, they form a many-celled gap. It should be noted that it is important to distinguish the differences between a cell, a patch and a gap.

The cells are defined as the small area formed when the random lines are drawn across the area. The cells are the units composed of patches and gaps. Patches consist of any number of contiguous cells, which are colored as black, and gaps consist of any number of contiguous cells, which are

colored white.

In order to draw random lines, the following method can be used. It can be assumed that the desired area in which the lines are to be drawn is circumscribed by a circle of radius r. The center of the circle can be considered as the pole of a polar coordinate frame and then an initial line can be drawn through it. Next, taking pairs of random polar coordinates (p,θ), a line can be drawn which passes through the point with the specific coordinate, such as (p_1,θ_1) and it is perpendicular to the line connecting (p_1,θ_1), and the pole of the polar coordinate. This is a random line, and therefore the method is called random line mosaic method [58]. Figure 2.2 shows a random line mosaic developed based on this method.

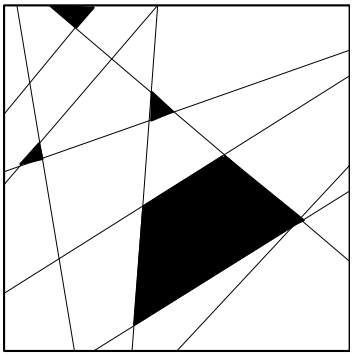

Figure 2.2: Random Line mosaic (L-mosaic).

2.3.2 S-mosaic pattern model

Another type of mosaic pattern is called S-mosaic, which can be constructed as follows: a pattern of random dots should be drawn in the map area for a 2D S-mosaic. Then each of the dots can be associated with a cell. Each segment of a cell boundary is the locus of points which are equidistant from the two nearest dots. Now, each cell can be colored independently as black or white with probability of b and w, respectively [58]. Figure 2.3 shows a random set mosaic pattern.

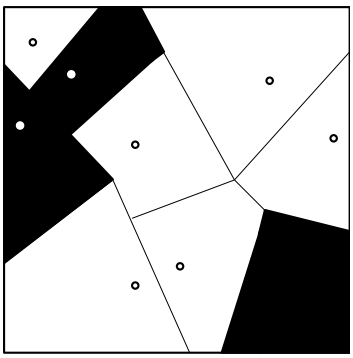

Figure 2.3: Random set mosaic (S-mosaic).

2.4 Mathematical modeling for L-mosaic

In the present study, we will focus on the application of L-mosaic in evaluating the residual stress variation. There exists different ways of comparing various kinds of mosaics such as: means and variances of random variables, including the number of sides per cell, cell perimeter, cell area, angular and edge length distribution, or comparing the theoretical autocorrelation functions.

To construct the mathematical model, it is more convenient to simplify a 3D model to a 2D model. This can be done by cutting the 3D mosaic with a 2D plane. Then the 2D mosaic pattern can be even more simplified by cutting it with a line, with the result being a 1D mosaic pattern. The line passing through the 2D mosaic pattern is reduced to the points on the transect, and between these points are the cut lengths of the cell which are called cell lengths. Figure 2.4 shows a 1D mosaic pattern.

It should be noted that since the properties of mosaic pattern depend on the properties of generated random points, these properties will be completely different for different random points [59]. Therefore, in the present study, the focus is on the mosaic pattern generated by the Poisson point field.

From the statistical theory, Miles [51] has shown when a 2D L-mosaic is generated from a Poisson field with density λ, the number of intersections on transect in a 1D L-mosaic would have a Poisson distribution of density of $\lambda = 2\tau/\pi$, where τ is a constant density.

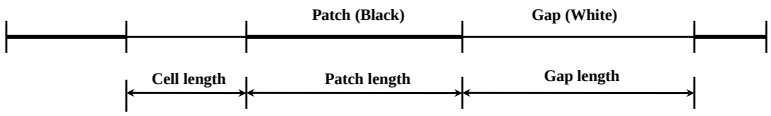

Figure 2.4: Transect through mosaic pattern.

Moreover, the probability density function (pdf) of an exponential function can be defined as:

$$f(x,\lambda) = \begin{cases} \lambda e^{-\lambda x} & \text{if} \quad x \succeq 0 \\ 0 & \text{if} \quad Otherwise \end{cases} \tag{2.6}$$

where λ is the parameter of the distribution and x is the random variable.

Therefore, the pdf for the cell length would be:

$$f(l_c,\lambda) = \lambda e^{-\lambda l_c} \tag{2.7}$$

where l_c is the cell length and λ is the cell distribution parameter. Additionally, in the case of multi-phase mosaic, the m colors correspond to the m phases. However, the multi-phase mosaic can be modeled as a two phase mosaic by choosing one color to be assigned to the patch group and the rest in the gap group. For instance, the j^{th} phase can be chosen as a phase called gap and all other phases regrouped together as the patch. As a result multi-phase mosaic has changed to a two phase mosaic [79]. The probability for the patch and gap can be defined as:

$$\begin{aligned} P_g &= P_j \\ P_P &= \sum_{i=1, i\neq j}^{m} P_i \end{aligned} \tag{2.8}$$

where subscripts g and p are denoted gap and patch, respectively.

Since, in a 1D mosaic pattern, the interest is on the gap and patch, the pdf for patch can be derived

as:

$$f(l_p, \lambda_{pj}) = \lambda_{pj} e^{-\lambda_{pj} l_p} \tag{2.9}$$

where λ_{pj} is the parameter of the distribution for the j^{th} patch, $\lambda_{pj} = P_j \lambda$ and l_p is the length of the patch. This is a mathematical model for the multi-phase mosaic pattern. Thus, by repeating above process for each phase and knowing $\sum_{j=1}^{m} P_j = 1$, the patch distribution parameter can be related to the cell distribution parameter as follows:

$$\sum_{j=1}^{m} \lambda_{pj} = \sum_{j=1}^{m} P_j \lambda = \lambda \tag{2.10}$$

Additionally, in the case of multi-phase mosaic, there is m governing distribution functions as defined in equation [78] and m independent controlling parameters (P_j, j=1,m-1).

2.4.1 The mean value for two-phase composites

The phase function for a two phase composite can be defined as:

$$X(x) = \begin{cases} x_1 & \text{if} \quad x \in \nu_1 \\ x_2 & \text{if} \quad x \in \nu_2 \end{cases} \tag{2.11}$$

where ν_1 and ν_2 are the volume of phase one and two, respectively.

The indicator function for phase i, for any point $x \in \nu_i$ is given by:

$$I_i(x) = \begin{cases} 1 & \text{if} \quad x \in \nu_i \\ 0 & \text{if} \quad otherwise \end{cases} \tag{2.12}$$

where ν_i is the volume of phase i. For a composite with two phases, the above equation can be simplified as: $I_1(x)$ and $I_2(x)$, thus the phase function can be redefined as:

$$X(x) = x_1 I_1(x) + x_2 I_2(x) \tag{2.13}$$

However, the expected value of an indicator function is the probability of that indicator function, therefore:

$$\begin{aligned} P[I_1(x)] &= \phi_1 \\ P[I_2(x)] &= \phi_2 \\ \phi_1 + \phi_2 &= 1 \end{aligned} \tag{2.14}$$

Replacing these values in the above equation would lead to:

$$\begin{aligned} E(X) &= x_1\phi_1 + x_2\phi_2 \\ E(X) &= x_1\phi_1 + x_2(1-\phi_1) \\ E(X) &= (x_1 - x_2)\phi_1 + x_2 \end{aligned} \tag{2.15}$$

$E(.)$ is the expectation operator.

2.4.2 Autocorrelation function for two-phase composite

Assuming the two-phase composite is homogenous and isotropic, the autocorrelation function of the composite can be written as:

$$R_x(\nu) = E(X(x)X(x+\nu)) = x_1^2 P[x_1, x_1] + 2x_1x_2P[x_1, x_2] + x_2^2P[x_2, x_2] \tag{2.16}$$

where $P[x_1, x_1]$ is the probability of both x and $x+\nu$ are in phase one, $P[x_2, x_2]$ is the probability of both x and $x+\nu$ are in phase two and $P[x_1, x_2]$ is the probability of x in phase one and $x+\nu$ in phase two [79].

It should be noted that $P[x_1, x_2] = P[x_2, x_1]$ and that is the reason for the second term having the factor of two. The autocorrelation function can be determined if these probabilities are defined. It can be seen that the autocorrelation function can be determined if these probabilities are defined. Based on Corson's equation [13] for the two-point probability distribution function of a homogeneous, isotropic two-phase random media, each of these probabilities can be defined as:

$$\begin{aligned} P[x_1, x_1] &= \phi_1\pi + \phi_1^2(1-\pi) \\ P[x_2, x_2] &= \phi_2\pi + \phi_2^2(1-\pi) \\ P[x_1, x_2] &= \phi_1\phi_2(1-\pi) \end{aligned} \tag{2.17}$$

where π is the probability of both x and $x+\nu$ belonging to the same phase. From this equation, it can be seen that π has a significant effect on the autocorrelation function.

2.4.3 Autocorrelation function for multi-phase composite

For multi-phase composite, the phase function can be written as:

$$X(x) = x_i I_i, x \in \nu_i \tag{2.18}$$

where i=1,2,$\cdots$,m, ν_i is the volume of phase i and m is the total number of phases within the composite.

Similar to the two phase composite, the mean value of the X can be derived as:

$$E(X) = \sum_{i=1}^{m} x_i \phi_i \tag{2.19}$$

where ϕ_i is the volume fraction of phase i.

Therefore, the autocorrelation function would be:

$$R_x(\nu) = E(X(x)X(x+\nu)) = \sum_{i=1}^{m}\sum_{j=1}^{m} x_i x_j P[x_i, x_j] \tag{2.20}$$

where

$$\begin{aligned} P[x_i, x_j] &= \phi_i \pi + \phi_i^2(1-\pi), i = j \\ P[x_i, x_j] &= \phi_i \phi_j (1-\pi), \quad i \neq j \end{aligned} \tag{2.21}$$

Thus, the autocorrelation function can be rewritten as:

$$R_x(\nu) = \sum_{i=1}^{m} x_i^2(\phi_i \pi + \phi_i^2(1-\pi)) + \sum_{i=1}^{m}\sum_{j=1}^{m} x_i x_j \phi_i \phi_j (1-\pi) \tag{2.22}$$

2.4.4 Autocorrelation function for L-mosaic pattern

The homogenous Poisson distribution can be defined as:

$$P[k] = \frac{(\lambda \mid \nu \mid)^k}{k!} e^{-\lambda|\nu|} \tag{2.23}$$

where k=$N(x, x+\nu)$ which is the number of points in length interval ν and it is controlled by the Poisson process.

Defining π as the probability of both x and $x+\nu$ being in the same cell, which is equivalent to the probability of no intersection point in ν, in other words when $k= 0$. Thus, for L-mosaic:

$$\pi = P[k = 0] = e^{-\lambda\nu} \tag{2.24}$$

$$R_x(\nu) = \sum_{i=1}^{m} x_i^2(\phi_i e^{-\lambda\nu} + \phi_i^2(1 - e^{-\lambda\nu})) + \sum_{i=1}^{m}\sum_{j=1}^{m} x_i x_j \phi_i \phi_j (1 - e^{-\lambda\nu}) \tag{2.25}$$

Figures 2.5 through 2.8 show how any increase in the relative distance and coarseness would decrease the autocorrelation function of the mosaic pattern.

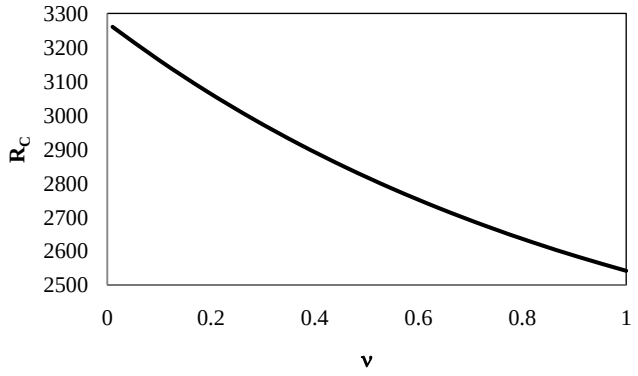

Figure 2.5: The effect of relative distance on stiffness autocorrelation function.

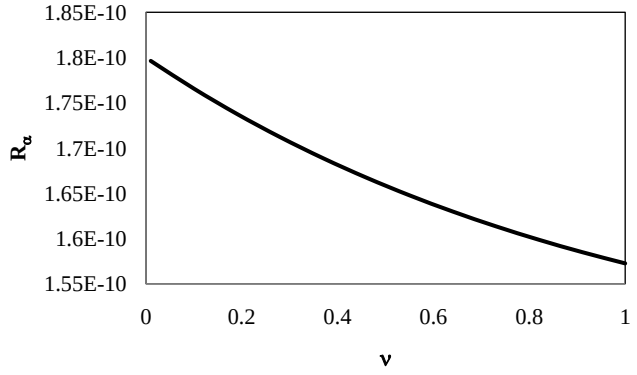

Figure 2.6: The effect of relative distance on thermal expansion autocorrelation function.

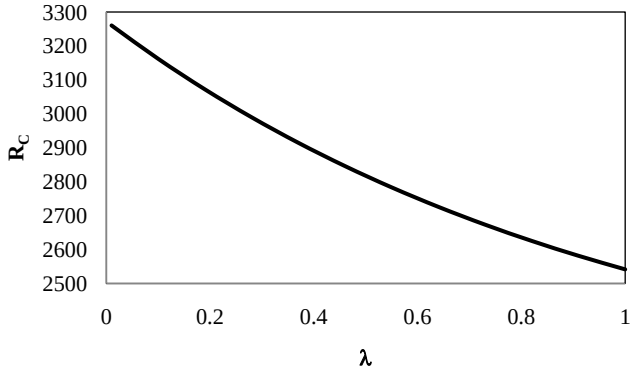

Figure 2.7: The effect of coarseness on stiffness autocorrelation function.

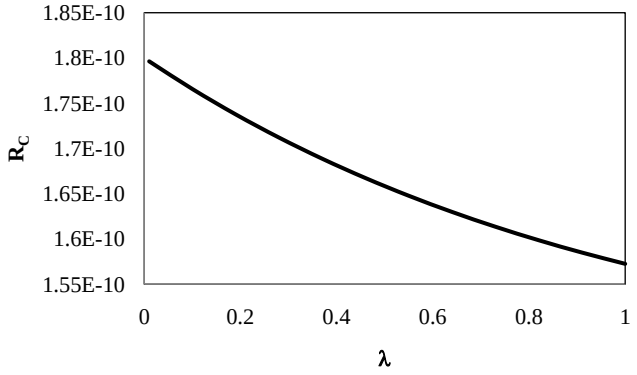

Figure 2.8: The effect of coarseness on thermal expansion autocorrelation function.

2.4.5 Autocorrelation function for S-mosaic pattern

Since the S-mosaic patterns are governed by the midpoints of the cells, the π can be defined as follows:

$$\pi = (1 + \lambda\nu)e^{-2\lambda\nu} \tag{2.26}$$

Thus the autocorrelation function for a two phase composite based on S-mosaic pattern would be defined as:

$$R_x(\nu) = (x_1^2\phi_1 + x_2^2\phi_2)(1 = \lambda\nu)e^{-2\lambda\nu} + (x_1\phi_1 + x_2\phi_2)^2[1 - (1 + \lambda\nu)e^{-2\lambda\nu}] \tag{2.27}$$

2.5 The mean value of modulus of elasticity and thermal expansion

Assuming the micro-structures are static or can be approximated as static, the structure functions would be independent of time [73], the modulus of elasticity and thermal expansion coefficient of each phase can be defined as the follows:

$$C(x) = \begin{cases} C_1 & \text{if} \quad x \in \nu_1 \\ C_2 & \text{if} \quad x \in \nu_2 \end{cases} \tag{2.28}$$

$$\alpha(x) = \begin{cases} \alpha_1 & \text{if} \quad x \in \nu_1 \\ \alpha_2 & \text{if} \quad x \in \nu_2 \end{cases} \tag{2.29}$$

where C_1 and C_2 are the modulus of elasticity, α_1 and α_2 are the thermal expansion coefficients of phase one and phase two, respectively.

Combining these equations with the indicator functions result in:

$$C(x) = C_1I_1(x) + C_2I_2(x) \tag{2.30}$$

$$\alpha(x) = \alpha_1I_1(x) + \alpha_2I_2(x) \tag{2.31}$$

However, the mean value or expected value of the modulus of elasticity can be obtained by:

$$E(C(x)) = E(C_1I_1(x) + C_2I_2(x)) \Rightarrow E(C(x)) = E(C_1).E(I_1(x)) + E(C_2).E(I_2(x)) \tag{2.32}$$

Since it has been mentioned that the expected value of the indicator function is the probability of the indicator function, the mean value of the *C(x)* would be:

$$E(C(x)) = E(C_1).\phi_1 + E(C_2).\phi_2 \tag{2.33}$$

where E is the expectation operator and ϕ_1 and ϕ_2 are the volume fraction of phase one and two, respectively.

Replacing the volume fraction of phase two in terms of volume fraction of phase one would result as:

$$E(C(x)) = E(C_1).\phi_1 + E(C_2).(1-\phi_1) \Rightarrow E(C(x)) = (E(C_1) - E(C_2)).\phi_1 + E(C_2) \tag{2.34}$$

Following the similar approach would give the mean value of the thermal expansion coefficient as:

$$E(\alpha(x)) = (E(\alpha_1) - E(\alpha_2)).\phi_1 + E(\alpha_2) \tag{2.35}$$

2.6 The autocorrelation function of modulus of elasticity and thermal expansion

The autocorrelation function is the second order information of spatial arrangements of the randomly distributed constituent phases. The random nature of various micro-structures can be characterized by morphological models. In the present study, the autocorrelation functions for multi-phase composites are developed based on L-mosaic patterns.

As was mentioned, there exist two common kinds of mosaic patterns, L-mosaic and S-mosaic. It should be noted that the L-mosaic can be used for simulation of those micro-structures that are composed of grains with high angularities and the S-mosaic can be used for low angular grains [78]. Following the explained method for developing the autocorrelation functions for a two-phase composite based on L-mosaic pattern yields:

$$\begin{aligned} R_C(\nu) &= (C_1\phi_1 + C_2\phi_2)^2[1 - e^{-\lambda\nu}] + (C_1^2\phi_1 + C_2^2\phi_2)e^{-\lambda\nu} \\ R_\alpha(\nu) &= (\alpha_1\phi_1 + \alpha_2\phi_2)^2[1 - e^{-\lambda\nu}] + (\alpha_1^2\phi_1 + \alpha_2^2\phi_2)e^{-\lambda\nu} \end{aligned} \tag{2.36}$$

where λ and ν are the coarseness and the relative distance between two points within the composite. $R_C(\nu)$ and $R_\alpha(\nu)$ are the autocorrelation functions for modulus of elasticity and thermal expansion, respectively.

2.7 Numerical results and discussions

From the expected values of the modulus of elasticity and thermal expansion, it can be shown that:

$$\begin{aligned} E(C(x)) &= E(C(x+\nu)) \\ E(\alpha(x)) &= E(\alpha(x+\nu)) \end{aligned} \tag{2.37}$$

Thus, substituting the expected values and autocorrelation functions into Equation 2.5 for the covariance of the stresses with leads to the following equation.

$$\begin{aligned} cov(\sigma(x),\sigma(x+\nu)) = \epsilon^2(C_1\phi_1 + C_2\phi_2)^2[1-e^{-\lambda\nu}] + (C_1^2\phi_1 + C_2^2\phi_2)e^{-\lambda\nu} \\ -2\theta\epsilon(C_1\phi_1 + C_2\phi_2)^2[1-e^{-\lambda\nu}] + (C_1^2\phi_1 + C_2^2\phi_2)e^{-\lambda\nu}E(\alpha(x)) \\ +\theta^2((\alpha_1\phi_1 + \alpha_2\phi_2)^2[1-e^{-\lambda\nu}] + (\alpha_1^2\phi_1 + \alpha_2^2\phi_2)e^{-\lambda\nu}) \\ ((C_1\phi_1 + C_2\phi_2)^2[1-e^{-\lambda\nu}] + (C_1^2\phi_1 + C_2^2\phi_2)e^{-\lambda\nu}) - E(\sigma(x))E(\sigma(x+\nu)) \end{aligned} \tag{2.38}$$

Since concrete is a two-phase composite including the cement paste and aggregates as two defined phases, the fluctuation of thermal stresses within concrete can be investigated using the above equation.

The mechanical properties and thermal expansion coefficients of each phase can be found in Table 2.1.

Table 2.1: The properties of the phases within the concrete

Phase	**Modulus of Elasticity (GPa)**	**Thermal expansion coefficient (/°C)**
Cement paste	12	$18 * 10^{-6}$
Aggregate	80	$6 * 10^{-6}$

Figure 2.9 through 2.16, show the effect of modulus of elasticity and thermal expansion on stress covariance under various conditions.

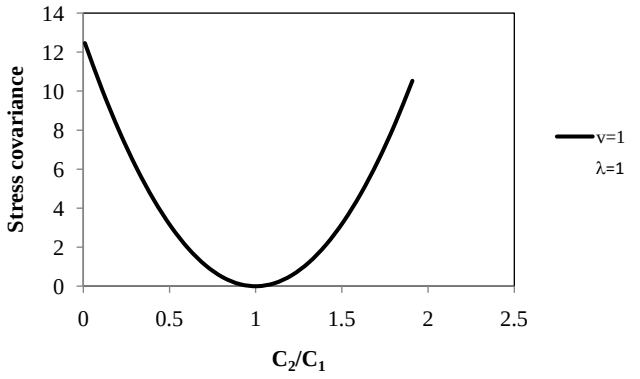

Figure 2.9: The effect of modulus of elasticity on the covariance with fixed volume fraction, fixed relative distance and fixed coarseness.

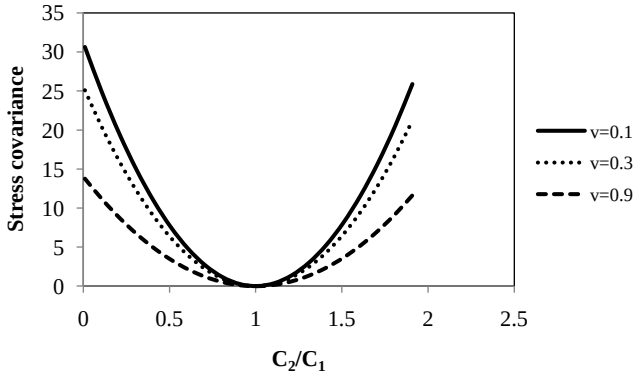

Figure 2.10: The effect of modulus of elasticity on the covariance with fixed volume fraction and fixed coarseness.

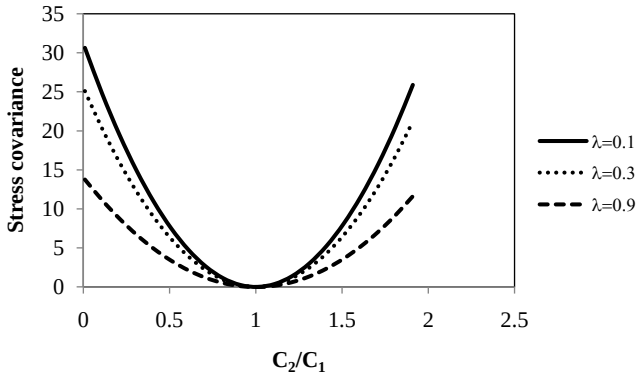

Figure 2.11: The effect of modulus of elasticity on the covariance with fixed volume fraction and fixed relative distance.

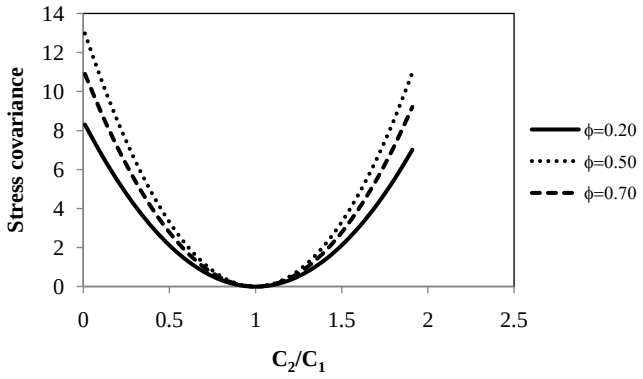

Figure 2.12: The effect of modulus of elasticity on the covariance with fixed relative distance and fixed coarseness.

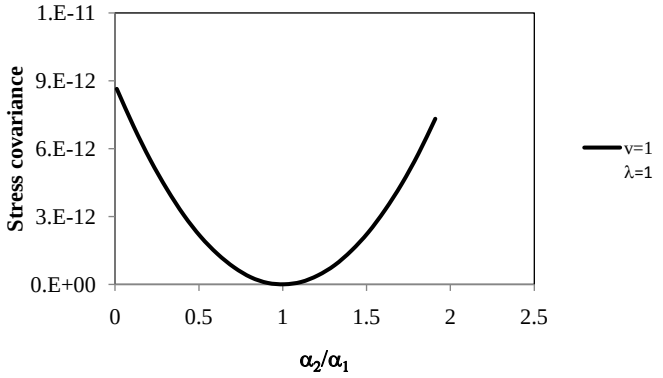

Figure 2.13: The effect of coefficient of thermal expansion on the covariance with fixed volume fraction, fixed relative distance and fixed coarseness.

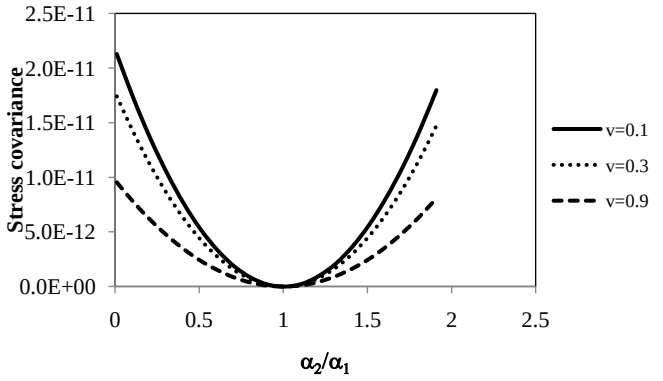

Figure 2.14: The effect of coefficient of thermal expansion on the covariance with fixed volume fraction and fixed coarseness.

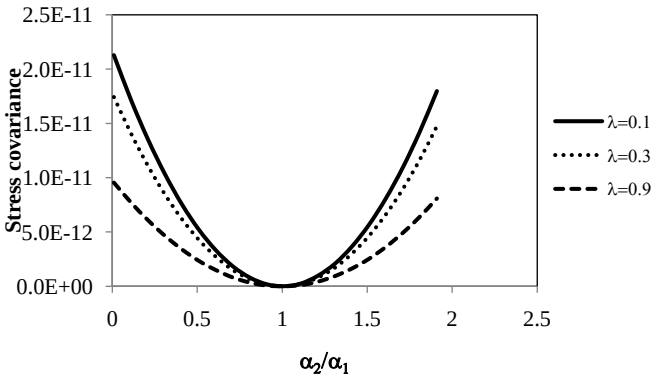

Figure 2.15: The effect of coefficient of thermal expansion on the covariance with fixed volume fraction and fixed relative distance.

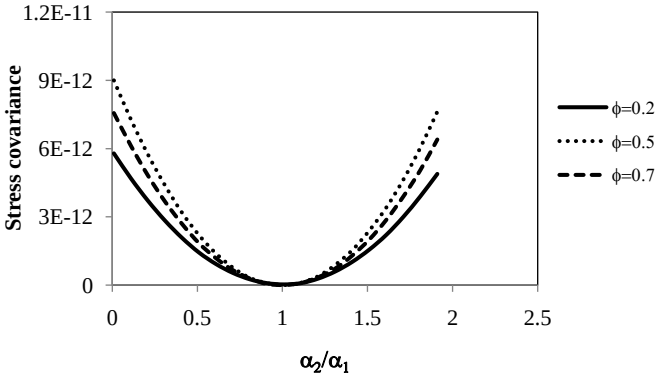

Figure 2.16: The effect of coefficient of thermal expansion on the covariance with fixed relative distance and fixed coarseness.

As can be seen from Figure 2.9 through 2.12, by increasing the ratio of C_2 to C_1 from zero to one, the covariance is decreasing, regardless of the value of coarseness or relative distance. This means that when the two phases have similar stiffness (modulus of elasticity), the variation of thermal stress is small; while if the two phases have dissimilar stiffness, the variation of thermal stress becomes large. However, by increasing the coarseness and relative distance, as expected, the covariance is decreased as well. This makes sense, because the stress variation due to heterogeneity of microstructure is a localized phenomenon, when large aggregate particles are used in concrete (coarser grained internal structure) any two particles get farther apart, the stress variation between the particles do not change as abruptly with respect to each other as in the fine-grained concrete. The effect of the ratio of coefficient of thermal expansion can be seen from Figure 2.13 through 2.16. Basically, it depends on the difference between the two CTEs, the larger the difference, the higher the stress variation. When the two CTEs are equal (thermally homogeneous), there is no thermal stress variation.

It is interesting to see in both modulus of elasticity and thermal expansion cases, the effect of volume fraction reaches the maximum when ϕ =0.5 (see Figures 2.12 and 2.16). This means that when there is no dominant phase exists in the composite, the thermal stress variation reaches the maximum.

Looking closely at Figures 2.9 through 2.16, reveals that the effect of the grain size and the grain distribution are much more significant than the volume fraction. Most previous research focused on the volume fraction, which is the first order statistics of the microstructure, however, these results showed that the effect of volume fraction is not as influential as the grain size and grain distribution. These findings confirm that the higher order correlations statistics of the microstructure are necessary in studying the thermal stress variation , which is dependent on the microstructure of the composite.

2.8 Application of the numerical results

Concrete can be considered as a two-phase composite with aggregate as one phase and a cement-paste matrix as another. The coarseness can be defined based on the volume fraction of aggregate and grading curve of the aggregate (particle size distribution). Xi [78] has shown the expression of coarseness λ for concrete can be defined as:

$$\lambda = \frac{\pi}{2E(D)} \frac{1}{1-\phi_a} \tag{2.39}$$

where the $E(D)$ is the average size of the aggregate and ϕ_a is the volume fraction of the aggregate in the mixing design. Figures 17 through 22 show the effect of the aggregate size and the aggregate volume fraction on the coarseness, stiffness, and thermal expansion autocorrelation functions.

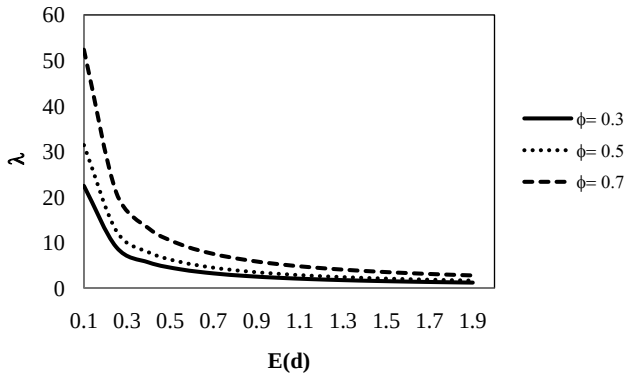

Figure 2.17: The effect of average aggregate size on coarseness for various aggregate volume fraction.

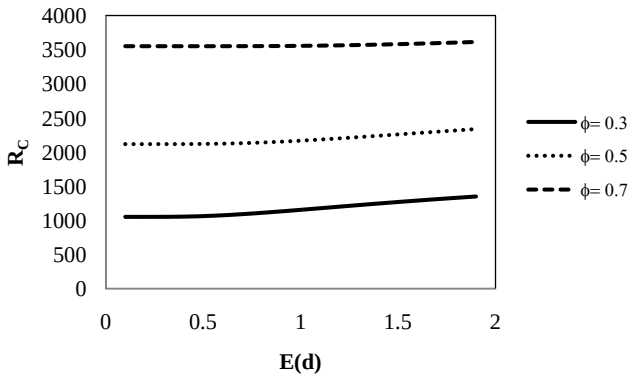

Figure 2.18: The effect of average aggregate size on stiffness autocorrelation function for various aggregate volume fraction.

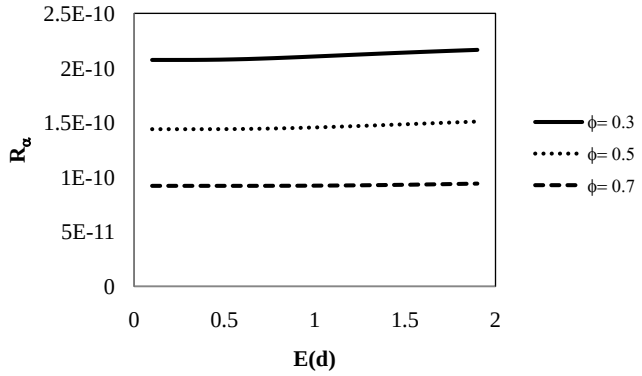

Figure 2.19: The effect of average aggregate size on thermal expansion autocorrelation function for various aggregate volume fraction.

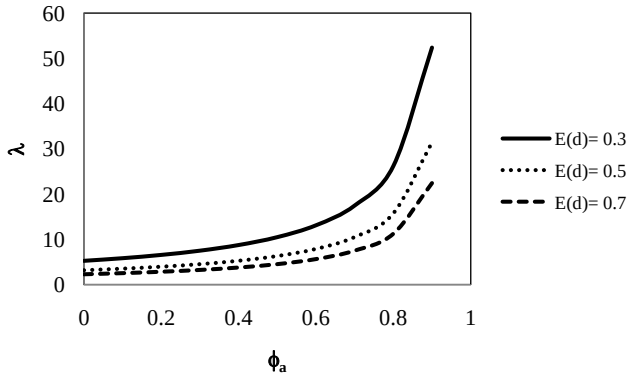

Figure 2.20: The effect of aggregate volume fraction on coarseness for various aggregate average size.

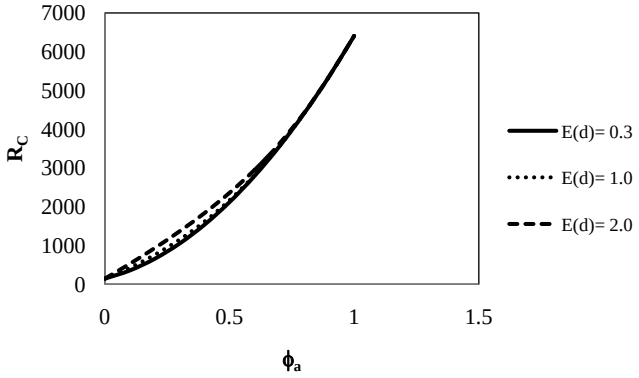

Figure 2.21: The effect of aggregate volume fraction on stiffness autocorrelation for various aggregate average size.

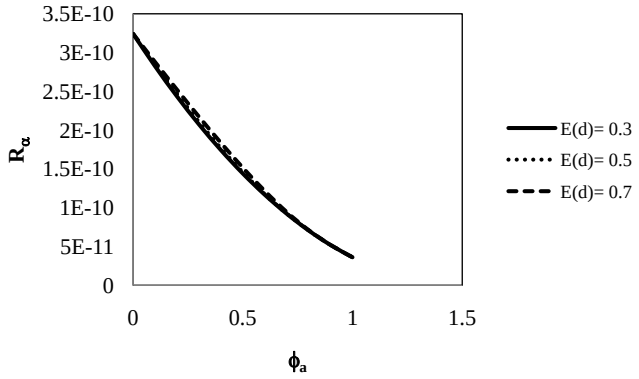

Figure 2.22: The effect of aggregate volume fraction on thermal expansion autocorrelation for various aggregate average size.

Figure 2.17 shows that for a fixed aggregate volume fraction any increase in the average aggregate size would decrease the coarseness. For a fixed average aggregate size, any increase in the volume fraction of the aggregate would increase the coarseness. It should be noted that for small average aggregate size, any change in the aggregate volume fraction would change the coarseness dramatically, while for bigger average aggregate size, any change in the aggregate volume fraction would not influence the coarseness as much.

Figure 2.18 shows that for a fixed aggregate volume fraction, any increase in the aggregate average size would increase the stiffness autocorrelation slightly. However, for a fixed aggregate average size, any increase in the aggregate volume fraction would increase the stiffness autocorrelation as well. This is due to the fact that the aggregate is stiffer than cement paste. One can also observe that for higher aggregate volume fraction, the change in the aggregate average size does not affect the stiffness autocorrelation function as much.

Figure 2.19 shows that for a fixed aggregate volume fraction, any increase in the aggregate average size would not make a significant difference on the thermal autocorrelation. However, for a fixed aggregate average size, any increase in the aggregate volume fraction would decrease the thermal autocorrelation, which is due to the fact that the thermal expansion of the aggregate is less than the thermal expansion of the cement paste.

Figure 2.20 shows that for a fixed aggregate average size, any increase in the aggregate volume fraction would increase the coarseness. However, for a fixed aggregate volume fraction, any increase in the aggregate average size would decrease the coarseness. This effect is more significant for higher aggregate volume fraction than the lower aggregate volume fraction.

Figure 2.21 shows that for a fixed aggregate average size, any increase in the aggregate volume fraction would increase the stiffness autocorrelation. This is mainly because of aggregate being stiffer than the cement paste. However, for a fixed aggregate volume fraction, any increase in the average aggregate size would increase the stiffness autocorrelation slightly. This effect is more obvious for the smaller aggregate volume fraction than the higher aggregate volume fraction.

Figure 2.22 shows that for a fixed aggregate average size any increase in the aggregate volume

fraction would decrease the thermal expansion autocorrelation, which is mainly due to the lower thermal expansion coefficient of the aggregate in compared with the thermal expansion coefficient of the cement paste. However, for a fixed aggregate volume fraction, any increase in the average size of the aggregate would lead to a slightly higher thermal expansion autocorrelation. This effect is more recognized in the lower aggregate volume fraction than the higher aggregate volume fraction.

Looking closely at these figures also reveals that the average aggregate size and volume fraction have the opposite effect on the coarseness and autocorrelation function. Overall, these findings show the importance of higher order autocorrelation function on the study of crack propagations within any composite.

2.9 Conclusions

A mathematical model is developed relating the covariance of thermal stress and the grain sizes, the volume fractions, the mechanical properties, and thermal expansion coefficients of the constituent phases. The effects of the influential parameters are numerically analyzed. The application of the theoretical model specifically to concrete was studied. The general findings from this study are as follows:

(1) The internal structure of composite materials such as concrete and mortar can be represented by mosaic patterns. There are various types of mosaic patterns. Among them, the statistical features of L-mosaic pattern were discussed in detail and their application to studying the variation of internal thermal stress was investigated.

(2) The covariance of thermal stress depends on the autocorrelation functions of elastic modulus and coefficient of thermal expansion of the composite, which, in turn, depend on the autocorrelation function of mosaic patterns.

(3) An increase in the distance between two desired points within a composite decreases the autocorrelation functions of mosaic patterns.

(4) Both stiffness and thermal expansion autocorrelation functions decrease with increasing coarseness of the grain structure.

(5) The average grain size and grain distribution have the strongest effect on both stiffness and thermal expansion autocorrelation functions. As a result, they also have the strongest effect on the thermal stress variation.

(6) The volume fraction of constituent phase is one of the most important factors in both stiffness and thermal expansion autocorrelation function. However, its effect is less than the effect of grain size distribution. Thus, the models incorporating only the volume fraction, which is the first order statistics of the internal structure, are not capable of capturing the thermal stress variation very well.

(7) The stiffness of each phase has the most effect on both stiffness and thermal expansion autocorrelation functions. If the stiffness of the phases are close, then the thermal expansion of each phase would make an influential effect on the autocorrelations.

(8) In the application of the theoretical model to concrete, the effect of the aggregate average size and aggregate volume fraction on stiffness autocorrelation is more significant than the thermal expansion autocorrelation. This is mainly due to the significant difference between the stiffness of the aggregate and cement paste. The difference between the coefficient of thermal expansion of the aggregate and cement paste is relatively small.

Chapter 3

EXPERIMENTAL STUDY ON PHASE CHANGE MATERIALS IN CONCRETE

This chapter presents the results of an experimental investigation of using phase change materials (PCMs) in Portland cement concrete. The objective of the research is to improve thermal properties of concrete as a structural material. Compression test, flexural test, drying shrinkage test, as well as thermal conductivity test are conducted. PCMs are used in concrete mixtures as both sand replacement and additives. The results revealed that in the replacement method, the loss of compressive strength due to addition of PCM is not significant, and the specific heat of concrete increased considerably. Thus, thermal conductivity of the new concrete is improved. Flexural test, drying shrinkage test and microstructure analysis provide a good understanding of the PCM-modified concrete. Overall, the results show that it is quite promising to maximize the enhancement of PCM on thermal properties of PCM-modified concrete and minimize the reduction on mechanical properties of the concrete.

3.1 Introduction

Mechanical properties such as strength and stiffness have been considered as the most important material properties for structural materials like concrete. Recently, thermal insulation and heat storage capacity of the structural materials have also been considered as important material properties for sustainable development of energy efficient buildings. Specifically, how to improve thermal resistance of concrete materials becomes an interesting and important research topic. One

of the effective methods to improve thermal resistance of concrete is to use phase change materials (PCMs) as an additive. PCMs have high heat of fusion when they melt and solidify at a certain temperature, and thus are capable of storing and releasing large amount of heat at the specific temperature [20].

Many researchers such as Hawes et al. [20] Lencer et al. [42] have studied different PCMs and their applications. Hawes et al. [20] and Sharma et al. [64] classified PCMs into three categories: organic, inorganic, and eutectic. Hawes et al. [17] have shown that by adding a proper type of PCM in a material, the thermal storage capacity of the material can be enhanced beneficially. They have shown that the organic PCMs materials, due to their compatibility with the building materials, would be the best choice for the application in the building envelopes. Chen et al. [11] used a specific type of phase change material made as small particles (called microencapsulated PCMs) embedded in energy-storing wallboard and their result indicated that by applying proper PCM to the inner surface of the wall, the thermal comfort of the building can be enhanced dramatically. Richardson et al. [62] analyzed the reduced unit weight of insulation materials when PCMs are used in the material. They concluded that the amount of mass which can be saved by using PCM provided a substantial benefit. Li et al. [45] investigated the thermal performance of granular PCM composite which was made of granular porous materials and PCMs and the result was quite promising.

Cabeza et al. [9] constructed a small house using concrete incorporating PCMs. Zhang et al. [83] studied the effect of a PCM on the thermal property of mortar. Most recently Hunger et al. [32] performed some experiments on self-compact concrete and they showed how the porosity of the concrete was increased by using PCM in their mix design, which implies that the strength of concrete with PCM may be reduced. Bentz and Turpin [7] investigated the effect of PCM in concrete with the lightweight aggregate (LWA) and they showed that by using a lower transition temperature PCM in a bridge deck, a significant portion of the freeze/thaw cycles can be potentially avoided.

The purpose of this chapter is to conduct a systematic study on the effect of PCMs on the

mechanical and thermal properties of concrete containing PCMs. Specifically, the compressive strength, flexural strength, drying shrinkage, and thermal behaviors of the PCM-modified concrete are investigated. These material properties are very important to ensure both short-term and long-term performance of the concrete. Moreover, microstructure of PCM-modified concrete is studied by a Scanning Electron Microscope (SEM). The results show how PCM micro-capsules are incorporated in the microstructure of cement paste.

3.2 Significance of the research

In order to build net-zero energy efficient buildings, it is important to apply every possible method to improve thermal performance of all components used in the building envelope, which implies that not only conventional insulation materials but also structural materials should be taken into account in terms of their contribution to thermal performance of the building. Meanwhile the importance of the mechanical properties of structural materials should not be disregarded. Addition of PCMs in concrete is definitely very effective to improve thermal properties of the concrete, but has some impact on mechanical properties of the concrete. Therefore, both thermal and mechanical properties of PCM-modified concrete should be studied, and the benefit of enhancing thermal properties will be maximized and the impact on mechanical properties of concrete will be minimized.

3.3 Materials used in the experimental program

A phase change material MPCM-28 wet cake manufactured by Microtek [29] was used in this study. The melting point of the MPCM-28 wet cake is 28 °C. This specific product was chosen based on its melting point which is the closest one to the room temperature among all other PCM products of Microtek. The PCM was microencapsulated as shown in Figure 1, which is an image of microstructure of MPCM-28 wet cake taking by a low vacuum scanning election microscopy (LVSEM). The white micro-spheres shown in Figure 3.1 are made of melamine formaldehyde (MF Melamine) polymers and the core material is paraffin (n-Octadecane). The encapsulated PCM

was selected in this study mainly because the polymeric material made of the microcapsules can survive the wet and high pH environment during casting process of the concrete. Table 5.6 shows MPCM-28's general properties based on the Microtek data sheet [29].

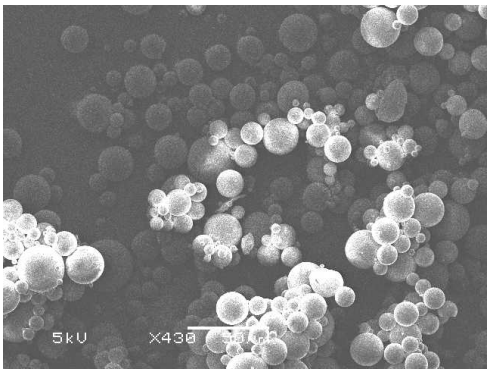

Figure 3.1: The microstructure of MPCM-28 wet cake.

When PCM is added to the mixture of concrete materials as an additional component, there are two ways to adjust the mix design of concrete. PCM can be used to replace a certain percentage of fine aggregate (sand) in the concrete mixture, which is called PCM replacement method; and PCM can also be used as additive in the concrete mixture, which is called PCM additive method. The effect of PCM on thermal properties of a concrete depends on the amount of PCM in the concrete. For a fixed amount of PCM, its effect on thermal properties of concrete is fixed. However, as shown in later sections, its effect on mechanical properties of the concrete is different depending on the mix design method. Therefore, there are two phases in this study. In the first phase, PCM was used to replace various volume percentages of fine aggregate in the concrete mixtures, and PCM was also used as additive in the concrete mixture. The PCM replacement and PCM additive resulted in different mix designs. The experimental results of the first phase revealed that PCM replacement is a better choice. Thus, the second phase of the study focused on thermal and mechanical behaviors of PCM-modified concrete with various volume percentages of PCM replacement of find aggregate.

With the PCM replacement method, different volume percentages of PCM were used to replace the same volume percentages of fine aggregate. For instance, when 5% of the fine sand

Table 3.1: General properties of MPCM-28

Typical Properties	
Appearance	White to slightly off-white color
Form	Wet cake (70% Solid, 30% Water)
Capsule Composition	85-90% wt.% PCM 10-15 wt.% Polymer Shell
Core Material	Paraffin
Particle Size (mean)	17-20 micron
Melting Point	28 °C (82°F)
Heat of Fusion	180-195 kJ/kg
Specific Gravity	0.9
Temperature Stability	Extremely Stable-less than 1% leakage when heated to 250°C
Thermal Cycling	Multiple

needs to be replaced by the PCM, the weight of the PCM can be readily calculated by knowing the density of PCM being equal to 0.9 kg/m^3. In the PCM additive method, the amounts of gravel and sand remain the same, and various amounts of PCM were added to the mixture.

The concrete mixtures consisted of 630 kg/m^3 fine aggregate (sand); 1160 kg/m^3 coarse aggregate; 350 kg/m3 Type I Portland cement; 200 kg/m^3 water, and four different amounts of microencapsulate PCM. The sieve analysis based on ASTM C136-06 [67] was conducted on the fine aggregate and the coarse aggregate being used in the concrete mixtures. Figure 7.1 shows the particle size distribution of the aggregates.

Table 3.2 and Table 3.3 show different mix designs using PCM replacement as well as PCM additives in the phase one of the study.

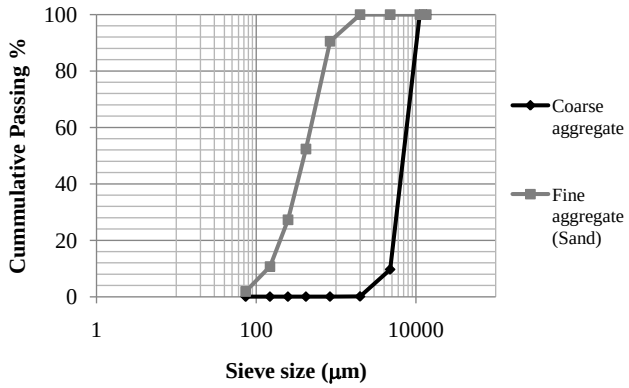

Figure 3.2: Particle size distributions of fine and coarse aggregate.

Table 3.2: Mix designs using PCM additive method

Group	**Cement (Kg)**	**Coarse aggregate (Kg)**	**Fine Aggregate (Kg)**	**PCM (gr)**	**Water (gr)**
PCM0	0.433	1.434	0.779	0	0.247
PCM5-A	0.433	1.434	0.779	13.17	0.247
PCM10-A	0.433	1.434	0.779	26.35	0.247
PCM15-A	0.433	1.434	0.779	39.52	0.247
PCM20-A	0.433	1.434	0.779	52.69	0.247

Table 3.3: Mix designs using PCM replacement method

Group	**Cement (Kg)**	**Coarse aggregate (Kg)**	**Fine Aggregate (Kg)**	**PCM (gr)**	**Water (gr)**
PCM0	0.433	1.434	0.779	0	0.247
PCM5-R	0.433	1.434	0.740	13.17	0.247
PCM10-R	0.433	1.434	0.701	26.35	0.247
PCM15-R	0.433	1.434	0.662	39.52	0.247
PCM20-R	0.433	1.434	0.623	52.69	0.247

As one can see in the both tables, 5%, 10%, 15% and 20% replacements (by volume) and additions were used as experimental parameters to examine the effect of PCM on compressive strength of the PCM-modified concrete. The same four amounts of PCM were used in the PCM additive method in order to examine the effects of the two different design methods on compressive strength of PCM-modified concrete (see Tables 3.2 and 3.3).

There are three steps in the mixing process. First, all the dry materials such as cement, fine aggregate and coarse aggregate are mixed for one minute. Second, the water is added gradually to the mix and the mixing lasts for another minute, and then PCM is added to the concrete mixture and this step takes one minute as well. It should be noted that it is important to add the PCM as the very last component in order to prevent the damage of micro-encapsulate during the mixing process.

Adding the PCM toward the end of the process, not only would avoid damage in the outer shell due to the high shear associated with mixing of concrete, but also would help to minimize the high pH value of the concrete.

3.4 Testing procedures

In order to have a better understanding of the effects of PCM on properties of concrete, the following tests were conducted: compressive strength test, flexural strength test, drying shrinkage test, and thermal conductivity test. These four tests were selected in the study because the PCM and the microcapsules are not high strength solid materials like regular concrete and thus their effect on the strength of concrete has been a major concern. Their effects on drying shrinkage of concrete are also important when the phase changes take place at different temperatures. The thermal conductivity test is especially important for PCM-modified concrete since the modifications in the thermal properties of the concrete due to added PCM will make the concrete suitable for many potential applications.

3.4.1 Compressive strength

This test was done according to ASTM C873/C873M-04e1 [68]. Six cylindrical specimens 2 $in \times 4$ in were cast for each mix design and the compression test was conducted on three of the cylinders at 7 days of age and the remaining three at 28 days of age. The compression test was conducted using a MTS machine with displacement control. The loading rate was kept constant at 0.0015 in/sec for all the specimens at all ages.

3.4.2 Three point bending flexural test

This test was done according to ASTM C293 [69]. Two 2 $in \times 2$ $in \times 8$ in prism specimens are prepared for this test. The three-point bending flexural test provides values for the modulus of elasticity in bending E_f, flexural stress σ_f, flexural strain ϵ_f as well as the flexural stress-strain response of the material. Moreover, flexural modulus obtained from this test can be used as an indication of a material's stiffness when it is loaded. It should be noted that the main advantage of this test is the ease of the specimen preparation and testing. On the other hand, there are some disadvantages, such as the results of the testing method are sensitive to specimen and loading geometry and strain rate.

The flexural stress and stain can be calculated based on the following equations:

$$\sigma_f = \frac{3pl}{2bd^2} \tag{3.1}$$

$$\epsilon_f = \frac{6Dd}{L^2} \tag{3.2}$$

where σ_f= Flexural stress, p= Load at the given point on the load deflection curve, d= Depth of the beam, ϵ_f= Flexural strain, D= Maximum deflection at the center, and L= Support span.

In this study, the flexural test was performed using an Instron testing machine with displacement control. The loading rate was 0.01 mm/s and the sampling rate was 0.1 per second.

It should be noted that in this test, the middle roller was set in the middle of the specimens and the side rollers were set at the thickness distance from the edges.

3.4.3 Drying shrinkage

The standard test method for drying shrinkage of concrete based on ASTM-C 157M [71] was used in this study. As it will be discussed in details later, using PCM replacement will lead to higher compressive strengths than using PCM additive; therefore, the drying shrinkage tests were conducted only on specimens in the PCM replacements method. Two mix designs for PCM replacement at 10% and 20% volume of sand were used for the specimens in the drying shrinkage test. These two mix designs were chosen to cover a lower range as well as the higher range of PCM content in the mix design. Two prism specimens 1 in × 1 in × 10 in were prepared for each mix design. Measurements were started after 7 days of curing in a standard curing room. The relative humidity of the lab was remained about 40% during the testing period.

3.4.4 Thermal properties

In general, thermal diffusivity α, density ρ and specific heat (or heat capacity) c_p of a material can be measured directly, and then thermal conductivity k of the material can be calculated by using the following equation:

$$k = \alpha \rho c_p \tag{3.3}$$

Direct measurement of thermal diffusivity is popular because it just requires measurement of temperature history due to a thermal perturbation on the sample. This is much easier than measuring heat flux as it is required in many steady state methods for obtaining thermal conductivity k [5]. Netzsch LFA 457 device was used for thermal diffusivity measurements.

On the other hand, Differential Scanning Calorimetry (DSC) for measuring the specific heat was conducted using Netzsch DSC 204 F1 Phoenix machine [61] at a scanning rate of 10 °C/min in the temperature range of -25 °C to 50 °C in a nitrogen atmosphere.

In general DSC analysis, two crucibles with the same size are heated through the same temperature versus time program. The reference crucible is always empty, while the other crucible, in turn, is empty, carries the standard (sapphire) sample, and finally, the sample with unknown

specific heat. By keeping crucible of the sample and the reference the same size, under the same temperature and made of the same material, the effects of parasitic convective and radiative losses are automatically canceled. Based on the difference in the heat (DSC signal) required for heating the samples, the ratio of specific heats of the sample and the standard can be easily determined. Equation 3.4 shows how this information is used to calculate the specific heat capacity of each sample.

$$C_{p,Sample} = C_{p,Standard} \frac{m_{Standard}}{m_{Sample}} \frac{DSC_{Sample} - DSC_{Baseline}}{DSC_{Standard} - DSC_{Baseline}} \tag{3.4}$$

It should be noted that the specific heat can only be calculated under exothermic process.

Moreover, for the DSC analysis the system should be programmed for the desired temperature range, which was -25 °C to 50 °C in this case. Thus, in the heating cycle (endothermic), first the temperature was brought down to -25 °C and it was hold for 4 minutes, then the heating cycle started up to 50 °C. When the temperature reached this highest desired temperature (50 °C) it is hold for 3 additional minutes. Next the cooling cycle (exothermic) would be started by cooling the system to the lowest desired temperature (-25 °C).

After the system was programmed for the required temperature range, the general approach in any DSC analysis was taken.

As it was mentioned before, first, both crucibles were empty under the heating and cooling process. Second, the reference crucible (the left hand crucible) remained empty, while the other one was holing sapphire (25 mg) under the same healing and cooling process, in which the system had been programmed. Finally, the third step, which was replacing the sapphire with the sample with unknown specific heat, started under the same healing and cooling process as the other two steps. Then following Equation 3.4 would lead to specific heat of the sample.

Similar to the specimens for drying shrinkage test, two mix designs for PCM replacement of 10% and 20% of sand were used for the specific heat test. Specimens with 10 $mm \times 10\ mm \times 1.5\ mm$ were cut from concrete specimens and their thermal diffusivity is measured at 7 days and 28 days of

age. Since the microcapsules of PCM are very small, the sample size of 10 $mm \times 10\ mm \times 1.5mm$ can be used to study the effect of PCM on thermal properties of the cement paste incorporating PCM micro-capsules.

3.5 Experimental Results and discussions

3.5.1 Compressive and flexural strengths

The average compressive strengths of the two groups of samples at 7 days and 28 days are shown in Table 3.5 and Table 3.4.

Table 3.4: Compressive strengths and strength reductions using PCM as additive

		7 days of age		28 days	
Group	**PCM-cement ratio**	**Average Stress (Ksi)**	**Percentage change**	**Average Stress (Ksi)**	**Percentage change**
PCM0	0	2.65	0	3.11	0
PCM5-A	0.009	1.92	27.41	2.35	24.42
PCM10-A	0.018	1.55	41.67	1.87	39.93
PCM15-A	0.028	1.67	36.96	1.92	38.38
PCM20-A	0.037	1.50	43.4	1.82	41.67

Table 3.5: Compressive strengths and strength reductions using PCM to replace sand

		7 days		28 days	
Group	**PCM-cement ratio**	**Average Stress (Ksi)**	**Percentage change**	**Average Stress (Ksi)**	**Percentage change**
PCM0	0	2.65	0	3.11	0
PCM5-R	0.009	2.21	16.6	2.82	9.30
PCM10-R	0.018	2.20	16.98	2.63	15.40
PCM15-R	0.028	2.46	7.17	2.58	17.19
PCM20-R	0.037	2.14	19.25	2.29	26.31

The strength reductions are shown in the same tables. Figure 3.3 shows the comparison of the test data obtained from the samples of 7 days old, and Figure 3.4 show the comparison of the test data obtained from the samples of 28 days old.

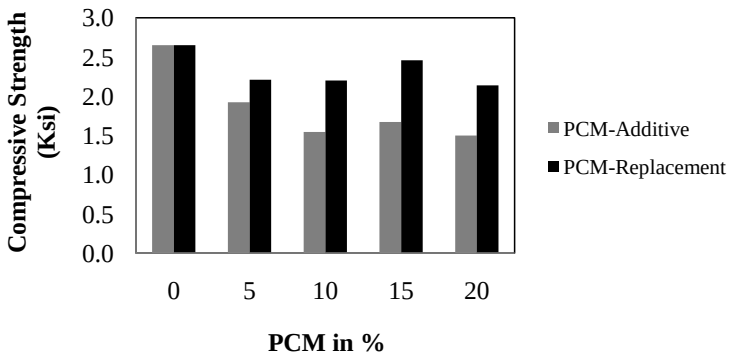

Figure 3.3: Comparison of compressive strengths at 7 days.

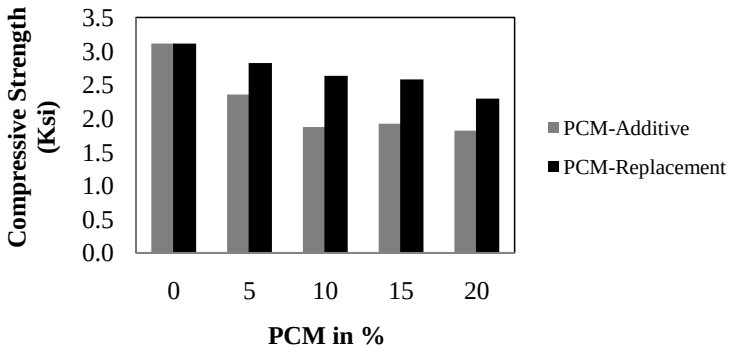

Figure 3.4: Comparison of compressive strengths at 28 days.

One can see that with increasing amount of PCM, the compressive strength of PCM-modified concrete decreases. This is an expected result since PCM is not a solid material with high strength and high stiffness. Therefore, its addition in the hardened concrete will definitely result in strength reduction. Our goal is to find the extent and trend of the strength reduction and minimize the strength reduction. In the present study, with a given amount of PCM in concrete, two different methods were used to add PCM in the concrete, i.e. the replacement method and the additive method. From Figure 3.3 and Figure 3.4, one can clearly see that the strength reductions associated with the PCM replacement method are less than those of the PCM additive method for all four amounts of PCM used in the present study.

This is an important result because improvement of thermal properties of a concrete material depends on the amount of PCM in the concrete. With a fixed amount of PCM in concrete, we must minimize the strength reduction of concrete due to addition of PCM. The present test data indicated that the PCM replacement method results in less strength reduction and thus should be adopted in the practice.

Then the question is why the PCM replacement method resulted in less strength reduction than the PCM additive method. This may be explained by the volume fractions of the constituents in PCM-modified concrete. Compressive strength of concrete depends on several mix design parameters such as water/cement ratio, cement content, gravel/sand ratio, etc. In the present study, water/cement ratio was kept constant for both PCM replacement and PCM additive methods. Therefore, the effect of other design parameters became important. Considering the PCM micro-capsules as soft sand particles, in the PCM replacement method, the total volume fraction of fine aggregate (natural sand plus PCM) remained as a constant with increasing amount of PCM in the mixture. So, the strength reduction of the concrete is due mainly to the increasing amount of soft aggregate (i.e. PCM micro-capsules) in the concrete. While in the PCM additive method, the total volume fraction of fine aggregte (natural sand plus PCM) increased and thus the volume fraction of cement decreased with increasing amount of PCM in the mixture. Thus, the strength reduction of the concrete is due to two concurrent mechanisms:

(1) Increasing the amount of soft aggregate (i.e. PCM microcapsules) in the concrete, which is the same as the PCM replacement method and.

(2) Decreasing the amount of cement (lowered cement content).

It is worthwhile to point out that from the test data shown in Figure 3.3 and Figure 3.4, the strength reduction due to the addition of PCM is not substantial up to 20% of volume replacement of fine aggregate, and there are many applications in which the reduced compressive strength will be still acceptable.

Based on the test data shown in Figures 3.3 and 3.4 and above analysis, it was decided that the rest of the experimental program (the phase two) will be conducted on the specimens prepared by the PCM replacement method. To this end, two groups of specimens were prepared: PCM10-R and PCM20-R. PCM10-R had 10% replacement of natural sand, which is a good representation for a medium range of PCM replacement. PCM20-R had 20% replacement of natural sand, which is a good representation for a high range of PCM replacement.

Three-point bending flexural test was conducted on PCM10-R and PCM20-R at 28 days. Figure 3.5 shows the test data of flexural strength tests. By increasing the amount of the PCM in the concrete mixture, the flexural strength of the concrete decreased. The extent of strength reduction is not significant from 10% to 20% replacement. Hawes [20] also showed that the flexural strength of the PCM-wallboards is comparable with the flexural strength of the conventional wallboards, which is a valuable confirmation on our test results. Comparing the compressive strength with the flexural strength, one can see that the flexural strength is about 20% of the compressive strength, which is quite acceptable.

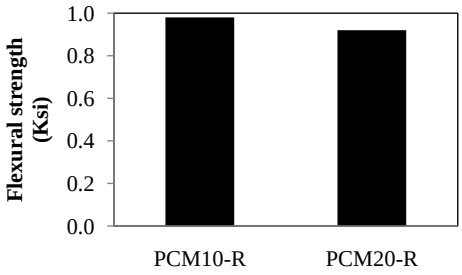

Figure 3.5: Flexural strengths of PCM-modified concrete.

3.5.2 Drying shrinkage

For the drying shrinkage test, two specimens were prepared for each group and they were kept in the curing room for 7 days, then the drying shrinkage test and measurement of length change were started in the room temperature. Figure 3.6 and Figure 3.7 show the test data for the drying shrinkage tests.

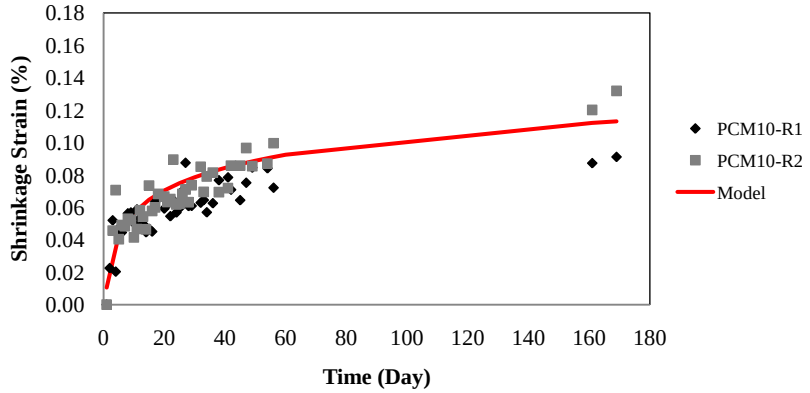

Figure 3.6: Drying shrinkage test data of PCM10-R.

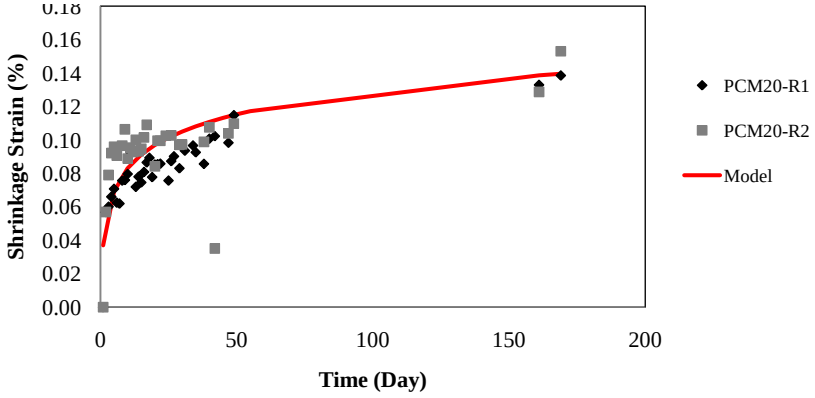

Figure 3.7: Drying shrinkage test data of PCM20-R.

The solid lines in the two figures represent curve fitting of the averaged test data. Then, the two solid lines were plotted in Figure 3.8 as a comparison of the drying shrinkage of PCM-modified concrete with 10% and 20% replacement. Figure 3.8 shows the comparison between the drying shrinkage of these two groups. The comparison of the two curves shows that by increasing the amount of the PCM in the concrete from 10% to 20% replacement, the drying shrinkage increases by about 15%.

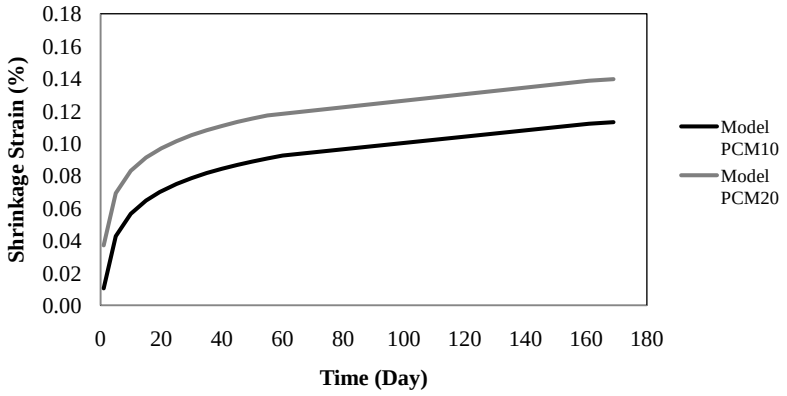

Figure 3.8: Comparison of drying shrinkage between PCM10-R and PCM20-R.

The driving force for drying shrinkage of concrete is cement paste. The amount of cement paste in concrete depends on the cement content and water/cement ratio. Higher cement content and higher water/cement ratio in concrete lead to higher potential of drying shrinkage. On the other hand, the potential of drying shrinkage is restrained by the solid framework formed by aggregates (gravel and sand) inside of concrete. With the same shrinkage potential generated by the cement paste, the actual shrinkage depends on the stiffness of the aggregates. The higher the stiffness of aggregate framework, the lower the actual drying shrinkage of the concrete is. In the phase two of the present study, the cement content and water/cement ratio were fixed, and thus the difference in the measured drying shrinkage came from the difference in the stiffness of the solid framework of aggregate. With 20% PCM replacement of fine sand, the stiffness of the aggregate framework is lower than that of the concrete with 10% replacement. Therefore, the shrinkage of PCM-modified concrete with 20% PCM replacement is higher.

Using the present test data, an empirical formula was developed for characterizing the drying shrinkage of PCM-modified concrete:

$$\epsilon_{sh} = 0.02lnt + (\frac{PCM}{100}) \times \frac{w}{c}^{(\frac{20}{PCM}+2)} \tag{3.5}$$

where w/c is the water/cement ratio, t is the time in days, PCM is the volume percentage of PCM replacement of fine aggregate in the concrete, which in this study is either 10 or 20. In the equation, the first term is the time dependent drying shrinkage, which represents the drying shrinkage of regular concrete; and the second term is not time dependent, which represents the additional shrinkage due to the addition of PCM.

In addition to the effect of PCM on the stiffness of solid framework of aggregate, there is another factor that may contribute to the higher shrinkage of PCM-modified concrete. As shown in Table 5.6, MPCM-28 wet cake contains 30% moisture and thus more PCM in the concrete mixture will bring in more moisture in the mixture. As a result more shrinkage strain will be observed in specimens with higher volume percentage of PCM. However, using the MPCM-28D which is another product of the Microtek [29] might be a good option for the future work. Because this product has the same melting point as the MPCM-28 wet cake, but it comes in 100% dry form, which might be a better choice for the dry shrinkage problem.

3.5.3 Thermal properties

Thermal behavior of the PCM-modified concrete shows interesting results. To understand these results better, the DSC analysis was performed on MPCM-28 wet cake alone. However, it is quite important to know that this specific PCM has 30% water content on the exterior of the capsules, therefore, before running the DSC analysis on any amount of mass, the water content should be eliminated from the particles, otherwise the DSC graph would not provide the accurate result and the joule per gram at the PCM's phase change temperature will be reduced due to the water weight. Figure 3.9 shows the specific heat of the MPCM-28 under different temperature.

It should be noted that the melting is a first order transition, which means when you reach

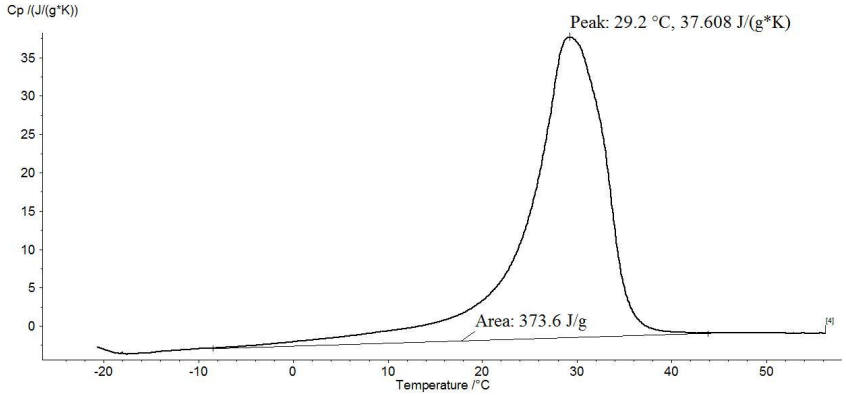

Figure 3.9: The specific heat of the MPCM-28 wet cake.

the melting temperature, the polymer's temperature will not rise until all the crystals have melted. Therefore, the heater under the sample crucible needs to insert a lot of heat into the polymer in order to melt the crystals and keep the temperature rising at the same rate as that of the reference crucible. This extra amount of the heat flow during the melting process appears as a big peak on the DSC analysis. Additionally, the latent heat of melting can be measured by measuring the area under the peak. The peak usually refers to the melting temperature and that is mainly because of putting a lot of energy to the polymer to make it melt. It should also be noted that the melting is an endothermic transition. Since the specific heat is calculated based on the ratio method, the peak observed on the DSC curve and *cp* curve are happening at the same temperature which is the melting temperature. Therefore, from Figure 3.9, it can easily be seen that the melting point is happening at 29.2 °C. This number is slightly different than the melting point of MPCM-28 wet cake and that is because the PCM particles contain 30% water and even though they have been dried out before DSC analysis, still some low percentage of water content remained on the exterior of the PCMs. Additionally, one can also observe the amount of the energy needed for the melting process is about 374 J/g which is the area beneath the c_p curve in the endothermic cycle.

Moreover, looking at Figure 3.10 shows that peak in the endothermic cycle is happening around 29.2 °C which is the same as the peak observed in Figure 3.9. However, the onset is at 23.2 °C, which is the temperature, in which the melting starts to happen. The other peak observed in

the exothermic cycle is 14.9 °C, in which is the solidification happens. The onset in this cycle is 23.9 °C, which is the temperature, in which the solidification starts to happen.

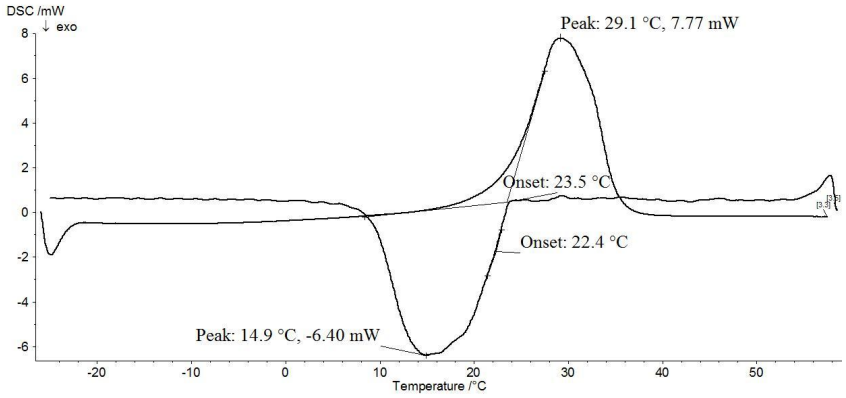

Figure 3.10: Differential Scanning Calorimetry of Phase change material.

Figure 3.11 shows the specific heat capacity of different PCM-modified concrete specimens at different ages. The peaks in specific heat curves for PCM-modified concretes are all in the range of the melting point of the MPCM-28. However, as it was mentioned in the DSC analysis of the MPCM-28 itself, the water content causes the difference between the peak point and the actual melting point of the MPCM-28 and since the PCM particles have been used in the mix without any drying process in advance, these peaks are not exactly at 28 °C (melting point of PCM). Also only 10% to 20% of fine sand was replaced by PCM in the concrete, and thus the actual amounts of PCM in the concretes are quite small. One important observation of Figure 3.11 is that increasing the amount of PCM will increase the specific heat capacity of the concrete. This increase is about 19% when PCM replacement changed from 10% to 20%. Another observation is that the older the specimens are, the higher the specific heat capacity is. In another word, aging is a significant factor in increasing the specific heat capacity of the concrete. For instance, in the case of PCM10-R, the specific heat has been increase by 24% from 7 days of age to 28 days of age.

As it was mentioned earlier, the thermal diffusivity was measured using Netzsch LFA 457 and the results for each sample in the room temperature is provided in Table 3.6. These data shows that the thermal diffusivity decreases with increasing the amount of PCM, while the aging

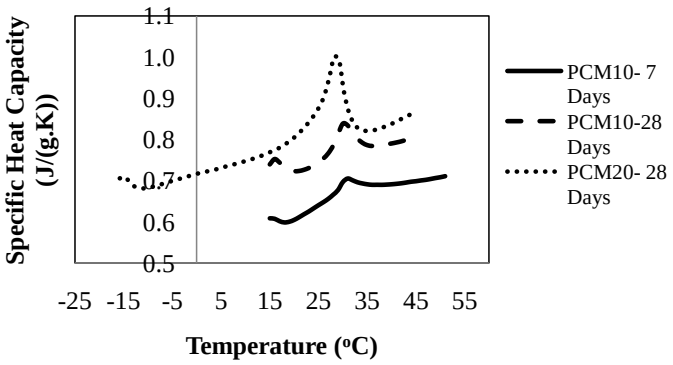

Figure 3.11: The specific heats of PCM-modified concretes with different amount of PCM at different ages.

has a opposite effect on the thermal diffusivity, meaning the older the specimens are, their thermal diffusivity is higher.

The specific heat, thermal diffusivity, density and Equation 5.3, would assist to determine the thermal conductivity of each PCM sample. Figure 3.12 shows the result of thermal conductivity of different PCM-modified concretes. This figure illustrates that increasing the amount of PCM in the mix would result in a lower thermal conductivity but the older the specimens are the higher the thermal conductivity value is; which is similar to the result of the heat capacity. Adding more PCM in the concrete results in higher specific heat and thus lower thermal conductivity, which are beneficial effects for improving thermal insulation property of building envelopes. Hunger [32] also concluded similar results in his work.

Table 3.6: Thermal diffusivity of PCM-modified concrete

Sample	**Age (Day)**	**Thermal diffusivity** (m^2/s)	**Density (gr/cc)**
PCM10	7	0.89	2.55
PCM10	28	1.14	2.28
PCM20	28	0.96	2.18

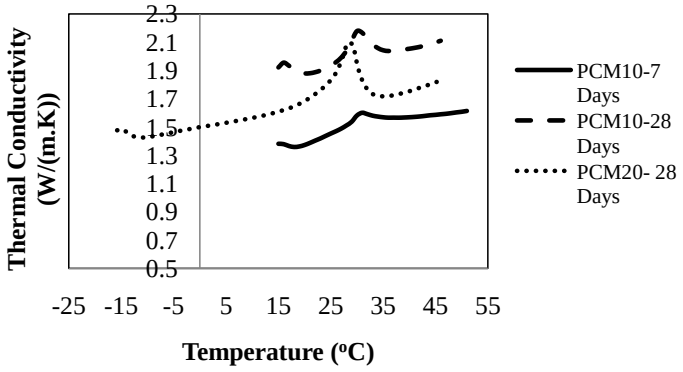

Figure 3.12: Thermal conductivity of PCM-modified concretes with different amount of PCM at different ages.

In general, materials with high thermal diffusivity rapidly adjust their temperature to that of their surroundings, and that is due to the fact that they can conduct heat quickly in comparison to their volumetric heat capacity [21]. Therefore, materials with low thermal diffusivity like PCMs are more desirable in the building envelopes.

3.5.4 Microstructure of PCM-modified concrete

Figure 3.13 and Figure 3.14 show the micrographs of the PCM micro-capsules within the concrete taken by a Scanning Electron Microscope (SEM). Several PCM particles are distributed throughout the mixture. These SEM images provide a good understanding of the bonding between cement paste and the PCM's outer layer, which is quite strong to ensure a high compressive strength of the PCM-modified concrete.

Figure 3.13: SEM micrographs of the PCM-modified concrete.

Some researchers showed that the PCM particles were destroyed or partially destroyed in the mixing process [32], it is quite clear that the PCM particles remained intact in the present study. There are two important experiences we had during the study for preventing the damage of PCM particles. One is to add the PCM particles in the concrete mixture in the very last step during the mixing process, and the other is to use a proper type of PCM with a strong outer polymer shell that can survive the mixing process. As it was mentioned before, adding the PCM at the end of

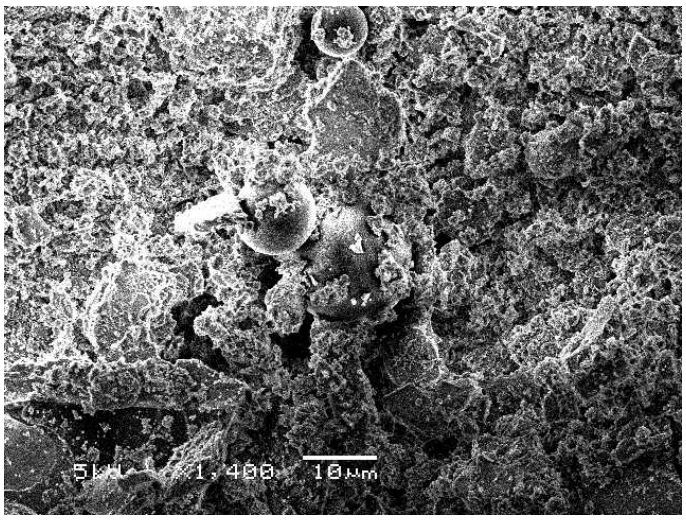

Figure 3.14: SEM image showing the bond between PCM's outer layer and the cement paste.

the mixing process would prevent the damage in the outer shell due to the high shear associated with the mixing process.

3.6 Conclusions

(1) With the addition of encapsulated PCM particles in concrete the compressive strength of the concrete decreases. The present test results showed that using PCM particles to replace fine aggregate particles in concrete mixes (called replacement method) resulted in a less strength reduction than using PCM as additive in the concrete (called additive method). The strength reduction is not too dramatic and there are many structural applications for the PCM-modified concrete.

(2) The flexural test results showed that there is a deduction in the flexural strength with increasing volume percentage of PCM, and that the flexural strength of PCM-modified concrete is in the range of 20% of the compressive strength, which is similar to flexural strength of regular concrete.

(3) Drying shrinkage test results showed that with increasing amount of PCM the drying shrinkage of the PCM-modified concrete increases, which is due to the low stiffness of the PCM particles

that reduces the overall stiffness of the aggregate framework in the concrete. Based on the shrinkage test data, an empirical equation was developed to predict the shrinkage of the PCM-modified concrete in terms of water-to-cement ratio and the PCM content.

(4) Differential Scanning Calorimetry (DSC) analysis of MPCM-28 wet cake was performed under the cooling and heating process for the temperature range of -25 °C to 55 °C in the nitrogen atmosphere. The results show how the PCM starts absorbing the heat at 29.2 °C and releasing the heat till it reaches it's solidification point of 14.9 °C.

(5) Thermal analysis results of the PCM-modified concrete showed that the phase change material can improve the thermal conductivity of the PCM-modified concrete. Any increase in the amount of the PCM in the concrete mixture would increase the heat capacity of the PCM-modified concrete, decrease the thermal diffusivity of the concrete, and thus decrease the thermal conductivity. Since the change in thermal diffusivity at different temperatures is not as significant as the change in the heat capacity, it can be said that using more PCM in the concrete mixture would provide a better material for the building in terms of thermal insulation.

(6) Test results of Scanning Electron Microscope (SEM) analysis showed that when the encapsulated PCM particles are added as the last component in the mixing process, there is almost no damage to the PCM outer layer, and there is a decent bonding between cement paste and the PCM particles.

Chapter 4

COMPOSITE MODELS FOR EFFECTIVE THERMAL CONDUCTIVITY AND DRYING SHRINKAGE OF PCM-CONCRETE

This chapter presents the results of generalized self consistent model for effective thermal conductivity and drying shrinkage of PCM-concrete. Two multi-phase, multi-scale models have been developed to predict the effective thermal conductivity and effective drying shrinkage.
The effect of temperature as well as the effect of volume fraction of the PCM on the effective thermal conductivity has been investigated. The effective drying shrinkage of PCM-concrete and its relation with the bulk modulus of PCM has also been investigated. The generalized self consistent model cannot capture the effective properties of PCM-concrete and needs to be modified.
The results of the modified generalized self consistent model for the effective thermal conductivity and drying shrinkage are promising. The modified generalized self consistent model illustrates that any addition in the PCM amount would decrease the effective thermal conductivity. The generalized self consistent model for effective drying shrinkage reveals that the use of stiffer PCM particles in the mix design would lead to higher shrinkage strain and this effect would be even more significant by increasing the amount of the PCM particles in the mix design.

4.1 Introduction

Composite materials have received considerable attention from the engineering society due to their remarkable engineering applications and this trend is likely to continue. Composite materials are engineered materials made of two or more constituent materials with significantly different

physical or chemical properties which remain separate and distinct on a macroscopic level within the finished structure. Multi-phase composite materials exhibit a remarkable complex microstructure. In the case of spherical inclusions, there exists various methods predicting the effective behavior of the composite material, including: Maxwell approximation, Self-consistent approximation (SC), Mori-Takana, Parallel model, etc. In some of the cases it is easy to obtain the exact solutions for the effective moduli, but in other cases it is not possible. However, in these cases, it is possible to obtain the bounds on the effective moduli, which is helpful in understanding the materials behavior.

Although, there are some critiques regarding the SC approximation which will generally violate bounds improved by the Hashin-Shtrikman bounds, it cannot be said that SC approximations are useless [73].

Milton [52] has shown that for some particular class of micro-structures the SC approximations for thermal conductivity reveals an accurate prediction. More explicitly, for a two-phase composite, this class consists of granular aggregates such that the spherical grains in each of the phase are comparable sizes and they are well separated on many length scales. At any particular length scale, the spherical grains of two phases are surrounded by a matrix consisting of much smaller well separated spheres of the two phases, which are also surrounded by a matrix.

One of the important properties of heterogeneous material is their effective thermal property such as thermal conductivity and drying shrinkage. Theoretical studies have shown that the effective thermal conductivity of composites is strongly dependent on the volume fraction, inclusion size and thermal conductivity of each of the constituents [16] and [57].

The generalized self consistent (GSC) method seems to be one of the most appropriate tools for homogenization unit cell inclusion that is an inclusion with surrounding ring matrix, which is itself embedded in the infinite effective medium.

This chapter focuses on the mathematical modeling of effective thermal conductivity and effective drying shrinkage of PCM-concrete. In the thermal conductivity model, thermal conductivity of aggregate, sand, cement paste and PCM particles as well as their volume fractions are taken into consideration. The effects of change in the volume fraction of PCM particles as well as tempera-

ture change on the effective thermal conductivity have been investigated. The predicted effective thermal conductivity based on the model was compared with the effective thermal conductivities of other model as well as experimental data.

In the drying shrinkage model, the PCM-concrete is treated as a four-phase composite. These four phases are: coarse aggregate, sand, cement paste and PCM particles. In order to predict the effective drying shrinkage, the drying shrinkage of each phase and PCM particles as well as their volume fractions are taken into consideration. The predicted effective drying shrinkage of the model was compared with experimental data.

4.2 Significance of the research

Energy efficiency of buildings is an important consideration. Improving thermal performance of structural components would have a significant effect on the overall performance of the building. Although, the experimental study would be helpful to estimate the effective thermal conductivity of each component, it is not always an easy approach. Additionally, the long term performance of each component such as drying shrinkage is a time consuming process. Thus, an analytical approach would be helpful to understand the effective property of a multi-phase composite such as the effective thermal conductivity and the effective drying shrinkage.

4.3 Effective thermal conductivity of multi-phase composite

4.3.1 Parallel model

The Parallel model for a composite consists of M phases with defined volume fractions can be specified as:

$$\sigma_e = \sum_{i=1}^{M} \phi_i \sigma_i \tag{4.1}$$

It should be noted that in the Parallel model, it is assumed that the layer of the components of physical structures are oriented in a parallel to the direction of heat flow. In addition, the Parallel model gives the maximum value of the thermal conductivity. Therefore, the Parallel model can be

Figure 4.1: Parallel model.

used for the upper bound limit.

4.3.2 Series model

The Series model for a composite consists of M phases with defined volume fractions can be specified as:

$$\frac{1}{\sigma_e} = \sum_{i=1}^{M} \frac{\phi_i}{\sigma_i} \tag{4.2}$$

It should be noted that in the Series model, it is assumed that the layer of the components of physical structures are oriented perpendicular to the direction of heat flow. In addition, the Series model gives the minimum values of the thermal conductivity. Therefore, Series model can be used for the lower bound limit.

4.3.3 Maxwell model

The Maxwell equation for generalized suspensions with matrix with thermal conductivity σ_1, *M-1* different types of spheres ($M \succeq 2$) with volume fractions $\phi_2, \phi_3, ..., \phi_M$ and thermal conduc-

Figure 4.2: Series model.

tivities $\sigma_2, \sigma_3, ..., \sigma_M$ can be defined as [73]:

$$\frac{\sigma_e - \sigma_1}{\sigma_e + (d-1)\sigma_1} = \sum_{i=1}^{M} \phi_i [\frac{\sigma_i - \sigma_1}{\sigma_i + (d-1)\sigma_1}] \tag{4.3}$$

4.3.4 Generalized self-consistent model

The generalized self consistent model (GSC) originally was developed by Christensen for the elastic property [12]. In this model, the existence of a characteristic dimension of the inhomogeneity as well as the existence of the scale properties averaging has been assumed. In addition, it has been assumed that the scale of the inhomogeneity in the order of magnitude is smaller than the characteristic dimension of the problem of interest. Considering this assumption would let a heterogeneous composite material be divided into many regions or elements that the volume fraction of each phase within each element is constant. Figure 4.3 shows this partitioning of a multi-phase composite into different elements.

This figure can be even more simplified by assuming spherical phases with a defined radius. Figure 4.4 shows the simplified partitioning of a multi-phase composite.

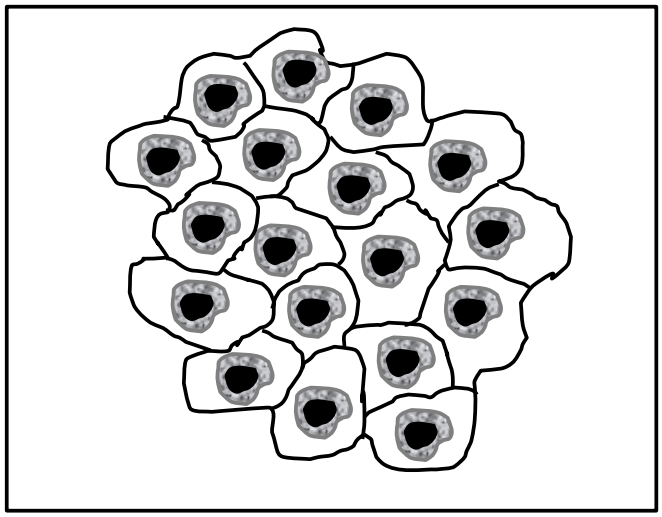

Figure 4.3: Partitioning multi-phase composite into different elements.

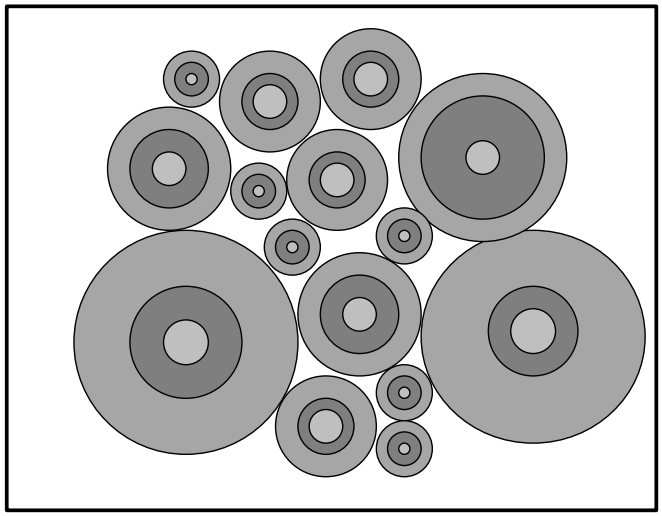

Figure 4.4: Partitioning multi-phase composite using spherical elements.

As it can be seen in Figure 4.4, the basic elements of the microstructure are spherical elements composed of different phases. As it was mentioned earlier, it is assumed that the volume fractions of all the elements are the same, thus the radius ratios of each of the phases within different element remains the same as well. The Christensen model is based on a two-phase composite; however most of the composites are multi-phase composites. Following the basic idea of a two-phase composite, the model can be further extended to a multi-phase composite model. A schematic figure of a four-phase composite has been shown in Figure 4.5. Based on the Christensen model, the effective

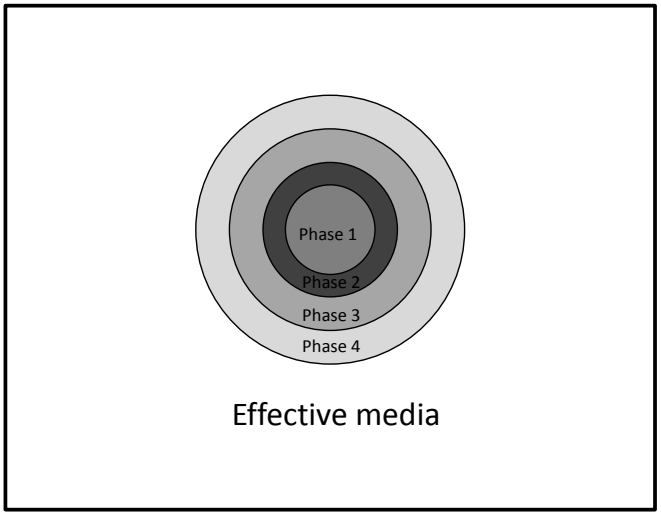

Figure 4.5: Schematic of a four-phase composite.

thermal conductivity of a two phase composite is:

$$k_{eff} = k_m[1 + \frac{c}{\frac{1-c}{3} + \frac{k_m}{k_i - k_m}}] \tag{4.4}$$

where k_m is the thermal conductivity of the matrix, k_i is the thermal conductivity of the inclusion and c is the volume fraction of the inclusion $= (a/b)^3$.

Figure 4.6 illustrated the basic generalization of the two-phase to five-phase model, which can also be extended to the n-phase model as well. Since the continuity conditions have been used in the derivation of the above equation, and c is only dependent on the size of the spheres, each of the two neighboring phases can be combined and their effective property can be calculated to be

considered in order to get the effective property of the whole composite. Generalizing this equation

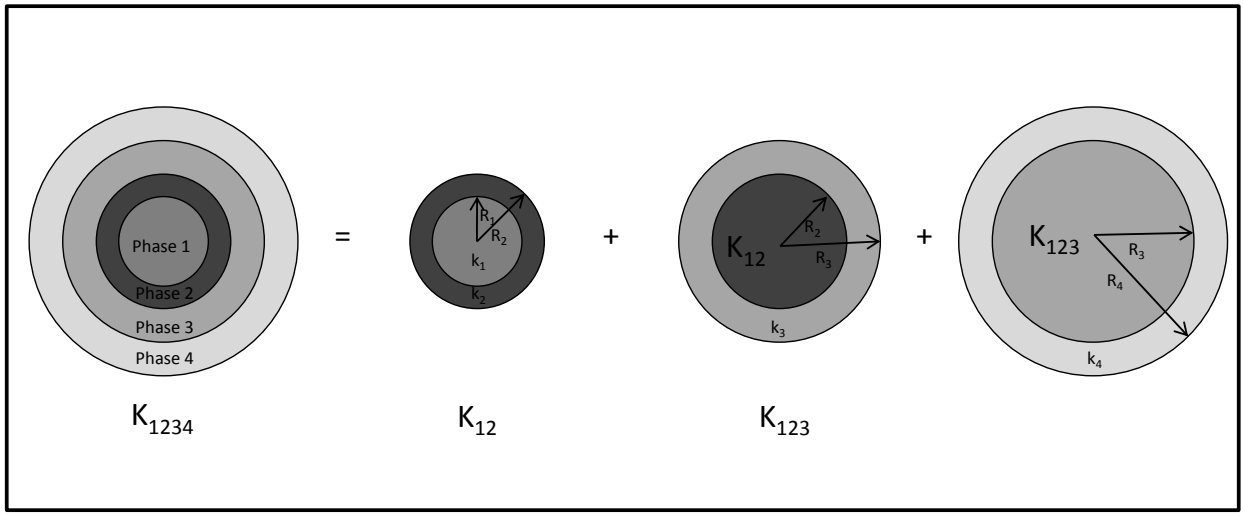

Figure 4.6: Generalization of two-phase model to four-phase model.

to a four-phase composite would be as follows:

$$k_{12} = k_2[1 + \frac{c_{12}}{\frac{1-c_{12}}{3} + \frac{k_2}{k_1 - k_2}}] \tag{4.5}$$

$$k_{123} = k_3[1 + \frac{c_{123}}{\frac{1-c_{123}}{3} + \frac{k_3}{k_{12} - k_3}}] \tag{4.6}$$

$$k_{1234} = k_4[1 + \frac{c_{1234}}{\frac{1-c_{1234}}{3} + \frac{k_4}{k_{123} - k_4}}] \tag{4.7}$$

where the k terms are the thermal conductivity of each of the phases. Although the c terms are not the volume fraction of each phase, they can easily be linked to the volume fractions of the phases as:

$$c_{12} = \frac{R_1^3}{R_2^3} = \frac{\phi_1}{\phi_1 + \phi_3} \tag{4.8}$$

$$c_{123} = \frac{R_2^3}{R_3^3} = \frac{\phi_1 + \phi_2}{\phi_1 + \phi_3 + \phi_3} \tag{4.9}$$

$$c_{1234} = \frac{R_2^3}{R_3^3} = \frac{\phi_1 + \phi_2 + \phi_3}{\phi_1 + \phi_3 + \phi_3 + \phi_4} = \phi_1 + \phi_2 + \phi_3 + \phi_4 \tag{4.10}$$

The effective thermal conductivity of n-phase composite can be determined as:

$$k_{eff,i} = k_i[1 + \frac{c_i}{\frac{1-c_i}{3} + \frac{k_i}{k_{eff,i-1} - k_i}}] \tag{4.11}$$

where:

$$c_i = \begin{cases} \frac{\sum_{i=1}^{i} \phi_i}{\sum_{i=1}^{i+1} \phi_i} & \text{if} \quad i \neq n \\ 1 - \phi_i & \text{if} \quad i = n \end{cases} \tag{4.12}$$

4.4 Effective shrinkage of multi-phase composite

Following a similar approach adopted in the effective thermal conductivity of multi-phase composite would lead to an equation for effective dry shrinkage of multi-phase composite [80].

$$\epsilon_{eff,i}^{sh} = \frac{k_{eff,i}\epsilon_{eff,i-1}^{sh} c_i(3k_i + 4G_i) + k_i\epsilon_i^{sh}(1 - c_i)(4G_i + 3k_{eff,i-1})}{k_i(3k_{eff,i-1} + 4G_i) - 4c_iG_i(k_i - k_{eff,i-1})} \tag{4.13}$$

where K and G are the bulk modulus and shear modulus respectively, and c can be defined as follows:

$$c_i = \begin{cases} \frac{\sum_{i=1}^{i} \phi_i}{\sum_{i=1}^{i+1} \phi_i} & \text{if} \quad i \neq n \\ 1 - \phi_i & \text{if} \quad i = n \end{cases} \tag{4.14}$$

4.5 Application of effective thermal conductivity of multi-phase composite

PCM-concrete is a good example of multi-phase composite. Therefore the effective thermal conductivity of the PCM-concrete can be calculated based on the above equation. Christensen model is based on the same size particle distribution but in PCM-concrete each of these phases has different length scale, which requires multi-scale analysis in addition to multi-phase analysis. Therefore, PCM-concrete can be considered as a four-phase composite: phase 1 is the coarse aggregate, phase 2 is the sand, phase 3 is the PCM particles, and phase 4 is the cement paste. Knowing the thermal conductivity of each of the phases as well as the volume fraction of the phases would assist in obtaining the effective thermal conductivity of the PCM-concrete.

In the preliminary study of the PCM-concrete done by Meshgin et al. [49], experimental data on thermal conductivities of two different PCM-concretes called PCM10-R and PCM20-R were obtained. PCM10-R and PCM20-R are referred to 10% and 20% sand volume replacement by

PCM particles. MPCM-28 wet cake which is a product of Microtek [29] has been used in this study. The data obtained from these two groups will be used in this study as verification of the present GSM model.

It should be noted that in the GSM model, it was assumed that the temperature effect on thermal conductivity of all the phases except PCM is not significant. Moreover, thermal conductivity of MPCM-28 wet cake has been calculated based on the specific heat. Specific heat of MPCM-28 wet cake has been obtained by Differential Scanning Calorimetry (DSC) using the Netzsch DSC 204 F1 Phoenix machine at a scanning rate of 10 °C/min (50 °F/min) in the temperature range of -25 °C (-13 °F) to 55 °C (131 °F) in a nitrogen atmosphere. Figure 4.7 shows the thermal conductivity of MPCM-28 wet cake under various temperatures.

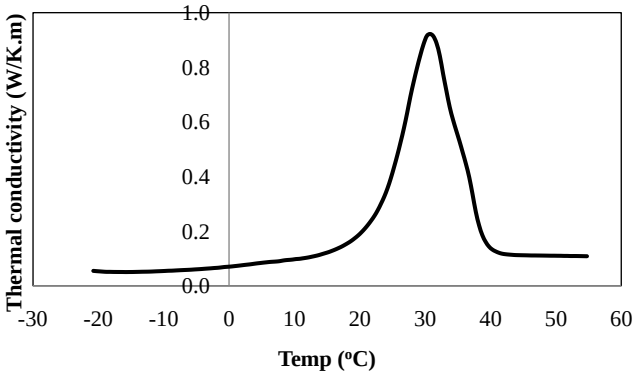

Figure 4.7: Thermal conductivity of MPCM-28 wet cake.

Figure 4.8 shows the multi-scale model of the PCM-concrete. As one can see from this figure, the PCM-concrete has four phases with different particle sizes. In the largest scale, PCM-concrete can be considered as a two phase composite considering coarse aggregates as inclusion and the rest of the phases as matrix surrounding the inclusion. However, the matrix can be modeled as another two phase composite considering the largest size particle as the inclusion and the rest as the matrix. This process can be continued until the smallest size particle being modeled as the inclusion and only one phase left as a surrounding matrix.

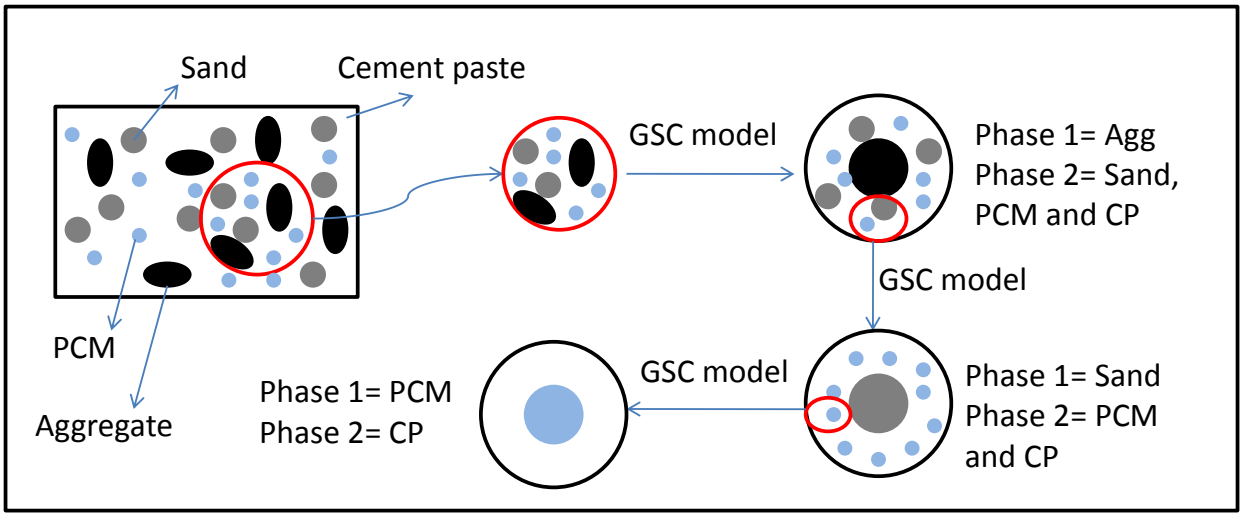

Figure 4.8: Multi-scale modeling of PCM-concrete.

4.6 Application of effective shrinkage of multi-phase composite

The effective shrinkage of the PCM-concrete can be calculated based on effective shrinkage equation. As it was mentioned earlier, PCM-concrete is a four-phase composite. Considering the first three phases and assuming that the aggregates and sand do not shrink, thus the cement paste is the only phase out of these three phases which would participate in the shrinkage of the PCM-concrete.

Following similar approach for each two phases in each scale would lead to the effective thermal conductivity. These steps can be written as:

$$\epsilon^{sh}_{eff,12} = 0 \tag{4.15}$$

$$\epsilon^{sh}_{eff,123} = \frac{k_3\epsilon^{sh}_3(1-c_3)(4G_3+3k_{eff,12})}{k_3(3k_{eff,12}+4G_3)-4c_3G_3(k_3-k_{eff,12})} \tag{4.16}$$

$$\epsilon^{sh}_{eff,123} = \frac{k_{eff,123}\epsilon^{sh}_{eff,123}c_4(3k_4+4G_4)+k_4\epsilon^{sh}_4(1-c_4)(4G_4+3k_{eff,123})}{k_4(3k_{eff,123}+4G_4)-4c_4G_4(k_4-k_{eff,123})} \tag{4.17}$$

Therefore, by knowing the shrinkage of the cement paste and PCM particles as well as the volume fraction of the phases, the effective shrinkage of the PCM-concrete can be achieved. In the preliminary study conducted by Meshgin et al. [49], it was shown that the shrinkage of normal concrete

can be calculated based on:

$$\epsilon^{sh}_{eff,123} = \epsilon_{con} = 0.02 \ln t \tag{4.18}$$

Thus the shrinkage of the cement paste can be calculated based on the backward calculation. Moreover, obtaining the bulk modulus and shear modulus of each of the phases would lead to the effective shrinkage of the whole composite. These parameters can be calculated based on the data available in the literature. For instance, knowing the Poisson's ratio of the PCM particles would assist to determine the value for $\frac{G_2}{k_2}$, which is equal to $\frac{3(1-2\nu)}{2(1+\nu)}$.

4.7 Results and discussions

Based on the previous study conducted by Meshgin et al. [49], the experimental data on thermal conductivity as well as drying shrinkage for the two groups of PCM-concrete called PCM10-R and PCM20-R is available. As it has been explained in the details on the reference, PCM10-R and PCM20-R have 10 and 20 percent sand volume replacement by PCM particles.

Figure 4.9 and Figure 4.10 show the results for the effective thermal conductivity of different methods under different temperatures for PCM10-R and PCM20-R, respectively. As one can see from these figures, the GSC model cannot predict the effective thermal conductivity of the PCM-concrete accurately. This is due to the limitation of GSC model. The GSC model can account only for simple microstructure information, such as volume fraction and inclusion shape. Additionally, all the inclusions and the matrix phase should have thermal conductivity within the same range. In case of the inclusions with higher thermal conductivity than the matrix phase, the relation coincides with the lower bound and vice versa. In this specific case, since the PCM has much lower thermal conductivity than the surrounding matrix, the effective thermal conductivity of PCM-concrete has a tendency to reach the upper bound (Parallel model). Thus, this model should be either modified or replaced by another model which can capture more complex microstructures.

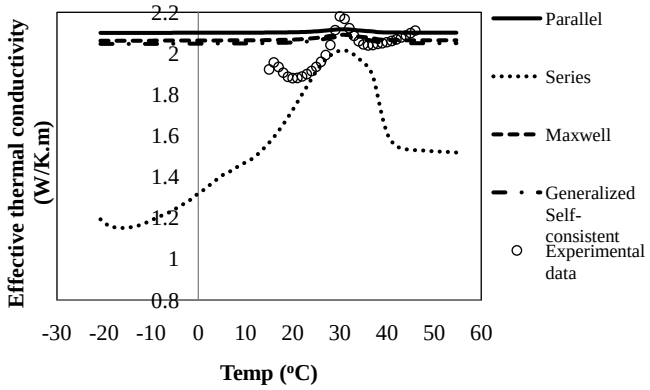

Figure 4.9: Effective thermal conductivity of PCM10R based on GSC model.

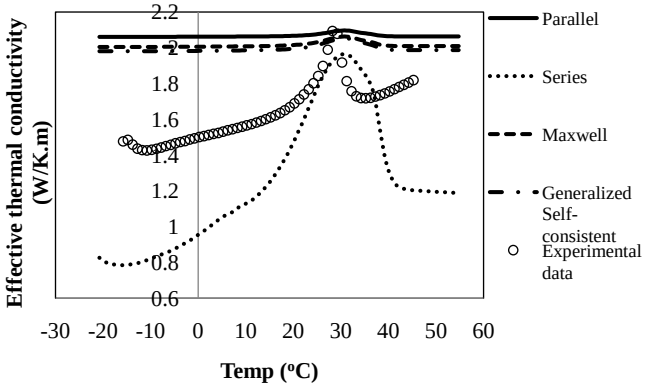

Figure 4.10: Effective thermal conductivity of PCM20R based on GSC model.

Since the focus of this study is the application of the GSC model, the authors decided to modify this model by considering the PCM particles as a thin ring surrounding the cement paste, to be able to compensate for their low thermal conductivity in compared to aggregate and cement paste.

Figure 4.11 and Figure 4.12 show the results based on the modified GSC model. As one can see, the model can capture the effective thermal conductivity of PCM-concrete more accurately than original GSC model. Additionally, the effective thermal conductivity of both PCM10-R and PCM20-R based on the modified GSC model falls between the upper and lower bound limits obtained from the Parallel and Series models. It should be noted that the peak observed in both PCM10-R and PCM20-R is due to the effect of the PCM particles. Moreover, these peaks are referring to the melting point of the PCM particles, which is around 28 °C for these specific PCM particles.

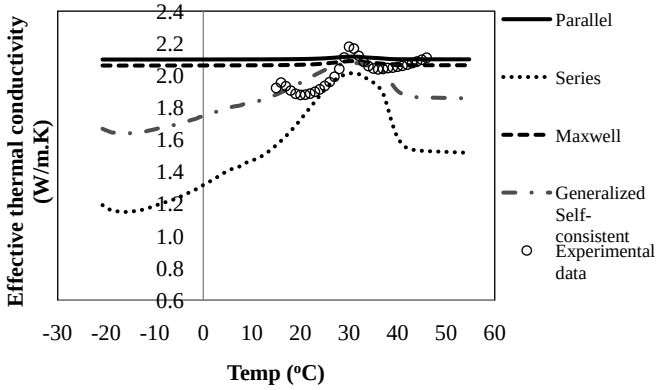

Figure 4.11: Effective thermal conductivity of PCM10R based on modified GSC model.

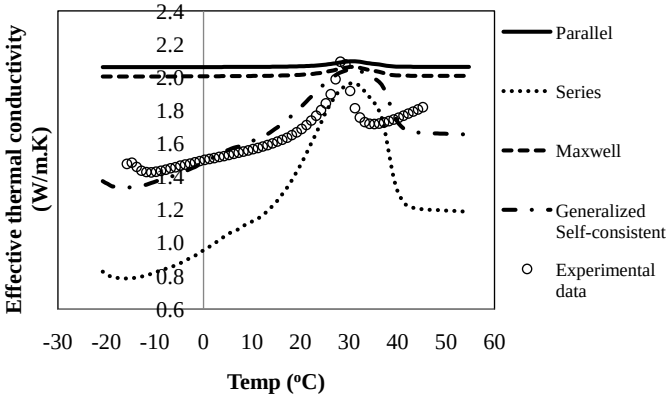

Figure 4.12: Effective thermal conductivity of PCM20R based on modified GSC model.

The comparison of Figure4.11 and Figure 4.12 reveals that adding the amount of the PCM in the mix design would lead to lower thermal conductivity, which is beneficial in terms of energy saving.

Figure 4.13 shows how the volume fraction of the PCM would affect the effective thermal conductivity of PCM-concrete. As was expected, increasing the amount of the PCM would decrease the effective thermal conductivity of the PCM-concrete and this is due to the fact that the PCM particles have a low thermal conductivity.

It should be noted that since the amount of the PCM has been calculated based on the percentage of the sand volume, the maximum volume fraction of the PCM in our specific mix design is 0.209. Moreover, since the thermal conductivity of the PCM changes under different temperature, this specific graph shows the change in the effective thermal conductivity only under room temperature (20°C).

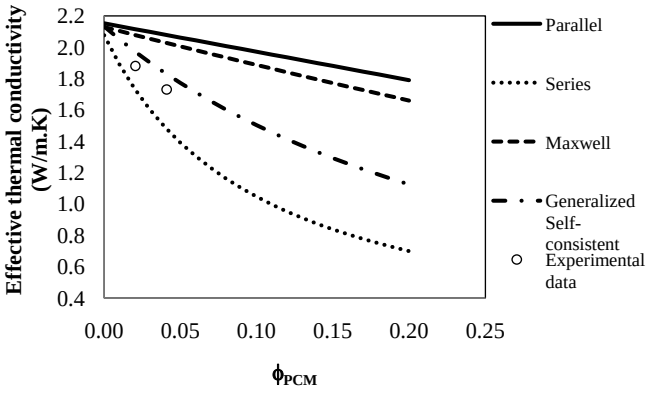

Figure 4.13: The effect of PCM volume fraction on the effective thermal conductivity.

Since only two different volume fractions data are available, the experimental data is limited in this case. Additionally, there is slightly difference between this data and the predicted value from the model. This is due to the fact that this data is not at the exact temperature as the model. Figure 4.14 and Figure 4.15 shows the effective shrinkage of PCM-10R and PCM-20R. The modified GSC model for the effective drying shrinkage as well as the analytical model obtained in the previous study conducted by Meshgin et al. [49] correlate well with the experimental data.

As it can also be seen from these figures, both models are within the upper and lower bounds obtained from the Parallel and Series models, respectively.

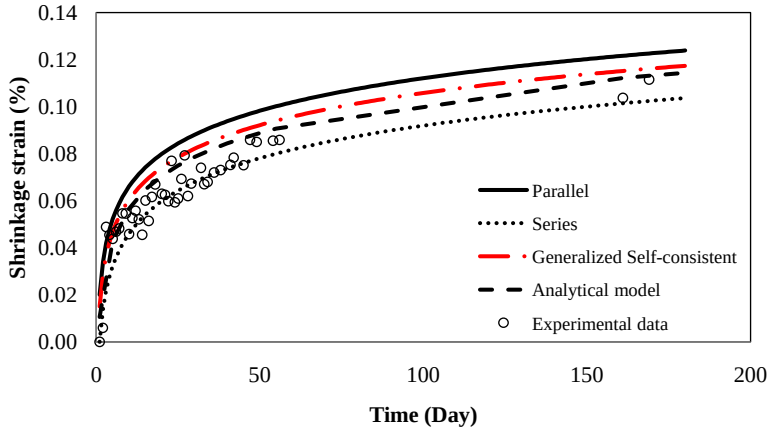

Figure 4.14: Effective shrinkage of PCM-10R based on GSC model.

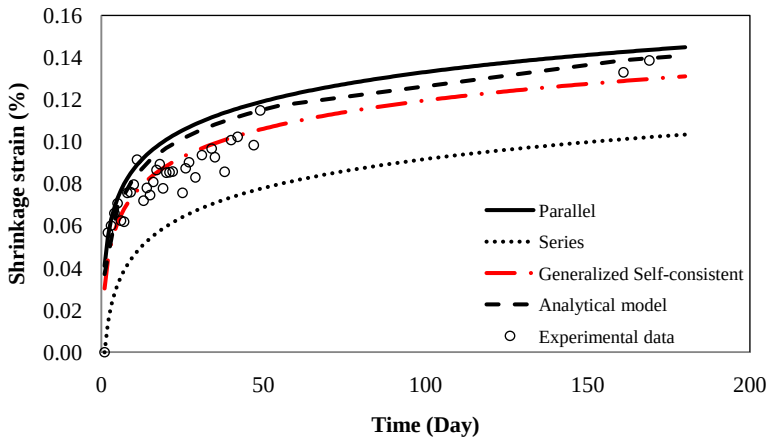

Figure 4.15: Effective shrinkage of PCM-20R based on GSC model.

Additionally, Figure 4.16 and Figure 4.17 show how the change in the ratio of the bulk modulus of PCM to the bulk modulus of the concrete affects the effective shrinkage of PCM-concrete. In other words, using stiffer PCM particles would increase the effective shrinkage of the PCM-concrete and this value would be even higher in the case of using more PCM particles in the mix design.

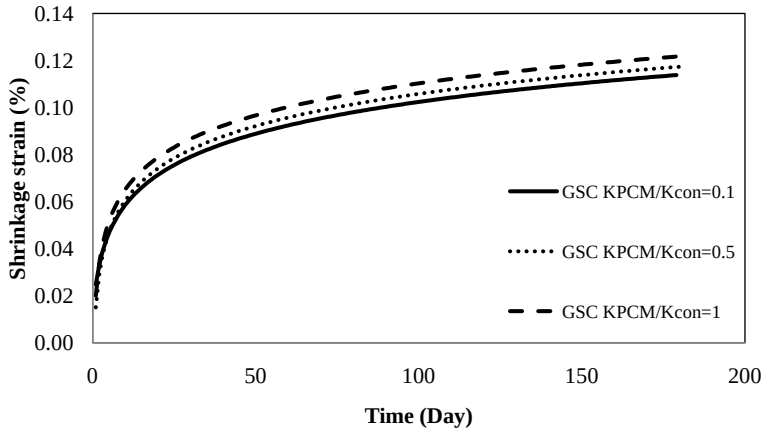

Figure 4.16: Comparison of the change in the bulk modulus ratio of PCM to concrete in PCM10-R.

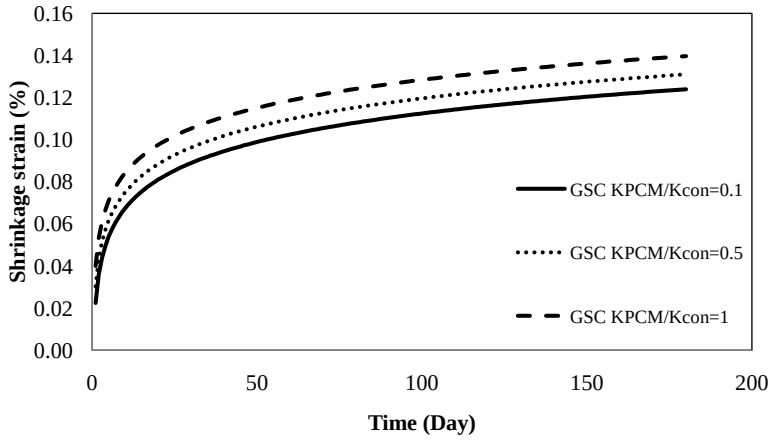

Figure 4.17: Comparison of the change in the bulk modulus ratio of PCM to concrete in PCM20-R.

4.8 Conclusions

In this study, the effective property of PCM-concrete has been investigated. Generalized self consistent (GSC) models were developed to predict the effective thermal conductivity and drying shrinkage of PCM-concrete. The GSC model fails to predict the effective thermal conductivity of the PCM-concrete accurately. This is mainly due to the fact that this model can account only for simple microstructure information, such as volume fraction and inclusion shape. Additionally, all the inclusions and the matrix phase should have thermal conductivity within the same range. Therefore the GSC model was modified by rearrange the spatial distribution of PCM phase in order to capture the effective thermal conductivity more accurately.

The modified GSC model predicts the effective thermal conductivity better than other models. The modified GSC model shows how the effective thermal conductivity decreases by increasing the amount of the PCM in the mix design. It also shows the results for both PCM-10R and PCM-20R are within the upper and lower bound regions.

The modified GSC model for the effective drying shrinkage show promising results. The use of stiffer PCM particles in the mix design leads to higher shrinkage strain and this effect will be even more significant by increasing the amount of the PCM particles in the mix design.

Chapter 5

EXPERIMENTAL STUDY ON RUBBERIZED MORTAR

Phase change materials (PCM) and rubber particles from recycled tires were used in Portland cement mortar with a potential application as insulation mortar. Series of tests were designed and conducted including compressive strength, flexural strength, thermal conductivity, drying shrinkage, and bond strength tests at 7 days and 28 days of age. Different types of additives were also used in the mix designs. The experimental results showed that mechanical properties of rubberized-mortar can be improved by adjusting the size of rubber particles and the amount of additives. With the same volume fraction of PCM and rubbers, the mechanical properties of PCM-modified mortar are either the same or better than that of rubberized-mortar. In terms of thermal properties, the rubber particles can reduce thermal conductivity of the mortar significantly, while the PCM can improve heat capacity of the mortar.

5.1 Introduction

One of the effective methods to improve energy efficiency of buildings is to improve thermal properties of insulation mortar. Insulation mortar is commonly used on the exterior wall of buildings, and it is a cementitious material made of Portland cement, fine aggregate, and various types of additives. An effective way to improve thermal properties of insulation mortar is to use phase change materials and recycled rubber particles such as scrap tires as additives. Phase change materials (PCM) have the ability to absorb and release energy at a certain temperature range, which makes them very effective to block the heat to transmit from exterior to interior of a building in the

summer and thus increase the level of comfort of the building and reduce the cost of air conditioning [23]. In the last few decades, there has been an increase of interest in PCM applications. For instance, Li et al. [45] suggested incorporating a phase change material to make a granular phase change composite as an alternative solution to increase thermal behavior of the composite. Cabeza et al. [9] investigated the inclusion of PCMs in concrete wall in order to save energy. Roth et al. [63] mentioned the use of PCM in building technology. They mentioned the influence of PCM on building varies greatly based on different factors such as building types, climate effect, etc. Zhang et al. [83] investigated the effect of PCM on the heat property of mortar and concluded that the heat latent of the compound PCM material is 1.66 times of the pure phase change material. On mechanical properties of PCM-modified concrete, a study conducted by Meshgin et al. [49] has shown that adding a small amount of PCMs in the concrete does not have significant impact on the mechanical properties of the material.

On the other hand, disposal of waste tires is a major environmental issue for many metropolitan areas in the world. Therefore, how to effectively reutilize scrap tires has become an important research topic in recent years. Large quantities of scrap tires are generated each year globally. These stockpiles are dangerous not only due to potential environmental threat, but also from fire hazards and provide breeding grounds for different type of animals such as rats, mice, etc. Over the years, disposal of tires has become one of the serious problems in environments and land filling is becoming unacceptable due to the rapid depletion of available sites for waste disposal. Therefore, utilization of rubber particles in cementitious materials has received a great attention from the researches and engineers.

Scrap tires can be classified as:

(1) Scrap tires

Scrap tires refers to a whole tire, a slit tire, a shredded or chopped tire, a ground rubber, or a crumb rubber product.

(2) Slit tires

These are produced in tire cutting machines. These machines can slit the tire either into two halves or can separate the sidewalls from the tread of the tires.

(3) Shredded/Chipped tires

These tires involve primary, secondary or both shredding processes.

The size of the tire shreds in the primary process can vary from 300-460 *mm* in length by 100-230 *mm* wide, down to 100-50 *mm* in length, which depends on the manufacturer's shredder model and the condition of the cutting the edges. On the other hand, the tire chips are normally cut from 76 *mm* to 13 *mm* which requires both primary and secondary shredding.

(4) Ground rubber

These rubbers are usually sized as large as 19 *mm* to as small as 0.15 *mm* (No. 100 sieve), which is based on the type of size reduction equipment and intended applications.

(5) Crumb rubber

Crumb rubber consists of particles ranging in size from 4.75 *mm* (No. 4 Sieve) to less than 0.075 *mm* (No. 200 Sieve) [65].

Many researchers investigated the influence of the rubber particles in mortar. For instance, Topcu et al. [76] investigated the flexural and compressive strength of the rubberized-mortar and they showed that both of these values decreased by increasing the amount of the rubber in the mixtures. In another study, Topcu et al. [75] investigated the durability of mortar and concrete including rubber particles in the mix design and they observed that in the regions where the environmental conditions are not harsh, use of rubberized-mortar is quite appropriate, otherwise, cement with higher strength or cement resistant to sulfate should be used. Kang et al. [36] investigated the crack resistance and flexural behavior of cement-based materials by adding rubber particles. Their test results revealed that the rubberized-mortar and concrete specimens exhibit ductile failure and great deformation almost 2-4 times of the normal specimens. Raghavan et al. [60] evaluated the workability and mechanical properties of mortar containing shredded automobile

and truck tyres. They showed, the geometry of the rubber particles influenced the fracture behavior of rubberized-mortar. Also by increasing the amount of the rubber, flexural strength and plastic shrinkage cracking of rubberized-mortar decreased. Li et al. [44] showed that there is certain improvement of strength properties of rubberized-mortar by using redispersible polymer powder. Oikonomou et al. [55] studied the chloride penetration into the rubberized-mortar and they showed an increase in chloride ion penetration resistance.

The main focus of this paper is to study the effects of scrap tires as well as phase change material on both mechanical and thermal properties of insulation mortar. In the practice, some additives are mixed together with PCM and rubber particles in the insulation mortar in order to improve workability and mechanical properties of the mortar. Thus, the effects of some additives including ground calcium, redispersible polymer powder, methyl cellulose, and wood fiber on mechanical and thermal behaviors of the rubberized-mortar and PCM-mortar were also included in this study.

As it has been explained, when rubber particles and PCM are used as additive in insulation mortar, the thermal properties of the mortar will be improved and the mechanical properties of the mortar will either degrade or remain the same depending on the amount of PCM used in the mortar. The technical goal of the present study is to maximize the enhancement in thermal properties and minimize the adverse impact on mechanical properties of the mortar due to the addition of rubber and PCM particles. A systematic experimental study was designed and implemented to quantify the effect of each of the additives in terms of compressive strength, flexural strength, thermal conductivity, drying shrinkage, and bond strength of the mortar. In another word, the basic trends of the effects of rubber and PCM particles on properties of mortar are predictable based on previous research results, but the quantitative analysis and optimization of the mortar mix design parameters have not been done. With optimum design parameters to be obtained in this study, a new insulation mortar will be available which can enhance thermal resistance and capacity of exterior walls of timer and masonry structures to improve energy efficiency of the buildings.

5.2 Materials

There exist various mix designs based on the volume ratio of each component. However, the individual components are normally sold by weight, so the weight ratio can be considered instead of the volume ratio.

The good weight ratio for a mortar can be based on the cement fine aggregate ratio of 1 to 2.5∼3.0. Moreover, since there are some additives which need to be added to the mix design, it is quite important to know their ratios as well. Table 5.1 shows the acceptable range for each of the additives.

Table 5.1: Weigh ratio of the additives in mortar mix design

Rubber	0.1% of the total dry materials
Redispersible Polymer Powder (RPP)	1∼2% of the total dry materials
MC	0.3% of the total dry materials
Wood fiber (WF)	0.1% of the total dry materials
Water	0.22∼0.26% of the total dry materials

Each mix design consists of 630 kg/m^3 fine aggregate (sand); 350 kg/m^3 Type I Portland cement; 200 kg/m^3 water; rubber particles/PCM; ground calcium; Redispersible Polymer Powder; Methyl cellulose and wood fiber. The sieve analysis based on ASTM C136-06 [67] was conducted on the fine aggregate being used in the mortar mixtures. Figure 5.1 shows the particle size distribution of fine aggregate.

5.2.1 Rubber particles

As it has been mentioned earlier, the rubber particles come in different shapes and sizes. Two different sizes of 6 mesh (coarse rubber particle) and 8-10 mesh (fine rubber particle), which are the products of AcuGreen company located at Denver were used in this study. The sieve analysis based on the standard ASTM C136 - 06 [67] was conducted on these two rubber sizes used in this study. Figure 5.2 shows the particle distribution of them.

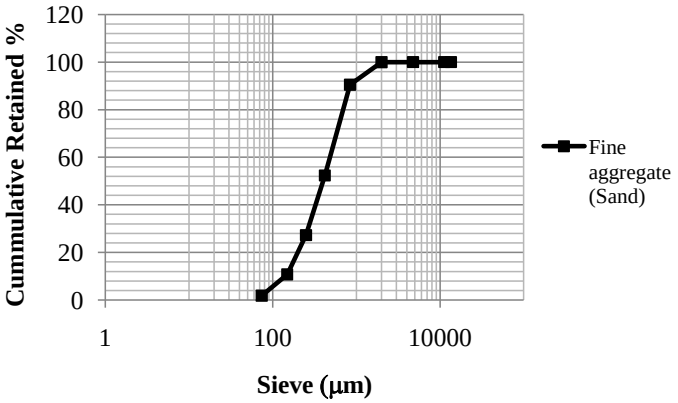

Figure 5.1: Particle size distributions of fine aggregate.

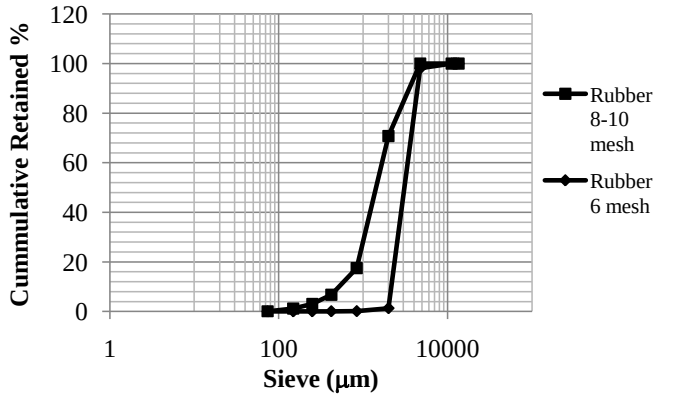

Figure 5.2: Particle size distribution of two size rubber particles.

5.2.2 Ground calcium

Commercially available ground calcium carbonate (GC) is usually used as fillers in cementitious materials and that is due to the fact that the size of the ground calcium particles are smaller than the cement particle size. Therefore, GC particles can fill the spaces between cement particles and provide a more dense internal structure of mortar or concrete.

In this study ground calcium 325 mesh, which is a product of Mineral Technologies [30] was used. Table 5.2 shows the typical properties of this product provided by the manufacturer.

Table 5.2: Properties of ground calcium

Characteristic	**Value**	**Unit**
Median particle size	13.0	Microns
Dry brightness	92	
Bulk density	0.73	grams/cc
Tap density	1.56	grams/cc
Oil absorption	12	
Specific gravity	2.7	

5.2.3 Redispersible polymer powder

Redispersible Polymer Powder (RPP) is easily redispersible in water. There has been extensive investigation on RPP in cementitious materials. RPP can increase the mortar density and adhesive bond strength, reduce water adsorption and improve water resistance. Since it can reduce water demands, it has such an excellent flow and leveling properties. It also has high flexural strength, abrasion resistance, water retention and good workability.

Redispersible Polymer Powder (RPP) used in this research is a product of Dow Chemical Company (DLP210) [27]. Table 5.3 shows the typical properties of this product.

Table 5.3: Physical properties of Redispersible Polymer Powder

Polymer Base	Vinyl acetate ethylene coploymer
Powder	
Appearance	White, free flowing powder
Residual moisture	Maximum 2 %
Bulk Density	0.395-0.545 g/ml
Ash Content	10-14 %
Glass transition temperature (Tg)	Ca. 6°C
Redispersion (ca. 50 % solids)	
Minimum film formation temperature	Ca. 0°C
pH	5.5-7.5

5.2.4 Methyl cellulose

Methyl cellulose (MC) is a chemical compound derived from cellulose. MC is a hydrophilic white powder in a pure form, which dissolves in cold water forming a clear viscous solution. It can be used for variety of purposes such as construction materials. MC has a major application as a performance additive in mortar. It is added to mortar dry mixes to improve the mortar's properties such as workability, open and adjustment time, water retention, viscosity, adhesion to surfaces, etc. [22].

Methyl cellulose (MC) used in this research is a product of Dow Chemical Company (Methocel K15 M) [27]. Table 5.4 shows the typical properties of this product.

Table 5.4: Methyl cellulose

Physical state	**Powder**
Color	White to off-white
Oder	Oder less

5.2.5 Wood fiber

Wood fibres (WF) are usually cellulosic elements that are extracted from trees, straw, bamboo, cotton seed, hemp, sugarcane, etc. The fiber is added to reinforce the cementitious materials in order to prevent them from cracking. Cement-bonded wood fiber is used to manufacture a wide variety of products primarily for the construction industry such as insulated concrete forms and it is mainly known for its use in green building. The material itself is 100% recyclable, and is known for its insulating and acoustic properties.

The wood fiber (TECHNOCEL 1004-7N) used in this research is a product of CFF [26]. Table 5.5 shows the material description provided in the data sheet.

Table 5.5: Properties of wood fiber

Characteristic	**Value**	**Unit**
Appearance	Grey fiber	
Loose density	75-110	g/l
Loss on drying	Max. 9.0	%
pH value	6.0-9.0	

5.2.6 Phase change material

Phase change material (PCM) is a substance with a high heat of fusion which melts and solidifies at certain temperature. Therefore, PCMs are capable of storing and releasing large amounts of energy.

In this study, MPCM-28 wet cake manufactured by Microtek [29] was used. Table 5.6 shows MPCM-28's general properties based on the Microtek data sheet [29].

5.2.7 Mixture design

Tables 5.7 and 5.8 show the mix design using rubber particles and phase change materials in this study. The first group and the second group were designed to observe the size effect of rubber particles on properties of the mortar. The third group was for the effect of rubber content

Table 5.6: General properties of MPCM-28

Typical Properties	
Appearance	White to slightly off-white color
Form	Wet cake (70% Solid, 30% Water)
Capsule Composition	85-90% wt.% PCM 10-15 wt.% Polymer Shell
Core Material	Paraffin
Particle Size (mean)	17-20 micron
Melting Point	28 °C (82°F)
Heat of Fusion	180-195 kJ/kg
Specific Gravity	0.9
Temperature Stability	Extremely Stable-less than 1% leakage when heated to 250°C
Thermal Cycling	Multiple

on mechanical and thermal behavior of the mortar. It should be noted that the rubber content is expressed in term of a percentage of total dry material in each mix design. In this group, the rubber content was increased up to 20% of the total dry material in the mix design. The forth group was for the effect of RPP in the mortar. In Groups 3 and Group 4, the same size of rubber particles as Group 1 (6 mesh) was used. In the last group, Group 5, the rubber particles were totally replaced with PCM, in order to compare the performance of mortar with only rubber particles and only with PCM. Since both rubber and PCM have similar density, their replacements are quite simple in the mix design.

Table 5.7: Mixture design using rubber particles

Group	**Cement (kg/m3)**	**Sand (kg/m3)**	**GC (kg/m3)**	**Rubber (kg/m3)**	**RPP (kg/m3)**	**MC (kg/m3)**	**WF (kg/m3)**	**Water (kg/m3)**
1	428.3	508.3	129.5	184.3 (6 mesh)	25.4	3.73	1.24	320.2
2	428.3	508.3	129.5	184.3 (8-10 mesh)	25.4	3.73	1.24	320.2
3	428.3	363.2	129.5	239.1 (130%)	25.4	3.73	1.24	297.6
4	428.3	508.3	129.5	184.3	32.8	3.73	1.24	322.0

Table 5.8: Mixture design using PCM

Group	**Cement (kg/m3)**	**Sand (kg/m3)**	**GC (kg/m3)**	**PCM (kg/m3)**	**RPP (kg/m3)**	**MC (kg/m3)**	**WF (kg/m3)**	**Water (kg/m3)**
5	428.3	508.3	129.5	184.3	25.4	3.73	1.24	320.2

The mixing process takes place in several steps. First, all dry materials such as cement, sand, rubber particles, RPP, GC, MC and WF were mixed. Second, the water was added gradually to the dry mix. For the last group, PCM was added to the mix at the very last step and this step should take at most one-three minute. It is important to add the PCM as the last component in order to prevent the damage of micro-encapsulates during the mixing process due to the shear forces between the solid particles.

5.3 Testing methods

In order to have a good understanding of any new material's behavior, series of experimental studies need to be performed. These experiments are varied based on the nature of the study. In this case, compression, flexural, thermal conductivity, drying shrinkage as well as bond test are among these experiments.

5.3.1 Compression test

This test was done based on ASTM C873 / C873M - 04e1 [1]. Six cylindrical specimens of 2 $in \times 4$ in were prepared for each mix design and the compression test was conducted on three of the cylinders at 7 days of age and the remaining three at 28 days of age. The compression test was conducted using Instron 5869 universal machine based on the displacement control. A 10,000 lb load cell was used during the compression test. The test end point was set at -3 mm, speed of the machine was set at 0.01 mm/s, the sampling period was set at 0.1 per second and detect controllers was enabled.

5.3.2 Three point bending flexural test

This test was done based on ASTM C293 [69]. Three 2 $in \times 2$ $in \times 4$ in rectangular prisms were prepared for this test. One out of three specimens was used for the 7 days flexural test and the other remaining two were used for the 28 days flexural test. The flexural test was conducted using Instron 5869 universal machine based on the displacement control. A 10,000 lb load cell was

used during the flexural test. The test end point was set at -3 *mm*, speed of the machine was set at 0.001 *mm/s*, the sampling period was set at 0.1 per second and detect controllers was enabled. By operating the loading machine quite carefully, the post peak response was obtained. As one can see from the speed of the machine, the load was applied with very slow rate of loading up to the peak.

The flexural stress and stain can be calculated based on the following equations:

$$\begin{aligned} \sigma_f &= \frac{3pl}{2bd^2} \\ \epsilon_f &= \frac{6Dd}{l^2} \end{aligned} \tag{5.1}$$

where

σ_f = Stress in the outer fibers at midpoint,

ϵ_f = Strain in the outer surface,

P = Load at a given point,

l = Support span,

b= Width of the beam,

d = Depth of the beam,

D = Maximum deflection of the center of the beam.

5.3.3 Thermal conductivity test

Heat can be transferred from one point to another point through different common methods such as: conduction, convection and radiation. There are different mathematical relationships to analyze each of these methods. For instance, equation 5.2 can be used for calculating the amount of heat conducted through different materials.

$$\triangle Q = kA\Delta T\Delta t/h \tag{5.2}$$

where

$\triangle Q$ = Total heat energy conducted,

A = Total area through which the conduction occurs,

ΔT = Temperature difference between the sides of the material

Δt = Time during which the conduction occurs,

h = Thickness of the material,

k = Thermal conductivity of the material.

In this study, the method used in the study of PCM in chapter three was adopted. In another word, specific heat and thermal diffusivity were measured and by using equation 5.3, thermal conductivity was calculated.

$$k = \alpha \rho c_p \tag{5.3}$$

where k is the thermal conductivity, α is thermal diffusivity, ρ is density and c_p is specific heat (or heat capacity).

It should be noted that Differential Scanning Calorimetry (DSC) for measuring the specific heat is conducted using Netzsch DSC 204 F1 Phoenix machine and Netzsch LFA 457 device was used for thermal diffusivity measurements.

5.3.4 Drying shrinkage

The standard test method for drying shrinkage of mortar based on ASTM-C 157 [71] was used in this study. Two prism specimens 1 in × 1 in × 10 in were prepared for each mix design. In order to take the most accurate measurements, two gage slugs were installed at the center of the top and bottom part of each specimen. Taking measurements started after 7 days of curing in a standard curing room. Figure 5.3 shows the device used for measuring the shrinkage of the specimens.

5.3.5 Tensile (pull off) bond test

This test was done based on the ASTM D4541-02 [70]. The pull-off test involves applying a direct tensile load to a partial core advanced through the overlay material and into the underlying mortar till failure occurs. The tensile load is applied to the partial core using a metal disk with a pull pin which is bonded to the overlay with an epoxy. A loading device with a reaction frame

Figure 5.3: Shrinkage device.

applies the load to the pull pin. The load should be applied at a constant rate, and the ultimate load should be recorded at the time of the failure. Figure 5.4 shows the device being used for the tensile bond test. There are different types of failure being observed through the tensile bond test. These are as follows:

(a) Failure at the bond surface.

(b) Failure between the disk and the overlay surface.

(c) Failure within the overlay material.

(d) Failure in the substrate.

It should be noted that in some of the cases the failure can be the combination of two or more of the above failures.

In this study, the wood mold 11.5 in $\times$ 7.5 in $\times$ 1 in was used. However, since the surface preparation is an important key in the bond test procedure, the following steps should be taken in order to prepare each specimen for the test:

(a) The surface in the test area should be wire brushed to remove any laitance and deposits. This should be done in order to achieve sufficient bond between the steel disk and the overlay surface.

(b) In order to minimize eccentricities during loading, care should be taken to ensure that the core is advanced perpendicular to the overlay surface.

Figure 5.4: Tensile (pull off) bond test device.

(c) After cleaning the top of the partial core, it should be dried and then bond a metal disk to the surface of the partial core with a fast setting epoxy. It should be noted that not to apply too much epoxy, since it would run down the sides of the core and possibly bond the core to the sides of the core hole. Moreover, in order to minimize the potential for loading eccentricities, the disk should be bonded to the middle of the partial core.

Figure 5.5 shows the specimen and specimen's preparation for the bond test.

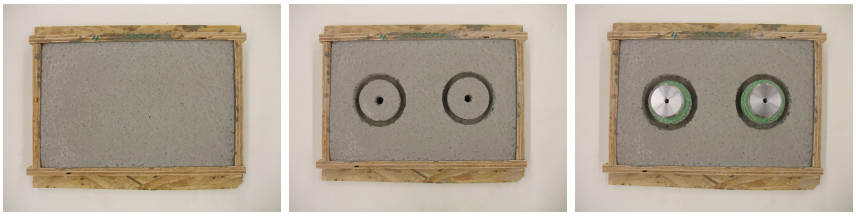

(a) Bond specimen (b) Cutting the core hole (c) Gluing the dolly

Figure 5.5: Tensile (pull off) bond test.

5.3.6 Scanning Electron Microscopy (SEM)

SEM images were taken using a microscope (JSM-6480LV (LVSEM)). The SEM images provide a better understanding of the internal structure of mortar in the microstructure level. In addition, the interfaces between rubber particles and cement paste, and PCM particles and cement paste can be observed.

5.4 Experimental Results and discussions

5.4.1 Compression and flexural tests

As it has been mentioned, compression test, flexural test, thermal conductivity, drying shrinkage and bond test were performed on specimens in each group.

Table 5.9 and Table 5.10 show the result of all the groups at 7 and 28 days of age. Figure 5.6 and Figure 5.7 show the comparison of compression and flexural strength of all the five groups at 7 and 28 days of age.

Table 5.9: Test results for all the groups at 7 days of age

Group	**Compression strength (Ksi)**	**Flexural strength (Ksi)**	**Compression/Flexural**	**Check $\leq$ 3.0**	**Bond test (Ksi)**
1	0.92	0.43	2.14	$\surd$	8
2	0.98	0.49	1.99	$\surd$	10
3	0.72	0.41	1.74	$\surd$	9
4	0.67	0.48	1.39	$\surd$	13
5	0.95	0.34	2.79	$\surd$	NA

Table 5.10: Test results for all the groups at 28 days of age

Group	**Compression strength (Ksi)**	**Flexural strength (Ksi)**	**Compression/Flexural**	**Check $\leq$ 3.0**	**Bond test (Ksi)**
1	1.10	0.53	2.09	Ok	15.0
2	1.01	0.49	2.04	Ok	18.0
3	0.62	0.45	1.38	Ok	15.0
4	0.72	0.47	1.54	Ok	23.0
5	1.05	0.41	2.58	Ok	62.5

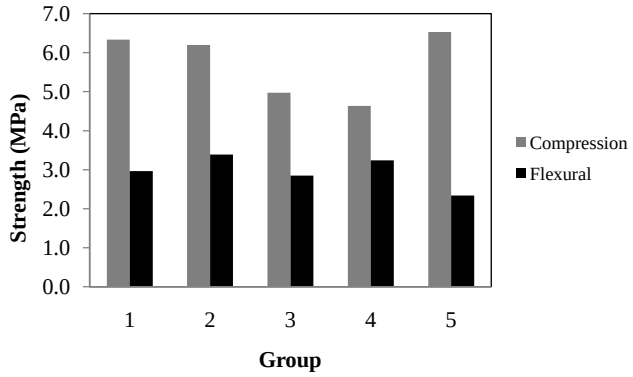

Figure 5.6: Comparison of compression and flexural strength of all groups at 7 days of age.

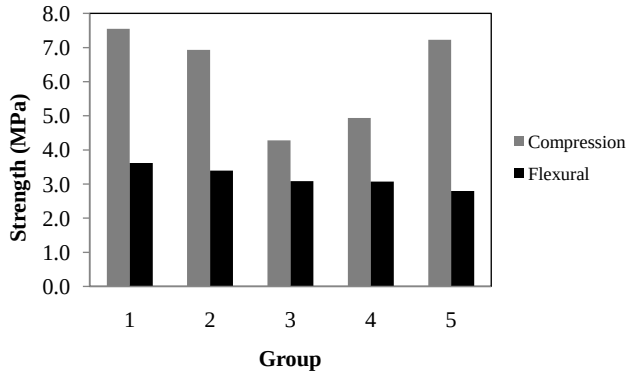

Figure 5.7: Comparison of compression and flexural strength of all groups at 28 days of age.

As one can see from both Figure 5.6 and Figure 5.7, the strength variations among the five groups are similar at 7 and 28 days. Comparing the test data of Group 1 and Group 2 for the effect of rubber particle size, one can clearly see that the size of rubber particles has a significant effect on the strengths at 7 days, and less significant effect at 28 days. So, it can be considered that the average rubber particle size can vary within the range of 6 to 10 mesh without a major effect on both compressive and flexural strength of the mortar. This conclusion was also confirmed by the test data from Xi et al. [81].

Comparing the test data of Group 3 with Group 1 and Group 2 for the effect of rubber particle content, one can see in both Figure 5.6 and Figure 5.7 that higher rubber content reduces the strengths, which is expected. A more careful observation of Figure 5.7 shows that the effect of rubber content on compressive strength is much more significant than its effect on the flexural strength. This may be explained by the stiffness and shape of rubber particles. In terms of stiffness, rubber particles are "soft" particles comparing with "stiff" sand particles and cement paste, and the "soft" rubber particles reduce compressive strength when the entire cross section is under compression in the compressive test. Therefore, with more "soft" rubber particles added in the mortar, the compressive strength of the mortar becomes lower. In terms of shape, rubber particles are thin flake shaped particles as shown in Figure 5.8 comparing with round shaped sand particles, and rubber particles acting like thin sheets of short fibers help to hold tensile stress when the lower portion of the cross section is under tension in the flexural test. Therefore, with more "flake shaped" rubber particles added in the mortar, the flexural strength of the mortar was not reduced like the compressive strength.

Figure 5.8: Rubber particles.

Comparing Group 4 with Group 1 and Group 2 for the effect of RPP, one can clearly see in both Figure 5.6 and Figure 5.7, with increasing amount of RPP, the compressive strength decreases and the flexural strength remains almost the same, which leads to a lower ratio of the compressive to flexural strength. Because the flexural strength is an indicator of tensile strength of mortar representing crack resistance of the material, the lower the strength ratio, the higher the crack resistance (relative to the compressive strength). Therefore, the main function of RPP is to reduce the compression/flexural strength ratio, which is an important feature of the mortar used on large area of building envelopes.

Group 5 was to compare the effect of PCM on the compressive and flexural strength with the effect of rubber particles. In the mix design of Group 5, the same amount (weight) of PCM was used to replace the rubber particles used in Groups 1 and Group 2. Since the densities of PCM and rubber are about the same, the PCM volume fraction in Group 5 was about the same as the rubber volume fraction in Group 1 and Group 2. One can see from Figure 5.6 and Figure 5.7 that the compressive strength of the PCM-modified mortar was about the same as rubberized-mortar, and the flexural strength of PCM-modified mortar was slightly lower than that of rubberized-mortar. This means that when the volume fractions of PCM and rubber are about the same, the effects of PCM particles and rubber particles on both compressive and flexural strength are about the same. However, the failure pattern of the PCM specimens was totally different from the failure pattern of rubberized-mortar under the flexural loading. Figure 5.9 shows the comparison of these two cases. PCM-modified mortar specimens exhibited a brittle and sudden failure in the flexural

testing, and the specimens were broken into two separate pieces at failure. This may be due to the spherical-shaped encapsulation of PCM particles as well as the very low tensile strength of the PCM material. While for the rubberized-mortar specimens, the flexural failure occurred gradually and smoothly, and the specimens did not break into separate pieces at the peak load.

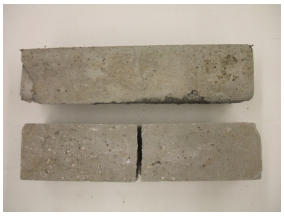

Figure 5.9: Comparison of PCM and rubber specimens under flexural testing.

Overall, when the phase change material is used as the sand volume replacement in insulation mortar, the reduction in compressive and flexural strengths are about the same as the reduction caused by the added rubber particles. From Table 5.7 and Table 5.8, the total amount of the dry material (all components except water) as well as the percentage of the rubber/PCM in each mix design can be easily calculated. Table 5.11 shows these values.

Table 5.11: Percentage of rubber/PCM in each mix design

Group	**Total dry material (kg/m^3)**	**Rubber or PCM / Total dry material**
1	1280.77	14%
2	1280.77	14%
3	1190.47	20%
4	1288.17	14%
5	1280.77	14%

The results from Table 5.9, Table 5.10 and Table 5.11 show that when 14 percent of the total dry material was added to the mix design by either PCM or rubber particles, the compression to flexural strength ratio have change significantly. More specifically, at 7 days of age, there is an increase of 31% (From 2.14 to 2.80) when PCM has been added in comparing with coarse rubber particles (6 mesh). The strength ratio increased by 53% (From 1.83 to 2.80) when PCM was added

in comparing with fine rubber particles (8-10 mesh). These values for strength ratios dropped to 23% (From 2.09 to 2.58) and 26% (From 2.04 to 2.58) at 28 days of age, respectively. It can be concluded that these ratios for smaller rubber particles are higher than the larger rubber particles, which shows the possibility of lowering the strength ratio by using the smaller rubber particles or powders. Additionally, the results shows the strength ratio was much lower for 28 days of age, which indicates that the aging effect was more significant for the flexural strength than the compressive strength for both PCM and rubber modified mortars.

5.4.2 Thermal conductivity

All thermal tests were conducted at 28 days of age. As mentioned earlier, thermal conductivity of a material can be calculated as the product of the density, thermal diffusivity, and specific heat of the material. In the present study, thermal diffusivity and specific heat of a mortar specimen were obtained first, and then the thermal conductivity was calculated. Figure 5.10 and Table 5.12 show the specific heat and thermal diffusivities of all groups of specimens, respectively. Figure 5.11 shows the calculated thermal conductivities.

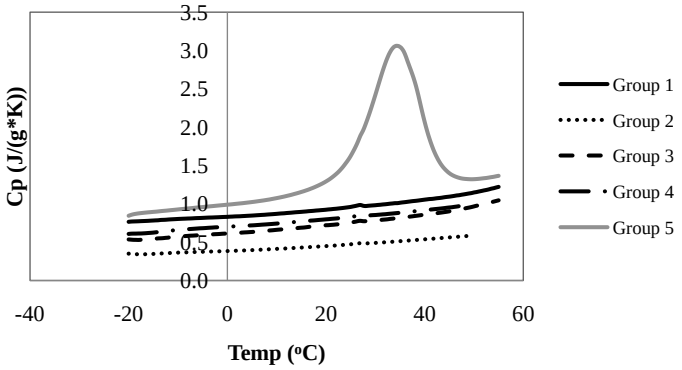

Figure 5.10: Specific heat of all the groups.

Table 5.12: Thermal diffusivity of all groups at room temperature

Group	**Thermal diffusivity (m^2/s)**	**Density(gr/cc)**
1	0.323	1.78
2	0.364	1.58
3	0.351	1.41
4	0.476	1.58
5	0.373	1.34

A careful observation of Figure 5.11 reveals that the small rubber particles (in Group 2) leaded to significantly low thermal conductivity (comparing Group 1 and Group 2). This means that the conductivity depends not only on the volume fraction of the rubber particles but also on the average size of the particles. Considering the rubber particles as inclusions in a two-phase composite material and the inclusion as insulator (with lower conductivity), then the smaller the average size of the distributed insulator, the lower the conductivity of the composite. Physically, this phenomena implies that with a fixed volume fraction of insulator, the insulator of smaller sizes has a more uniform spatial distribution in the mortar, and thus a higher resistance to the heat conduction (the resistivity is inversely proportional to the conductivity). Of course, the significance of this kind of size dependency is related to the volume fraction of the inclusion, and should not be considered as a general conclusion. More researches are needed in this area.

Comparing the test data of Group 3 with Group 2 in Figure 5.11, one can see that the thermal conductivity of the mortar decreases with increasing volume fraction of rubber particles. This can be easily explained by the low thermal conductivity of rubber particles. With more insulative particles added into the mixture, the conductivity of the composite will be lower. Another observation was that more RPP (Group 4) in the mixture slightly increased the thermal conductivity of rubberized-mortar.

In the case of the effect of PCM on the conductivity of the composite, it is quite clear that PCM-modified mortar (Group 5) had similar conductivities to the rubberized-mortar with larger size rubber particles (Group 1). However, there was a sharp peak for the PCM-modified mortar and the peak appeared around the melting point of the PCM particles. The peak in the conductivity is

due to the peak in the specific heat shown in Figure 5.10, which reflects the large amount of heat absorbed at the melting point of the PCM. This high peak in the heat capacity represents a major improvement in the insulation capacity of the mortar. It should be noted that since MPCM-28 wet cake was used in this study and this product has 30% water content in its exterior wall, the peak did not appear exactly at 28 °C which is its melting point.

As it was mentioned earlier, the thermal diffusivity of the PCM-modified mortar varies at elevated temperature; therefore, the thermal diffusivity test was run on the PCM-modified mortar at different temperatures. Figure 5.12 shows the results of the thermal diffusivity test on PCM-modified mortar.

As it can be seen from Figure 5.12, the thermal diffusivity curve has a peak around 33 °C, which is quite similar to the peak at the specific heat curve. The thermal conductivity of the PCM-modified mortar at different temperatures was calculated as it was explained earlier. Figure 5.13 shows the temperature effect on the thermal conductivity of the PCM-modified mortar.

It can be seen from both Figure 5.12 and Figure 5.13 that there exists a peak around the melting point of the PCM particles. However, the temperature effect on the thermal diffusivity after the melting point was not much different and remained within the same value as the peak, which was significantly higher than the thermal diffusivity before the melting point of the PCM particles.

5.4.3 Tensile (pull off) bond test

The bond tests were conducted at 7 and 28 days of ages and the results are shown in Table 5.9 and Table 5.10. It can be seen that using fine rubber particles results better bond (Group 2) than using the coarse rubber particles (Group 1). This is because the bond between rubber and wood is very poor, and thus the contact area between a rubber particle and wood can be considered as a defect in the interface. Since the strength of the interface depends on the largest defect, the large rubber particles tend to result in large defect and thus lower bond strength. Since RPP is a good binder, it is understandable that more RPP in the mixture provides a higher bonding strength

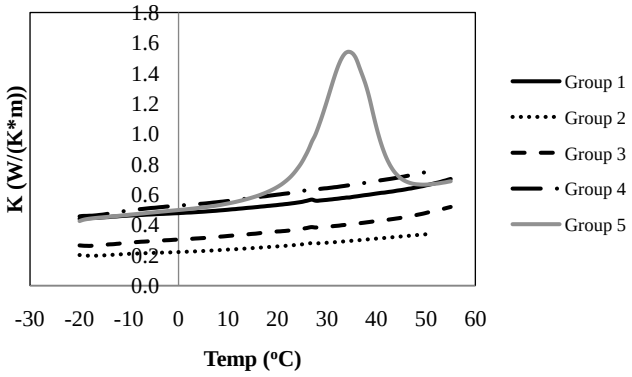

Figure 5.11: Thermal conductivity of all groups after 28 days of age.

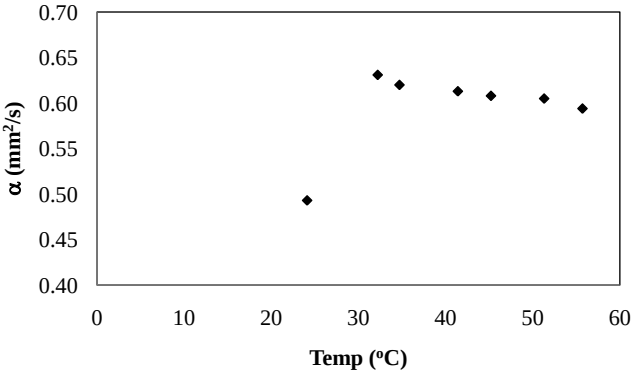

Figure 5.12: Thermal diffusivity of the PCM-modified mortar at different temperature.

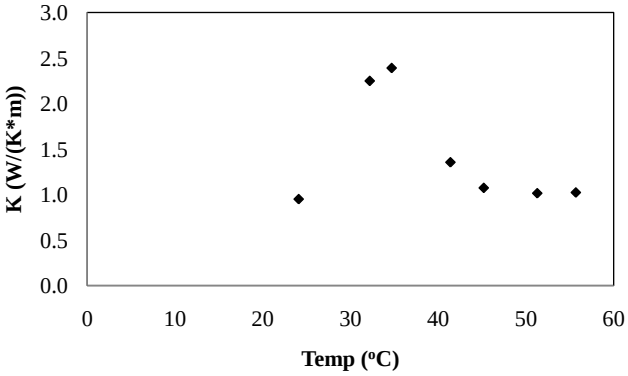

Figure 5.13: Thermal conductivity of the PCM-modified mortar at different temperature.

(Group 4).

The result of Group 5 is very interesting, which shows that the PCM-modified mortar performs the best among all groups in terms of the bond strength. That can be explained by the fact that the sizes of PCM particles (17-20 microns) are much smaller than the sizes of rubber particles (3-5 mm). The PCM particles are distributed in the cement paste and the majority of the bond strength comes from the bond between the cement paste and the wood.

5.4.4 Drying shrinkage

Figure 5.14 shows the dry shrinkage test results for all groups of specimens. As it can be clearly seen from the graph, the size of the rubber particles plays an important role. Basically, the drying shrinkage decreases significantly with decreasing size of rubber particles. As shown in Figure 5.14 the shrinkage of Group 2 was lower than that of Group 1. This is because some of the small rubber particles can be accommodated in various types of pores in the cement paste and therefore do not contribute to the formation of the "soft" framework in the solid. This "soft" framework is the main reason for the high drying shrinkage of rubberized-mortar comparing with the shrinkage of regular Portland cement mortar. With more rubber particles in the mixture, the contribution of the "soft" framework becomes more significant, leading to higher dry shrinkage strain (see the result of Group 3 in Figure 5.14).

Figure 5.14 shows the drying shrinkage of different groups.

As shown in the figure (see the result of Group 4 in Figure 5.14), RPP can reduce the dry shrinkage and this may be due to its function of reducing the water permeation in the microstructure of cement paste. Drying shrinkage is caused by moisture exchange between the environment and the cement paste. RPP is a polymeric material that can be considered as a type of sealant for the pore structure, and the moisture permeation in the pore network of cement paste is slowed down by RPP, and thus the drying shrinkage is reduced.

The effect of PCM on drying shrinkage of PCM-modified mortar is shown in Group 5 in Figure 5.14. The volume fraction of the PCM in Group 5 and the volume fraction of the rubber particles in

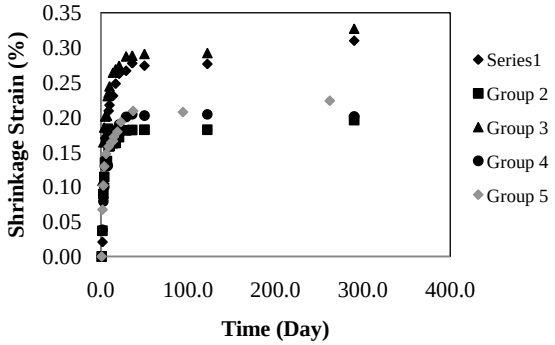

Figure 5.14: Comparison of drying shrinkage of all groups.

Group 1 are about the same, and the drying shrinkage of the PCM-modified mortar is much lower than that of the rubberized-mortar. The PCM particles (MPCM-28 wet cake) contains 30% water, and the extra water from the PCM increases the water-to-cement ratio of the mixture to a certain extent, which, in turn, may increase the drying shrinkage of the mortar. But, such an increase in the shrinkage is over shadowed by the effect of particle size of PCM. Since the average size of the PCM particles is 17-20 microns, smaller than the size of rubber particles used in the study, and the effect of small particles, as described earlier, was more significant than the effect of the slightly increased water-cement radio. As a result, the drying shrinkage of Group 5 (PCM-mortar) was lower than Group 1 (rubberized-mortar with large rubber particles).

5.4.5 Scanning Electron Microscopy (SEM) images

Figure 14 shows a SEM image for a rubberized-mortar sample. As one can see in Figure 14, the wood fibers are the narrow long lines distributed throughout the whole mixture. The fibers have good bond with surrounding cement paste. The black dot in the center of image is a rubber particle, and it has good bond with surrounding cement paste. This is one of the images collected in the study. SEM images showed the good bond between rubber particles and the cement paste.

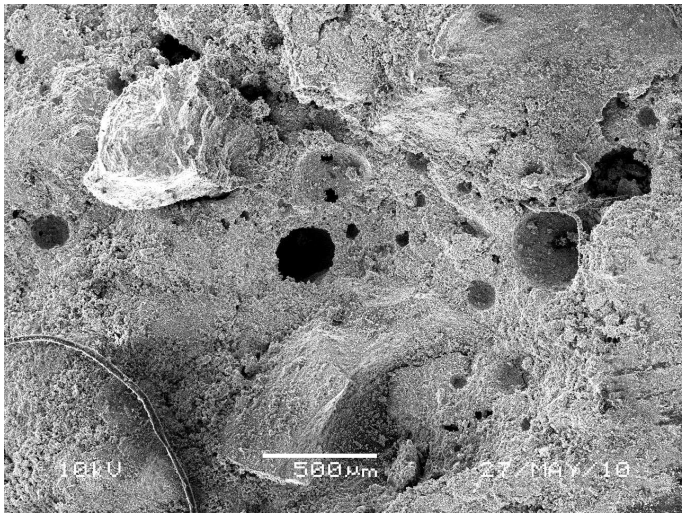

Figure 5.15: SEM image of rubberized-mortar.

5.5 Conclusions

(1) Mechanical and thermal properties of various PCM-modified and rubberized Portland cement mortars were experimentally studied. Compressive strength, flexural strength, bond strength, drying shrinkage, and thermal conductivity of the mortar samples were tested at different ages. Different types of additives were also used in the mix designs such as ground calcium (GC), redispersible polymer powder (RPP), methyl cellulose (MC), and wood fiber (WF).

(2) When the volume fractions of PCM and rubber particles are about the same, the effects of PCM particles and rubber particles on both compressive and flexural strength of the mortars are similar. With increasing PCM and rubber contents, the compressive and flexural strengths of the mortars decrease.

(3) The failure pattern of the PCM specimens is totally different from the failure pattern of rubberized-mortar under the flexural loading. PCM-modified mortar specimens exhibited a brittle and sudden failure in the flexural testing; while the flexural failure of rubberized-mortar specimens occurred gradually and smoothly, and the specimens did not break into separate pieces at the peak load.

(4) Within the size range of rubber particles used in the study (6-10 mesh), the effect of rubber particle size is not significant on the compressive or flexural strength.

(5) The addition of RPP in the mortar decreases the compressive to flexural strength ratio. The effects of RPP on the two strengths are different: the compressive strength was reduced and the flexural strength remained about the same.

(6) Using smaller rubber particles and lower rubber content help to improve the bond strength of the mortar. Using RPP in the mixture can improve the bond strength significantly. The PCM-modified mortar performs the best in terms of bond strength.

(7) The thermal conductivity results show that the smaller and more rubber particles result in lower thermal conductivity. This means that the thermal conductivity of mortar depends not only on the volume fraction of the rubber particles but also on the average size of the particles. The smaller the rubber particle size, the lower the conductivity of the rubberized-mortar. Application of PCM results in a peak on the thermal conductivity curve, which is happening around the melting point of the PCM.

(8) The drying shrinkage of mortar is affected significantly by PCM, rubber particles, and RPP. Lower rubber content and more RPP in the mixture help to reduce the drying shrinkage. With the same volume fraction for PCM and rubber particle, the drying shrinkage of PCM-modified mortar is much lower than that of rubberized-mortar.

(9) SEM images showed that the interface bond between rubber particles and surrounding cement paste is very good, so is the bond between wood fibers and cement paste.

Chapter 6

COMPOSITE MODELS FOR EFFECTIVE THERMAL CONDUCTIVITY PCM-RRUBBERIZED-MORTAR

This chapter presents the results of generalized self consistent model for effective thermal conductivity of rubberized-mortar, PCM-rubberized-mortar and PCM-mortar. A multi-phase, multi-scale model has been developed to predict the effective thermal conductivity. The effect of temperature as well as the effect of volume fraction of both PCM and rubber on the effective thermal conductivity has been investigated. Unfortunately, the generalized self consistent model cannot capture the effective properties of rubberized-mortar, PCM-rubberized-mortar and PCM-mortar accurately and it needs to be modified. The modification has been done considering both PCM and rubber powder as outer rings in the model as an approach to account on their low thermal conductivity in comparing with other phases. The result of the modified generalized self consistent model for the effective thermal conductivity is capturing the experimental data better. The modified generalized self consistent model illustrates that any addition in the PCM amount and rubber powder would decrease the effective thermal conductivity. Also, the model has verified for another PCM-mortar with different mixing design.

6.1 Introduction

The disposal of solid waste has created a lot of problems in the last decades. For instance, in the United States alone, more than 242,000,000 scrap tires have been produced each year [14]. These stockpiles are dangerous not only because of the environmental issue, but also because of

the fire hazards and providing inhabitation for various species [72]. One of the possible solutions is to reuse tire rubbers in a variety of rubber products in building envelopes.

There have been several studies incorporating the waste tire rubbers in concrete and mortar. Topcu et al. [75] investigated the durability of rubberized-mortar and rubberized-concrete. Their results showed that the rubberized-mortar could be used in seawater, cement with higher strength and cement resistant to sulfate. However, it is appropriate to use the rubberized-mortar in places where the high temperature effect does not exist. Huynh et al. [33] studied some of the properties of rubberized-mortar and they found out that any increase in the rubber content in the mortar mix would decrease the flexural strength and plastic shrinkage of mortar. This reduction varies based on the shape and size of the rubber particles. Their results have also revealed that the geometry of rubber particles influences the fracture behavior of mortar as well. Oikonomou and Mavridou [55] examined the incorporation of tire rubber granules as a partial replacement for the sand in cement mortars. The results showed a decrease in mechanical properties, whereas an increase in chloride ion penetration resistance. Kang and Jiang [36] investigated the crack resistance of cement based materials by addition of rubber particles and they showed cracking time was retarded and the crack resistance was improved. Albano et al. [3] investigated the influence of scrap rubber particles through destructive and non-destructive testing, in order to find a liable application. Their results showed by the ultrasonic pulse velocity with time, one can infer that the addition of rubber decreased this variable, being the effect more notorious when rubber content increased. Additionally ultrasonic pulse velocity was relatively independent of particle size and coupling agent employed. Although several works have been done on different properties of rubberized composites, there are a few works investigated the thermal conductivity of composites containing rubber particles. For instance, Benazzouk et al. [6] investigated the thermal conductivity of cement composites by replacing rubber particles as volume replacement to cement. The results indicated a clear reduction in thermal conductivity of the composite with any addition of rubber particles.

Most of the studies on rubberized concrete and mortar are experimental studies. However, for the sake of time and expense of running different tests, it would be beneficial to study the effect of the

rubber in concrete mixture analytically. Huang et al. [31] treated rubberized concrete as a multi-phase composite material. They used Finite Element Analysis in order to investigate the effect of various design parameters on the composite strength. Their results revealed that any reduction in the maximum rubber size, using stiffer coarse aggregate, control of the aggregate size distribution as well as harder cement mortar would help the composite strength.

There are a few researchers focusing on the analytical study of the thermal conductivity of rubber in cementitious materials, such as Topcu et al. [76] who adopted artificial neural network and fuzzy logic and Benazzouk et al. [6] who developed a model based on self consistent method assuming air, rubber particles and cement paste are the three phases in the composite.

Mortar is a heterogeneous multi-phase material. On a macroscopic scale, it is a mixture of cement paste, fine aggregates, with different sizes and shapes. With regard to its mechanical behavior, mortar is often considered as a tow-phase composite structure, consisting of aggregate particles, the cement paste matrix in which they are dispersed, and the interfacial transition zone (ITZ) around the aggregate particles and cement paste [54].

In this work, the unique idea is to use rubber waste particles and phase change material known as PCM as raw materials in order to reduce the heat transfer into building to decrease the energy consumption. This chapter focuses on the mathematical modeling of effective thermal conductivity of rubberized-mortar, PCM-rubberized-mortar and PCM-mortar. In the thermal conductivity model, thermal conductivity of sand, cement paste, rubber and PCM particles as well as their volume fractions are taken into consideration. The effects of change in the volume fraction of PCM particles and rubber powder as well as temperature change on the effective thermal conductivity have been investigated. The predicted effective thermal conductivity based on the model has been compared with the effective thermal conductivities of other models as well as experimental data.

6.2 Significance of the research

Reducing the heat transfer into buildings would be a great assist to decrease the energy consumption of building enveloped. To do so, lowering the thermal conductivity of structural

components would be the very first approach. Experimental study would come to mind as a first method, however not always the best way to start the investigation. Generalized self consistent method has been adopted to study variety of properties in two phase composites, but there are several limitations to expand the basic method to a multi-phase composite. In this work, with the help of multi-scale as well as multi-phase approach, generalized self consistent model has been modified to predict the thermal conductivity of rubberized-mortar, PCM-rubberized-mortar and PCM-mortar more accurate.

6.3 Effective thermal conductivity of multi-phase composite

There are several models available in order to study the effective properties of any composites. Most of these models examine the effective properties of the composite based on the desired property of each phase as well as their volume fraction. Parallel, series, Maxwell, generalized self consistent are among these models.

6.3.1 Parallel model

The Parallel model for a composite consists of M phases with defined volume fractions can be specified as:

$$\sigma_e = \sum_{i=1}^{M} \phi_i \sigma_i \tag{6.1}$$

It should be noted that in the Parallel model, it is assumed that the layer of the components of physical structures are oriented in a parallel to the direction of heat flow. In addition, the Parallel model gives the maximum value of the thermal conductivity. Therefore, the Parallel model can be used for the upper bound limit.

Figure 6.1: Parallel model.

6.3.2 Series model

The Series model for a composite consists of M phases with defined volume fractions can be specified as:

$$\frac{1}{\sigma_e} = \sum_{i=1}^{M} \frac{\phi_i}{\sigma_i} \tag{6.2}$$

It should be noted that in the Series model, it is assumed that the layer of the components of physical structures are oriented perpendicular to the direction of heat flow. In addition, the Series model gives the minimum values of the thermal conductivity. Therefore, Series model can be used for the lower bound limit.

6.3.3 Maxwell model

The Maxwell equation for generalized suspensions with matrix with thermal conductivity σ_1, *M-1* different types of spheres ($M \succeq 2$) with volume fractions $\phi_2, \phi_3, ..., \phi_M$ and thermal conductivities $\sigma_2, \sigma_3, ..., \sigma_M$ can be defined as [73]:

$$\frac{\sigma_e - \sigma_1}{\sigma_e + (d-1)\sigma_1} = \sum_{i=1}^{M} \phi_i [\frac{\sigma_i - \sigma_1}{\sigma_i + (d-1)\sigma_1}] \tag{6.3}$$

Figure 6.2: Series model.

6.3.4 Generalized self-consistent model

The generalized self consistent model (GSC) originally was developed by Christensen for the elastic property [12]. In this model, the existence of a characteristic dimension of the inhomogeneity as well as the existence of the scale properties averaging has been assumed. In addition, it has been assumed that the scale of the inhomogeneity in the order of magnitude is smaller than the characteristic dimension of the problem of interest. Considering this assumption would let a heterogeneous composite material be divided into many regions or elements that the volume fraction of each phase within each element is constant. Figure 6.3 shows this partitioning of a multi-phase composite into different elements. This figure can be even more simplified by assuming spherical phases with a defined radius. Figure 6.4 shows the simplified partitioning of a multi-phase composite.

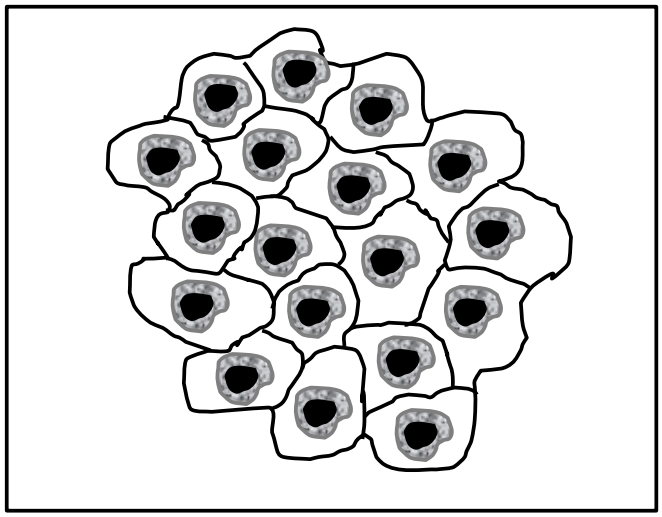

Figure 6.3: Partitioning multi-phase composite into different elements.

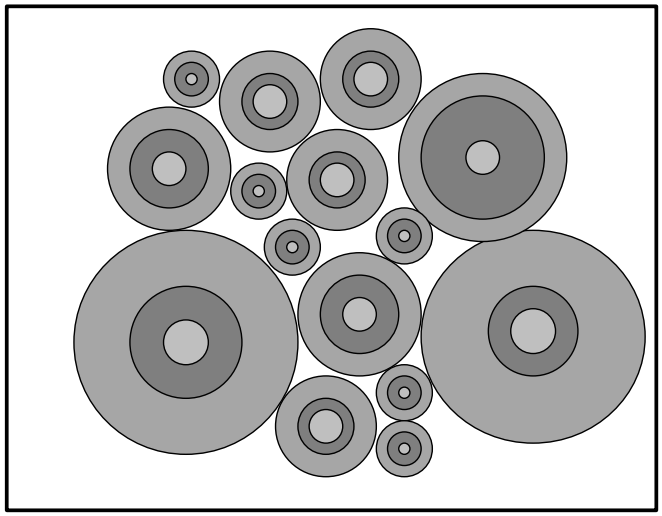

Figure 6.4: Partitioning multi-phase composite using spherical elements.

As it can be seen in Figure 6.4, the basic elements of the microstructure are spherical elements composed of different phases. As it was mentioned earlier, it is assumed that the volume fractions of all the elements are the same, thus the radius ratios of each of the phases within different element remains the same as well. The Christensen model is based on a two-phase composite; however most of the composites are multi-phase composites. Following the basic idea of a two-phase composite, the model can be further extended to a multi-phase composite model. A schematic figure of a four-phase composite has been shown in Figure 6.5. Following the original self-consistent scheme

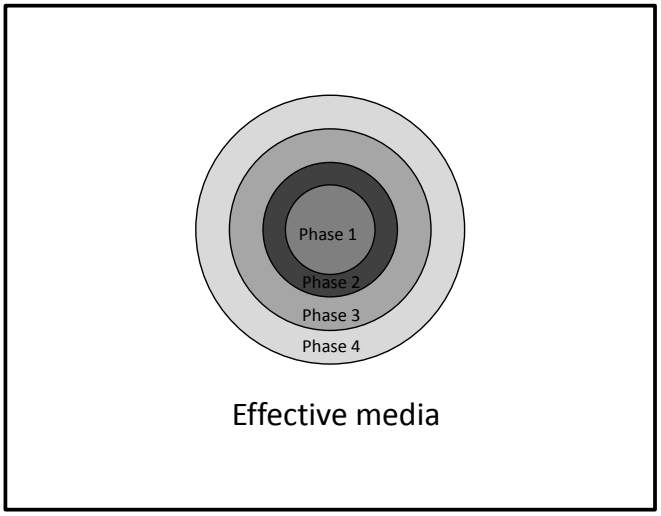

Figure 6.5: Schematic of a five-phase composite.

(SCS) [12] assuming a spherical inclusion of radius a is embedded in a concentric sphere matrix of radius b, which itself is embedded in an infinite effective medium possessing the unknown effective thermal conductivity k_{eff}. The ratio of the radii a/b can easily be linked to the volume fraction of inclusions through $\phi = (a/b)^3$. The governing equations can be defined as:

$$\nabla T^2 = 0 \Rightarrow \begin{cases} \nabla T_i^2 = 0 & \text{if} \quad 0 \leq r \leq a \\ \nabla T_m^2 = 0 & \text{if} \quad a \leq r \leq b \\ \nabla T_{eff}^2 = 0 & \text{if} \quad r \geq b \end{cases} \tag{6.4}$$

Using spherical coordinates with axial symmetry about x_3 axis would assist to define:

$$\nabla^2 = \frac{1}{r^2}\frac{\partial}{\partial r}(r^2\frac{\partial}{\partial r} + \frac{1}{r^2\sin\theta}\frac{\partial}{\partial r}(\sin\theta\frac{\partial}{\partial\theta}) \tag{6.5}$$

Since the solution to the Laplace equation is in the form of:

$$T = (Ar + \frac{B}{r^2}\cos\theta) \tag{6.6}$$

The following equation can be written for each phase:

$$\begin{cases} \nabla T_i = A_i r\cos\theta & \text{if} \quad 0 \le r \le a \\ \nabla T_i = (A_m + \frac{B_m}{r^2})\cos\theta & \text{if} \quad a \le r \le b \\ \nabla T_i = (A_{eff} + \frac{B_{eff}}{r^2})\cos\theta & \text{if} \quad r \ge b \end{cases} \tag{6.7}$$

It should be noted that the B_i must be set equal to zero to avoid singularity at the inclusion. In order to solve five unknown in the above equations, the continuity equations should be written.

$$k_i\frac{\partial T_i}{\partial r} = k_m\frac{\partial T_m}{\partial r} \tag{6.8}$$

$$k_m\frac{\partial T_m}{\partial r} = k_{eff}\frac{\partial T_{eff}}{\partial r} \tag{6.9}$$

Solving the above equations simultaneously would lead to the effective thermal conductivity of a two-phase composite as:

$$k_{eff} = k_m[1 + \frac{c}{\frac{1-c}{3} + \frac{k_m}{k_i - k_m}}] \tag{6.10}$$

where k_m is the thermal conductivity of the matrix, k_i is the thermal conductivity of the inclusion and c is the volume fraction of the inclusion $= (a/b)^3$.

Figure 6.6 illustrated the basic generalization of the two-phase to five-phase model, which can also be extended to the n-phase model as well. Since the continuity conditions have been used in the derivation of the above equation, and c is only dependent on the size of the spheres, each of the two neighboring phases can be combined and their effective property can be calculated to be considered in order to get the effective property of the whole composite. Generalizing this equation

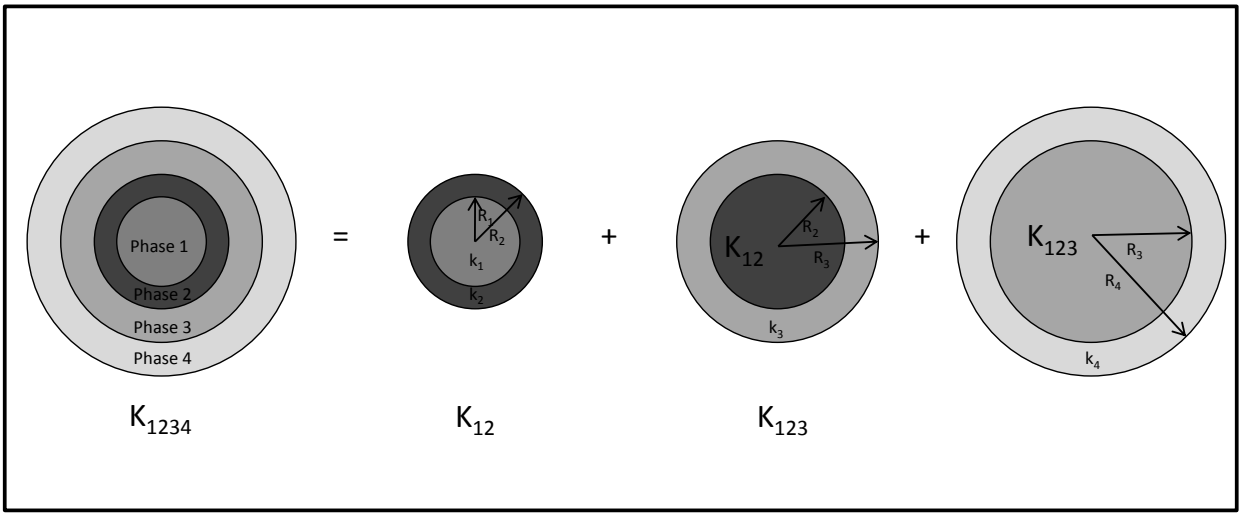

Figure 6.6: Generalization of two-phase model to five-phase model.

to a four-phase composite would be as follows:

$$k_{12} = k_2[1 + \frac{c_{12}}{\frac{1-c_{12}}{3} + \frac{k_2}{k_1 - k_2}}] \tag{6.11}$$

$$k_{123} = k_3[1 + \frac{c_{123}}{\frac{1-c_{123}}{3} + \frac{k_3}{k_{12} - k_3}}] \tag{6.12}$$

$$k_{1234} = k_4[1 + \frac{c_{1234}}{\frac{1-c_{1234}}{3} + \frac{k_4}{k_{123} - k_4}}] \tag{6.13}$$

where the k terms are the thermal conductivity of each of the phases. Although the c terms are not the volume fraction of each phase, they can easily be linked to the volume fractions of the phases as:

$$c_{12} = \frac{R_1^3}{R_2^3} = \frac{\phi_1}{\phi_1 + \phi_3} \tag{6.14}$$

$$c_{123} = \frac{R_2^3}{R_3^3} = \frac{\phi_1 + \phi_2}{\phi_1 + \phi_3 + \phi_3} \tag{6.15}$$

$$c_{1234} = \frac{R_2^3}{R_3^3} = \frac{\phi_1 + \phi_2 + \phi_3}{\phi_1 + \phi_3 + \phi_3 + \phi_4} = \phi_1 + \phi_2 + \phi_3 + \phi_4 \tag{6.16}$$

The effective thermal conductivity of n-phase composite can be determined as:

$$k_{eff,i} = k_i[1 + \frac{c_i}{\frac{1-c_i}{3} + \frac{k_i}{k_{eff,i-1} - k_i}}] \tag{6.17}$$

where:

$$c_i = \begin{cases} \frac{\sum_{i=1}^{i} \phi_i}{\sum_{i=1}^{i+1} \phi_i} & \text{if} \quad i \neq n \\ 1 - \phi_i & \text{if} \quad i = n \end{cases} \tag{6.18}$$

6.4 Application of effective thermal conductivity of multi-phase composite

In the preliminary study conducted by Na et al. [53] experimental data on thermal conductivity of three types of mortars are collected. In all these groups, 50% of the sand volume has been replaced, either by PCM, or rubber powder or combination of PCM and rubber powder. They are called PCM-mortar, rubberized-mortar and PCM-rubberized-mortar, respectively.

When the replacement is done based on PCM and rubber, in order to eliminate the effect of one over the other, 25% of the sand volume has been replaced by PCM and the rest of 25% has been replaced by rubber powder. The detail of the mix design can be found in the reference.

MPCM-28 wet cake which is a product of Microtek [29] has been used in this study. The data obtained from these three groups would be a good verification for the developed GSM model.

PCM-mortar, rubberized-mortar and PCM-rubberized-mortar are good example of multi-phase composite, therefore the effective thermal conductivity of them can be calculated based on above equation. Christensen model is based on same size particle distribution. However in PCM-mortar, rubberized-mortar and PCM-rubberized-mortar, each phase has different grain scale, which requires multi-scale analysis in addition to multi-phase analysis.

Figure 6.7 shows the multi-scale model of the PCM-rubberized-mortar. As one can see from this figure, the PCM-rubberized-mortar has four phases with different size particles. In the largest scale, PCM-rubberized-mortar can be considered as a two phase composite considering fine aggregates (sand) as inclusion and the rest of the phases as matrix surrounding the inclusion. However, the matrix can be modeled as another two phase composite considering the largest size particle as the inclusion and the rest as the matrix. This process can be continued until the smallest size particle being modeled as the inclusion and only one phase left as a surrounding matrix. The same process

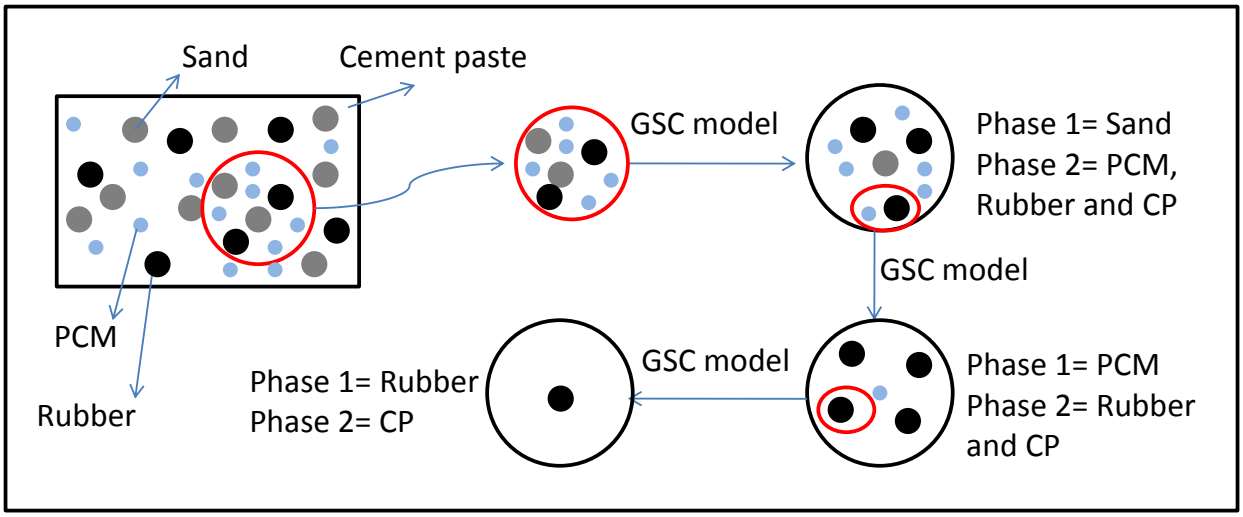

Figure 6.7: Multi-scale modeling of PCM-rubberized-mortar.

can be followed for PCM-mortar and rubberized-mortar. Keeping in mind, the multi-scale process in these two groups is one step shorter than PCM-rubberized-mortar.

Knowing the thermal conductivity of each of the phases as well as the volume fraction of the phases would assist us to obtain the effective thermal conductivity of the rubberized-mortar, PCM-rubberized-mortar and PCM-mortar.

It should be noted that in the GSM model, it was assumed that the temperature effect on thermal conductivity of all the phases except PCM and rubber powder is not significant. Moreover, thermal conductivity of MPCM-28 wet cake and rubber powder have been calculated based on the specific heat. Specific heat of MPCM-28 wet cake and rubber powder have been obtained by Differential Scanning Calorimetry (DSC) using Netzsch DSC 204 F1 Phoenix machine at a scanning rate of 10 °C/min in the temperature range of -25 °C to 55 °C in a nitrogen atmosphere. Figure 6.8 shows the thermal conductivity of MPCM-28 wet cake under various temperatures. Figure 6.9 shows the thermal conductivity of rubber powder under the same temperature range as MPCM-28 wet cake.

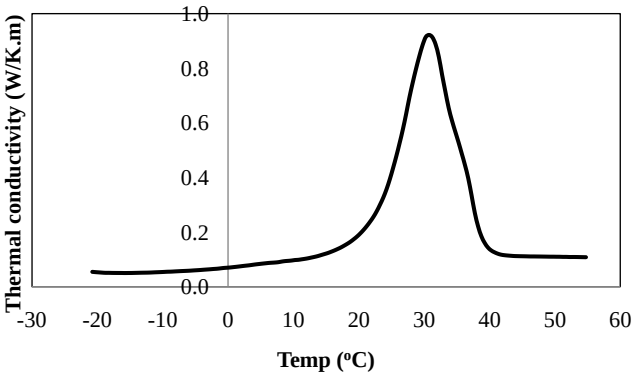

Figure 6.8: Thermal conductivity of MPCM-28 wet cake.

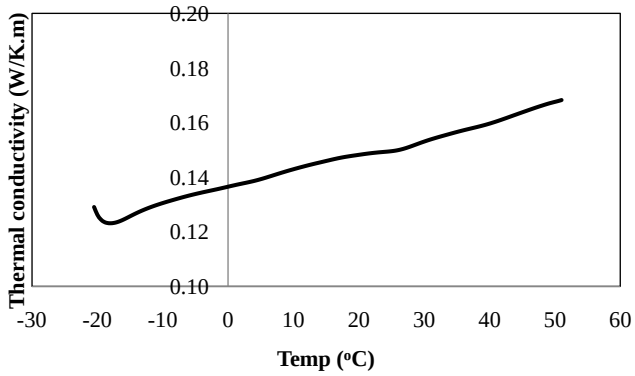

Figure 6.9: Thermal conductivity of rubber powder.

6.5 Results and discussions

Based on the pervious study conducted by Na et al. [53], the experimental data on thermal conductivity for three groups of rubberized-mortar, PCM-rubberized-mortar and PCM-mortar is available. As it has been explained in details on the reference, 50 percent sand volume has been replaced by either PCM particles or rubber powder or combination of both.

Figures 6.11, 6.12 and 6.10 illustrate the results for the effective thermal conductivity of rubberized-mortar, PCM-rubberized-mortar and PCM-mortar based on Parallel, Series, Maxwell and generalized self consistent model.

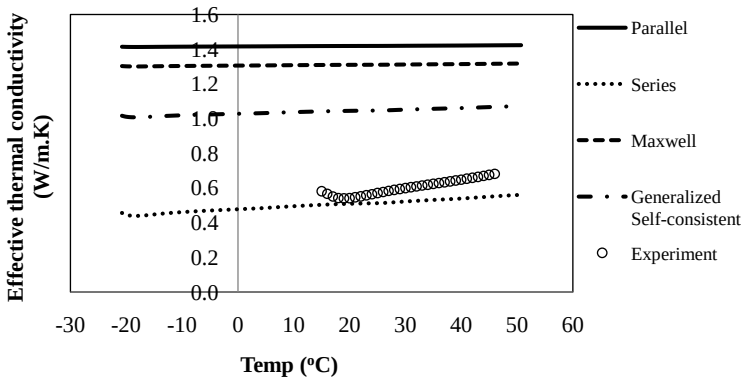

Figure 6.10: Effective thermal conductivity of rubberized-mortar based on GSC model.

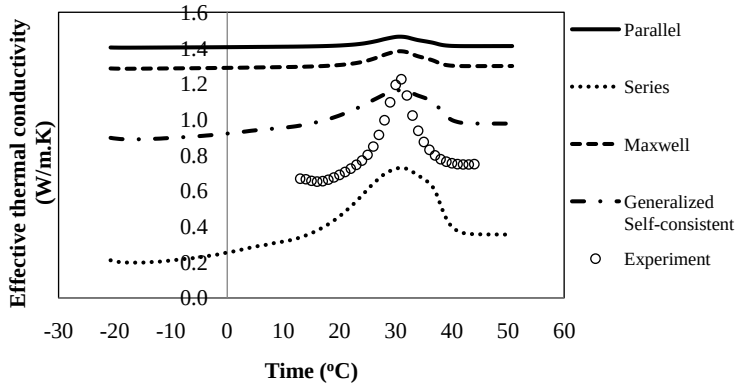

Figure 6.11: Effective thermal conductivity of PCM-rubberized-mortar based on GSC model.

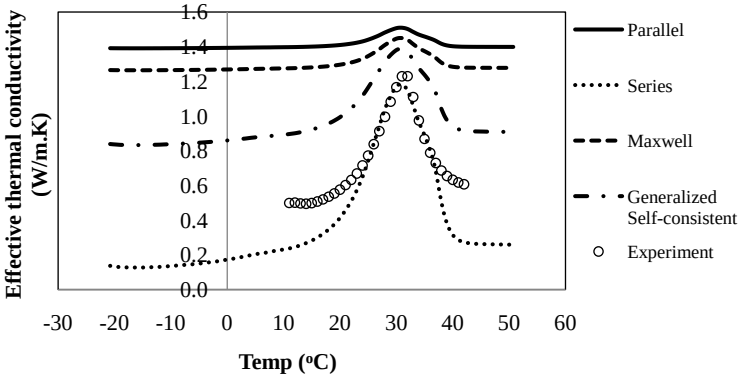

Figure 6.12: Effective thermal conductivity of PCM-mortar based on GSC model.

In all these figures, the experimental data has been added to the figures to show how accurately these models can capture the effective thermal conductivity of the composites. As one can see from these figures, the GSC model cannot predict the effective thermal conductivity of these composites accurately. This is due to the limitation of GSC model. The GSC model can account only for simple microstructural information, such as volume fraction and inclusion shape. Additionally, all the inclusions and the matrix phase should have thermal conductivity within the same range. In case of the inclusions with higher thermal conductivity than the matrix phase, the relation coincides with the lower bound and vice versa. In our specific case, since the PCM and rubber particles have much lower thermal conductivity than the surrounding matrix, the effective thermal conductivity of these composites have not been captured with neither models. Thus, this GSC model should be either modified or being replaced by another model which can capture more complex micro-structures.

Since the focus of this study is the application of the GSC model, the authors decided to modify the model by considering the PCM and rubber particles as thin membrane surrounding the cement paste, to be able to compensate for their low thermal conductivity in comparing with cement paste. Figures 6.13 and 6.14 show the results based on the modified GSC model.

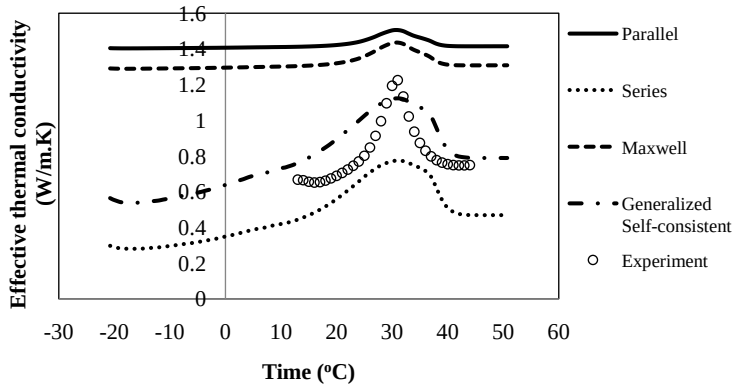

Figure 6.13: Effective thermal conductivity of PCM-rubberized-mortar based on modified GSC model.

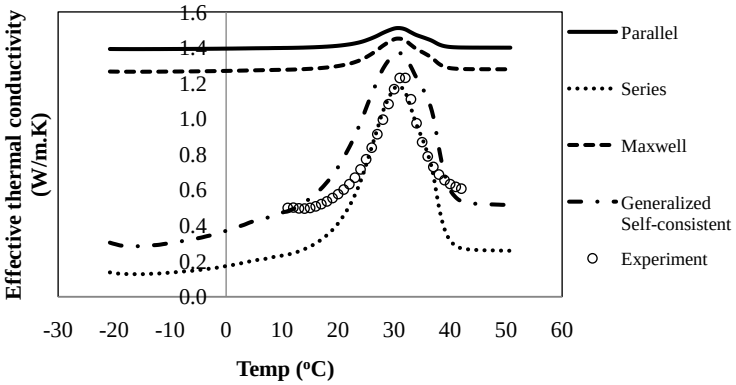

Figure 6.14: Effective thermal conductivity of PCM-mortar based on modified GSC model.

As one can see, the model can capture the effective thermal conductivity of PCM-rubberized-mortar and PCM-mortar more accurately than unmodified GSC model. However, Figure 6.15 shows the improvement in the model behavior capturing the effective thermal conductivity of the rubberized-mortar, but still not too close to the experimental data. The reason is, the rubber particles have different size and shapes and by modeling them as a thin membrane around the cement paste, only their low thermal conductivity has been taken into account. However, their shape and their size need to be considered in the model in order to capture their thermal conductivity more accurately. This problem is not significant in PCM-rubberized-mortar and PCM-mortar, since the PCM particles come only in one shape (spherical shapes) and their size varies in a smaller range (17-20 micron). There is no doubt that any model which can consider the microstructure of the composite would perform better than GSC model.

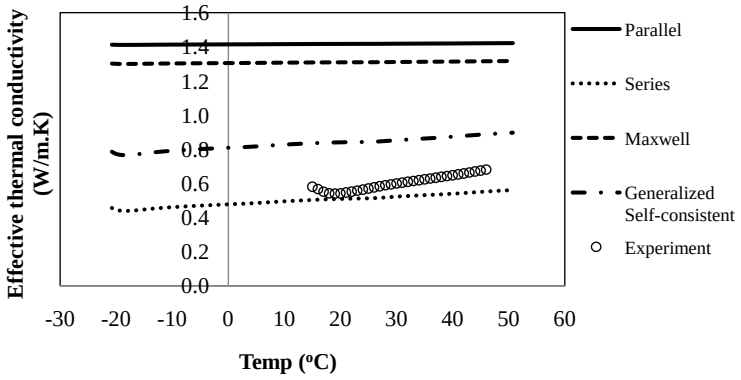

Figure 6.15: Effective thermal conductivity of rubberized-mortar based on modified GSC model.

The results from the modified GSC model are slightly different from the experimental data, because the thermal conductivity of all the phases except PCM and rubber particles were assumed to be constant under different temperature. Moreover, the thermal conductivity of all these phases were obtained from the literature, however, if the exact thermal conductivity analysis would be performed on each of the phases individually, the modified generalized self consistent model would predicted more accurate results. Additionally, the effective thermal conductivity of all these composites based on the modified GSC model falls between the upper and lower bound limits obtained

from Parallel and Series model. It should be noted that the peak observed in both rubberized-PCM-mortar and PCM-mortar is due to the effect of the PCM particles. Moreover, these peaks are referring to the melting point of the PCM particles, which is around 28 °C for these specific PCM particles. It should be noted that 28 °C is the melting point of the MPCM-28 dry powder, but since MPCM-28 wet cake has been used in the mix design, the melting point is slightly different than the dry powder. This is due to the amount of the water which exists in MPCM-28 wet cake. It should be noted that both modified GSC and the Series model can capture the correct trends of the effective properties. In terms of the spatial arrangement of the constituent phases, the series arrangement is the best spatial structure that allows the minimum amount of PCM or rubber particles with low thermal conductivity to block the maximum amount of heat. In the parallel arrangement, most of heat will pass through the phase with the least thermal resistance. Therefore, PCM plays a very minor role in Parallel model.

Figure 6.16 shows the effect of any change in the volume fraction of both PCM and rubber on the effective thermal conductivity. It should be noted, the volume fraction of both PCM and rubber can not increase beyond 0.227 for this specific mixing design.

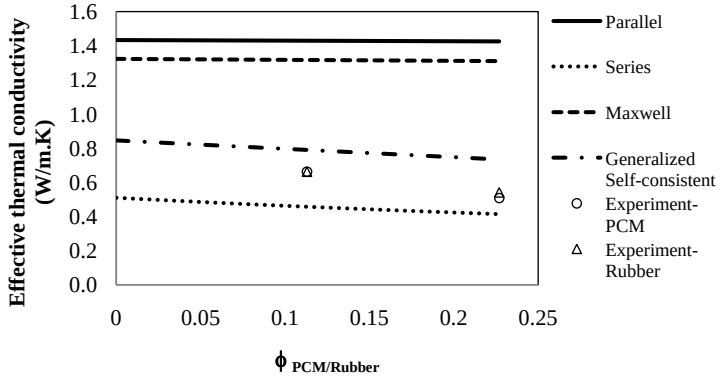

Figure 6.16: The effect of PCM/rubber volume fraction on the effective thermal conductivity.

One can see that more PCM would lead to lower thermal conductivity in comparing with more rubber content in the mix design. This can easily be explained based on the fact that the PCM particles have lower thermal conductivity in comparing with rubber particles. This effect is

so small in our example since very small portion of the sand has been replaced by either PCM or rubber (max volume fraction of PCM/rubber= 0.227).

This model has also been verified for another PCM-mortar with different mix design. The experimental study can be found in reference [50]. The modified generalized self consistent model was adopted to capture the effective thermal conductivity of PCM-mortar and rubberized-mortar as well as their effective shrinkage. Figures 6.17 and 6.18 show how this model can capture the effective thermal conductivity of rubberized-mortar and PCM-mortar.

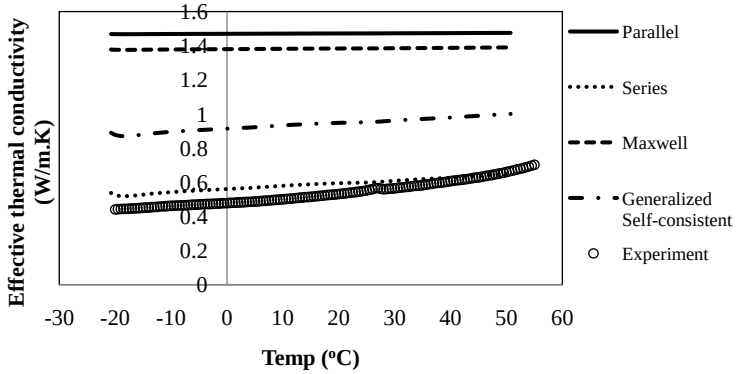

Figure 6.17: Effective thermal conductivity of rubberized-mortar (rubber particle) based on modified GSC model.

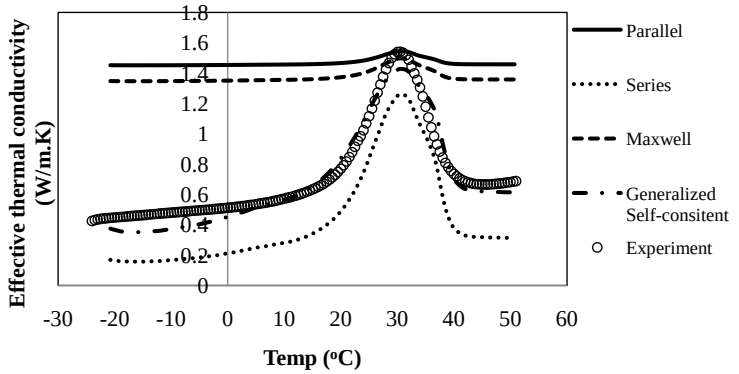

Figure 6.18: Effective thermal conductivity of PCM-mortar based on modified GSC model.

These results confirm that the modified generalized self consistent model can capture the effective thermal conductivity much better than the generalized self consistent alone. However, as it was mentioned earlier, in the case of rubberized-mortar, the size of the particles need to be considered, but in the PCM-mortar, all PCM particles sizes are within the same rage, so the size effect is not extreme as it is in the rubberized-mortar case.

6.6 Conclusions

In this chapter, the effective property of rubberized-mortar, PCM-rubberized-mortar and PCM-mortar has been investigated. Generalized self consistent (GSC) model was developed to predict the effective thermal conductivity of them. The GSC model fails to predict the effective thermal conductivity of the rubberized-mortar, PCM-rubberized-mortar and PCM-mortar accurately. This is mainly due to the fact that this model can account only for simple microstructure information, such as volume fraction and inclusion shape. Additionally, all the inclusions and the matrix phase should have thermal conductivity within the same range. Therefore the GSC model should be either modified or replaced by another model, which can capture more complex micro-structures. The modified GSC model predicts the effective thermal conductivity well when compared to other models.

The modified GSC model shows how the effective thermal conductivity would decrease by increasing the amount of the PCM or rubber the mix design. It can also capture the behavior of PCM-rubberized-mortar and PCM-mortar better than the rubberized-mortar and that is mainly because of the size and shape effect of the rubber particles in the mix design. The results for PCM-rubberized-mortar and PCM-mortar correlated well with the experimental data but in the case of rubberized-mortar, the modified generalized self consistent over predicts the effective thermal conductivity by 33% in comparing with experimental data.

It should be noted that the model has been verified by another PCM-mortar with different mixing design and the results confirms the latter findings.

Chapter 7

EXPERIMENTAL STUDY ON RUBBERIZED CONCRETE

7.1 Introduction

One of the focuses of this chapter is to use rubber particles in concrete, which includes coarse aggregate with sizes larger than 4.75 mm (4 mesh). Another focus is to improve thermal properties of the rubber concrete by incorporating phase change materials.

Much research has been done on how to reutilize waste tires in concrete. Similar to rubber mortar, when rubber particles are added to the concrete mixture, the strength and stiffness of the rubber concrete is decreased. Research has focused on how to reduce the reduction in the mechanical properties of the rubber concrete. One method is to use certain types of chemicals and polymers to treat the surface of rubber particles before mixing with the other components, called the surface pre-treatment method. The purpose of the surface treatment is to improve the bond between the rubber and surrounding cement paste, which is the weak link of the composite material.

Li et al. [43] investigated a rubberized-concrete with surface treatment of NaOH experimentally and concluded that NaOH surface treatment does not work for larger sized tire chips. They also observed that steel belt wires in waste tires improve the strength of rubberized-concrete and truck tires perform better than the car tires. This conclusion is understandable since the steel belts would reinforce the rubberized-concrete. Gneyisi et al. [15] investigated the mechanical properties of rubberized-concrete with and without silica fume and they concluded that the addition of more silica fume into the mix design can prevent the reduction of compressive strength of the

rubberized-concrete. Topcu et al. [74] analyzed the rubberized-concrete as a composite material and verified the elastic moduli obtained from their equation with the experimental data. In another study, Topcu et al. [75] focused on the durability of rubberized-concrete and their results revealed that in terms of durability, the optimum amount of rubber aggregate to produce concrete is 10% in volume which is quite economical and good in terms of recycling.

Balaha et al. [4] performed a series of experiments on rubberized-concrete and they confirmed the other researchers' results in terms of compressive and tension strength, however, they concluded that any increase in the amount of the rubber would decrease the bulk density of the rubberized-concrete. Zheng et al. [84] investigated the dynamic property of the rubberized-concrete and showed that the dynamic modulus elasticity of rubberized-concrete was lower than that of plain concrete. Also, the damping ratios of rubberized-concrete increased considerably with any increase in the rubber content. Kang et al. [36] studied the crack resistance and flexural behavior of cement-based materials by adding rubber particles. Their test results revealed that the rubberized-mortar and concrete specimens exhibit ductile failure and substantial deformation almost 2-4 times of the normal specimens.

As mentioned in chapter 5, in order to improve thermal properties of mortar, phase change material can be used. Similarly, PCM can also be used in concrete to improve its thermal properties. Many researchers such as Hawes et al. [20], Lencer et al. [42] have studied different PCMs and their applications in the construction industry. More specifically, Chen et al. [11] introduced a new PCM for energy-storing wallboard. Hawes et al. [19] examined the mechanisms of absorption of PCM in concrete. They observed that the hydrogen bonding can improve absorption under appropriate circumstances. In another study conducted by Hawes et al. [18] thermal performance of PCM in concrete was investigated. Kuznic et al. [41] carried out research with wall containing PCM and they observed that the PCM wall reduces the air temperature fluctuations in the room. Moreover, the PCM material included in the walls strongly reduces the overheating effect. Zalba et al. [82] studied the application of phase change materials (PCM) in free-cooling systems. Their statistical analysis showed that the thickness of the encapsulate has the most influence in the solidification

process. Castellon et al. [10] improved the thermal comfort in the buildings by using phase change materials. Bentz et al. [7] investigated the application of PCM in concrete and showed that PCM can reduce the number of freeze/thaw cycles experienced by concrete exposed to a winter environment. Hunger et al. [32] examined the behavior of self-compact concrete containing PCM. They showed that increasing the amount of PCM lead to a lower thermal conductivity and increased heat capacity.

7.2 Materials

Five different groups of rubberized-concrete, PCM-concrete and PCM-rubberized concrete were considered in this study. Each mix design consisted of 630 kg/m^3 fine aggregate (sand); 1160 kg/m^3 coarse aggregate; 350 kg/m^3 Type I Portland cement; 200 kg/m^3 water, and four different amounts of microencapsulate PCM/rubber particle.

The sieve analysis based on ASTM C136-06 [67] was conducted on the fine aggregate and the coarse aggregate being used in the concrete mixtures. Figure 7.1 shows the particle size distribution of the aggregates.

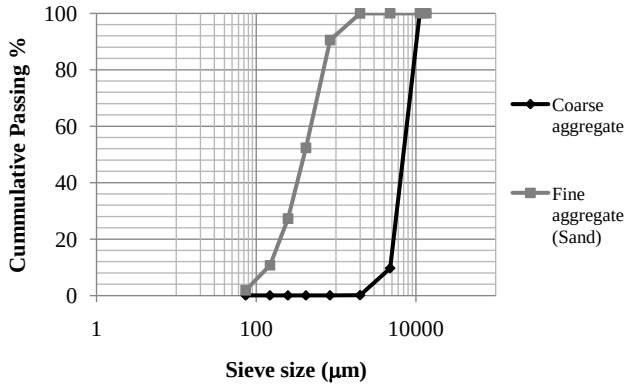

Figure 7.1: Particle size distributions of fine and coarse aggregate.

7.2.1 Rubber particles

Rubber particles come in different shapes and sizes. In this study, 6 mesh (coarse sized rubber) from AcuGreen, located in Denver, was used. The sieve analysis based on the standard ASTM C136- 06 [67] was conducted on this specific rubber size. Figure 7.2 shows the particle distribution of it.

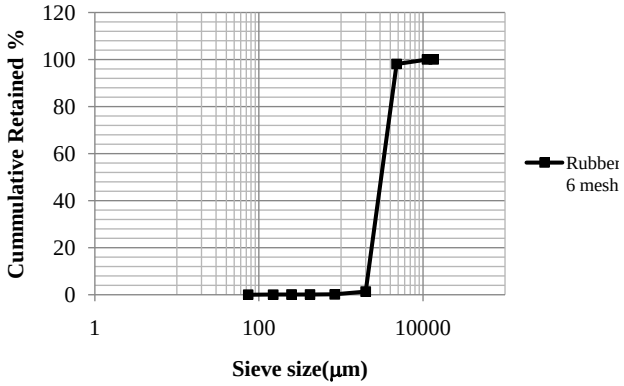

Figure 7.2: Particle size distribution of the rubber particles.

7.2.2 Polyvinyl alcohol

Polyvinyl alcohol (PVOH, PVA, or PVAL) is a water-soluble synthetic polymer. Its chemical formula is: CF3(CF2)7CH2CH2-SiCl3 or CF3(CF2)6-COCl. The PVA with low viscosity has low molar mass of 31,000-50,000 and 15,000-23,000 number average.

Since PVA has high tensile strength and flexibility and great adhesion property, there has been some research incorporating some PVA into cement mortar as well as concrete. Singh et al. [66] studied the effect of polyvinyl alcohol (PVA) on the hydration of ordinary Portland cement. Their results have shown that PVA increases the strength, but decreases the porosity. Kim et al. [37] studied the structure and properties of PVA-modified mortar and concrete and concluded that the addition of small amounts of PVA (up to 2 wt% PVA based on cement mass) will cause several changes in the microstructure and the properties of mortar and concrete. They also showed that the porous interfacial transition zones around sand grains and coarse aggregate were significantly

reduced in size and number.

To study the effect of the surface treatment of the rubber particles, 1.2-wt. %PVA of rubber was used. The PVA was manufactured at Celanese and the product name is Celvol 540 [25]. Based on the data sheet the PVA physical properties are provided in table 7.1.

Table 7.1: Physical properties of Polyvinyl Alcohol [25]

Appearance	White to cream granule powder
Bulk density	40 lbs/cu ft
Specific gravity of solid Of 10 wt% solution at 25°	1.27-1.31 1.02
Thermal Stability	Gradual discoloration about 100°; darkens rapidly above 150°; rapid decomposition above 200°
Thermal conductivity W/(m.k)	0.2
Electric resistivity, Ohm.cm	(3.1-3.8)×107
Specific heat J/(g.k)	1.5
Melting point (unplasticized) °	230 for fully hydrolyzed grades; 180-190 for partially hydrolyzed grades
$Tg°C$ (dry film)	75-85
Storage stability (solid)	Indefinite when protected from moisture
Flammability	Burns similarly to paper
Stability to sunlight	Excellent

Table 7.2 provided the typical properties of Celvol 540.

Dissolving PVA is the most critical step in solution preparation. Dispersing the particles in water has a major effect on its performance. Since the surface of the particles will swell quickly and then clump together, it is important to add the granules slowly to cool water (¡100 °F/38 °C) using good agitation, It should be noted that good agitation does not mean high shear value. It simply means adequate agitation to disperse the particles, without whipping air into the solution. If water greater than 100 °F is used, the particles will swell rapidly and will clump together, which would lead to incomplete dissolution. After this step, the suspension should be heated to at least 185 °F (85 °C) and the solution should be kept at this temperatures for a minimum of a half an hour. Additionally, based on the data sheet provided by the manufacture [25], the amount of the water added to the Celvol 540 particles should be less than 7% by weight of the solid. However,

Table 7.2: Properties of Celvol 540 [25]

Grade	Hydrolyis %	Viscosity cps	pH	Total volatiles % Max	Volatiles compound % Max	Ash % Max
Celvol 540	87.0-89.0	45-55	4.5-6.5	5	0.9	0.5

different ratios of 1% and 6% were used in our study.

7.2.3 Phase change material

Phase change material (PCM) is a substance with a high heat of fusion which melts and solidifies at a certain temperature. Thus, PCMs are capable of storing and releasing large amounts of energy. In this study, MPCM-28 wet cake manufactured by Microtek [29] was used.

7.2.4 Mixing process

Four different groups are prepared in this study including:

(a) Rubberized-concrete with surface treatment.

(b) Rubberized-concrete without surface treatment.

(c) PCM-concrete.

(d) PCM-rubberized-concrete, with surface treatment.

Different mixing process were adopted based on the type of the specimens. In the case of the rubber with surface treatment, the PVA solution was prepared first. Then, after the PVA solution was prepared, different methods were adopted in the mixing process. First, the PVA solution was cooled down to the room temperature, then, the rubber particles were added to it. Second, the rubber particles were added to the solution and they were kept at room temperature for around 24 hours. However, in both methods, it was necessary to ensure that all the particles were coated with the solution. Also, the amount of the PVA should not be more than 7% by weight of the solid

in the solution. In our study, two different percentage of the PVA (1% and 6%) were used in the solution.

It is also important to mention that the amount of rubber particles can be calculated based on the percentage of sand volume. The previous study has shown that using the rubber as sand volume replacement would lead to the higher compressive strength than using the rubber as additives. In this study different percentages of sand volume were replaced by rubber particles. For instance, when 5% of sand volume needed to be replaced by rubber, the volume of sand can be calculated, and knowing the density of rubber being equal to 1.0 kg/m^3, the mass of rubber can be calculated. Table 7.3 shows the mix design using for the rubberized-concrete with surface treatment.

Table 7.3: Mix design for rubberized-concrete with surface treatment

Group	**Cement (Kg)**	**Aggregate (Kg)**	**Sand (Kg)**	**Rubber (gr)**	**Water (Kg)**	PVA (gr)	**Water for PVA (gr)**	**Total water (Kg)**
RC0	0.433	1.434	0.779	0	0.247	0	0	0.247
RC5	0.433	1.434	0.74	14.64	0.244	0.176	2.75	0.247
RC10	0.433	1.434	0.701	29.27	0.242	0.351	5.5	0.247
RC15	0.433	1.434	0.662	43.91	0.239	0.527	8.26	0.247
RC20	0.433	1.434	0.631	58.55	0.236	0.703	11.01	0.247

When the surface treatment of the rubber particles was done, they added to the concrete mix design. It should be noted that the treated rubber should be added to the mixture last. Figure 7.3 shows the mixing process.

(a) PVA preparation (b) Rubber particles (c) Mixing with rubber

Figure 7.3: Preparation process for rubberized-concrete with surface treatment.

With the rubber without surface treatment, the mixing process was simpler. First all the dry materials were mixed and then the water was added to the mix. As with the other cases, the rubber particles were added to the mix last. Table 7.4 shows the mix design for the rubberized-concrete without surface treatment.

Additionally, in the case of PCM-concrete, the amount of PCM can be calculated based on the percentage of sand volume. For instance, when 5% of sand volume is needed to be replaced by PCM, the volume of sand can be calculated and then knowing the density of PCM being equal to 0.9 kg/m^3, the mass of PCM could be calculated. Again, it should be noted that the PCM should be added to the concrete as the last material. Table 7.5 shows the mix design for the PCM-concrete.

Finally, in the case of PCM-rubberized concrete, the same process as with the other cases was followed. However, in order to eliminate the influence of one over the other, the replacement of sand volume was done equally based on these two materials. Moreover, based on the observation in the previous study, the PCM should be added at the last minute to prevent the outer layer of the micro-capsulate from damaging. Table 7.6 shows the mix design for the PCM-rubberized-concrete.

Table 7.4: Mix design for rubberized-concrete without surface treatment

Group	**Cement (Kg)**	**Aggregate (Kg)**	**Sand (Kg)**	**Rubber (gr)**	**Water (Kg)**
RC0	0.433	1.434	0.779	0	0.247
RC5	0.433	1.434	0.74	14.64	0.247
RC10	0.433	1.434	0.701	29.27	0.247
RC15	0.433	1.434	0.662	43.91	0.247
RC20	0.433	1.434	0.631	58.55	0.247

Table 7.5: Mix design for PCM-concrete

Group	**Cement (Kg)**	**Aggregate (Kg)**	**Sand (Kg)**	**PCM (gr)**	**Water (Kg)**
PCM0	0.433	1.434	0.779	0	0.247
PCM5	0.433	1.434	0.74	13.17	0.247
PVM10	0.433	1.434	0.701	26.35	0.247
PCM15	0.433	1.434	0.662	39.52	0.247
PCM20	0.433	1.434	0.631	52.69	0.247

Table 7.6: Mix design for PCM-rubberized-concrete

Group	**Cement (Kg)**	**Aggregate (Kg)**	**Sand (Kg)**	**Rubber (gr)**	**PCM (gr)**	**Water (Kg)**	**PVA (gr)**	**Water for PVA (gr)**	**Total water (Kg)**
PCM-RC0	0.433	1.434	0.779	0	0	0.247	0	0	0.247
PCM-RC5	0.433	1.434	0.74	7.32	6.59	0.239	0.088	8.69	0.247
PCM-RC10	0.433	1.434	0.701	14.64	13.17	0.23	0.176	17.39	0.247
PCM-RC15	0.433	1.434	0.662	21.96	19.76	0.221	0.263	26.08	0.247
PCM-RC20	0.433	1.434	0.631	29.27	26.35	0.212	0.351	34.78	0.247

Figure 7.4 shows the mixing process for PCM-rubberized-concrete.

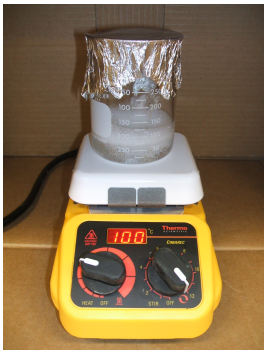

(a) PVA preparation

(b) Rubber particles

(c) Mixing with rubber

(d) Mixing with PCM

Figure 7.4: Preparation process for PCM-rubberized concrete.

7.3 Testing procedure

In order to have a good understanding of any new material's behavior, a series of experimental studies needed to be performed. These experiments were varied based on the nature of the study. In this case the focus was just on the compression test.

The compression was done based on ASTM C873 / C873M - 04e1 [68]. Six cylindrical specimens of 2 $in \times 4$ in were prepared for each mix design and the compression test was conducted on three of the cylinders at 7 days of age and the remaining three at 28 days of age. The compression test was conducted using a MTS machine based on the displacement control. The displacement rate was kept constant at 0.0015 in/sec for all the specimens at all ages.

7.4 Results and discussions

The compression test was performed on specimens in each group. First, the effect of the surface treatment using Polyvinyl alcohol on the rubber particle was investigated. In order to do so, a mix design with the highest amount of the rubber particles (RC20) was selected and the effect of the surface treatment based on different methods was investigated. Table 7.7 shows the mix design for investigating the effect of PVA on surface treatment.

Table 7.7: Mix design for the effect of PVA surface treatment

Group	**Cement (Kg)**	**Aggregate (Kg)**	**Sand (Kg)**	**Rubber (gr)**	**PVA (gr)**	**Water for PVA (gr)**	**Water (Kg)**	**Total water (kg)**	**Surface treatment**
RC20-wo	0.433	1.434	0.631	58.55	x	x	0.247	0.247	x
RC20-199-with-m1	0.433	1.434	0.631	58.55	0.703	69.55	0.247	0.317	Method one
RC20-199-with-m2	0.433	1.434	0.631	58.55	0.703	69.55	0.247	0.317	Method two
RC20-694-with-m2	0.433	1.434	0.631	58.55	0.703	11.01	0.247	0.258	Method two

As it can be seen the first group is just the rubberized-concrete with 20 percent sand volume replacement without any surface treatment. The second group is the rubberized-concrete with 20 percent sand volume replacement with surface treatment, not considering the water being used in the PVA preparation. It should be noted that the PVA preparation is based on one percent solid and ninety-nine percent water. The third group is the same as the second group, but adopting the second method of the surface treatment, which was explained earlier. This method is based on drying the treated rubber particles in the air for about 24 hours. The fourth group is the same as the third group, but the PVA amount the solution is based on six percent solid and ninety-four percent water. Figure 7.5 and Figure 7.6 show the result of the compression test for 7 and 28 days of these groups.

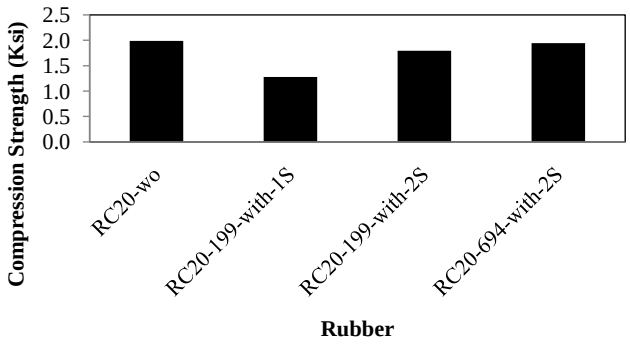

Figure 7.5: Comparison of the PVA surface treatment effect at 7 days of age.

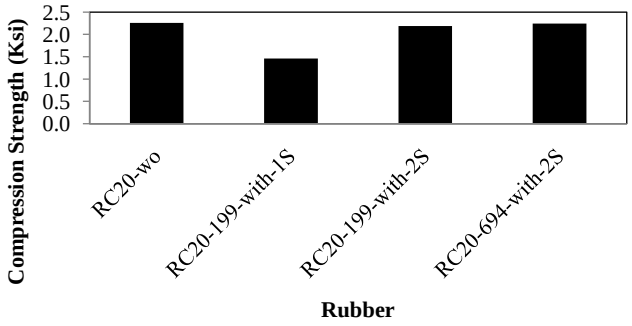

Figure 7.6: Comparison of the PVA surface treatment effect at 28 days of age.

The result revealed that the compression strength based on the second method of the surface treatment is quite similar to the result without any surface treatment. Moreover, how to prepare the PVA solution is another important factor in achieving higher compressive strength. More specifically, in the case of using one percent solid and ninety-nine percent water, the compressive strength is less than the case of 6 percent solid and ninety-four percent water in the solution. This is understandable based on the fact that the water content in the mix design is one of the most controlling factors in the compressive strength of the concrete. It should be noted even though the rubber particles were left in the room temperature for 24 hours and most of the water in the solution had evaporated, the amount of the remaining water on the rubber particles makes a difference in the compressive strength of the concrete.

Moreover, the first method of surface treatment affected the compressive strength of the rubberized-concrete significantly, due to the fact that the rubber particles were treated with the PVA solution and added to the mix design right after. Therefore, the amount of the water in the concrete is significantly higher than the other cases. Overall the result has shown that the compressive strength has not significantly improved by using PVA solution for the surface treatment.

Since the other focus of this study was investigating the behavior of rubberized-concrete, PCM-concrete and PCM-rubberized concrete, compression tests at 7 and 28 days of age were performed on various groups. Figures 7.7 and 7.8 show the result of all the groups at 7 and 28 days of age.

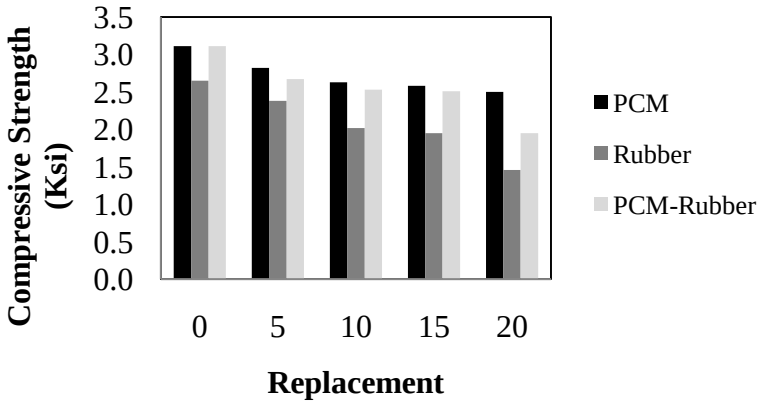

Figure 7.7: Comparison of the compressive strength of rubberized-concrete, PCM-concrete and PCM-rubberized-concrete at 7 days of age.

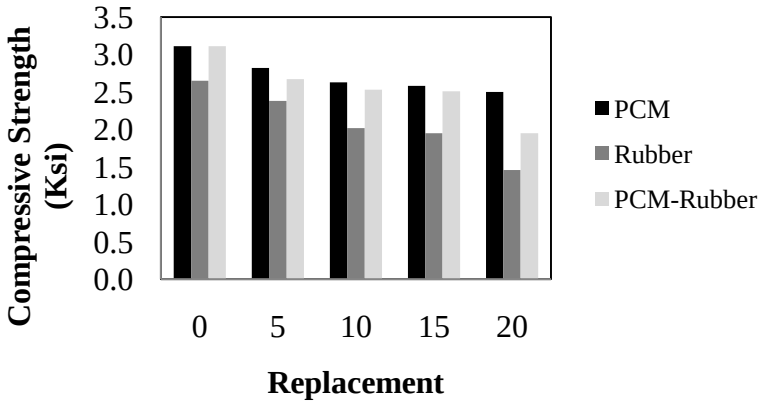

Figure 7.8: Comparison of the compressive strength of rubberized-concrete, PCM-concrete and PCM-rubberized-concrete at 28 days of age.

The figures show that the compressive strength of the rubberized-concrete is much lower than the compressive strength of the PCM-concrete. This is due to the fact that rubber is a softer material than PCM. On the other hand, PCM particles are smaller than the rubber particles, so the PCM particles can fill up the porous areas better than rubber particles. Additionally, the compressive strength of the PCM-rubberized concrete fell into the range between the PCM-concrete and rubberized-concrete, which satisfied our expectations.

Moreover, within each group, by increasing the amount of either rubber particles or PCMs, the compressive strength decreases because the sand volume is being replaced by these materials. Since both are much softer than the sand particles, the compressive strength should be decreased. Also, in the case of the rubberized-concrete, the rubber particles are much bigger than the sand particles, therefore this is another factor decreasing the compressive strength of the rubberized-concrete or PCM-rubberized concrete in comparing with normal concrete.

7.5 Conclusion

The mechanical properties of different mix designs of rubberized-concrete, PCM-concrete and PCM-rubberized concrete have been investigated in this study. Compression tests were performed at two different ages (7 days and 28 days). The compression test data shows that there is a significant difference between using the equivalent amount of Rubber or PCM in the mix design. Additionally, the effect of PVA on the surface treatment was investigated and the results revealed that the PVA does not help to increase the compressive strength of the rubberized-concrete.

Chapter 8

GUARDED HOT BOX TEST

8.1 Introduction

A small scale case study was conducted in our lab using an environmental chamber. Timber box structures (simulating residential houses) were built and selected mortars were applied on the exterior walls of the box. The box was placed in the environmental chamber, which features programmable temperature and relative humidity control. The chamber temperature was programmed. Both chamber temperature and the temperature in the box were monitored, and the two temperature profiles were compared to examine the effectiveness of mortar as an insulation material. This test is called hot box test. Several box structures were built using conventional premixed mortar and mortars with different optimum compositions. The test data was compared, and they will serve as prototype/practical applications in real construction.

8.2 Materials and mix designs

Some of the mix designs from Chapter 4 were selected for the study in this chapter. The selection criteria included both mechanical and thermal properties of mortars: compression strength, flexural strength, thermal conductivity, dry shrinkage, and bond strength. The selected mix designs used are as follows, and the mix designs are in Table 8.1.

(1) Ordinary cement-mortar (as a reference).

(2) Rubber-mortar with rubber particle (8-10 mesh).

(3) Rubber-mortar with rubber powder (200 mesh).

(4) PCM-mortar.

Table 8.1: Mix design for the hot box test

Group	**Cement** ($\mathbf{kg/m^3}$)	**Sand** ($\mathbf{kg/m^3}$)	**GC** ($\mathbf{kg/m^3}$)	**Rubber** ($\mathbf{kg/m^3}$)	**RPP** ($\mathbf{kg/m^3}$)	**MC** ($\mathbf{kg/m^3}$)	**WF** ($\mathbf{kg/m^3}$)	**Water** ($\mathbf{kg/m^3}$)
1	428.3	1182.5	129.5	0	25.4	3.73	1.24	320.2
2	428.3	508.3	129.5	184.3 (8-10 mesh)	25.4	3.73	1.24	320.2
3	428.3	508.3	129.5	184.3 (200 mesh)	25.4	3.73	1.24	320.2
4	428.3	508.3	129.5	184.3 (PCM)	25.4	3.73	1.24	320.2

8.3 Testing procedure

The top face of the box was used to apply the selected insulation mortar. The dimension of the top face was 12 in × 12 in × 1 in. Figure 8.1 shows the schematic of the test set-up.

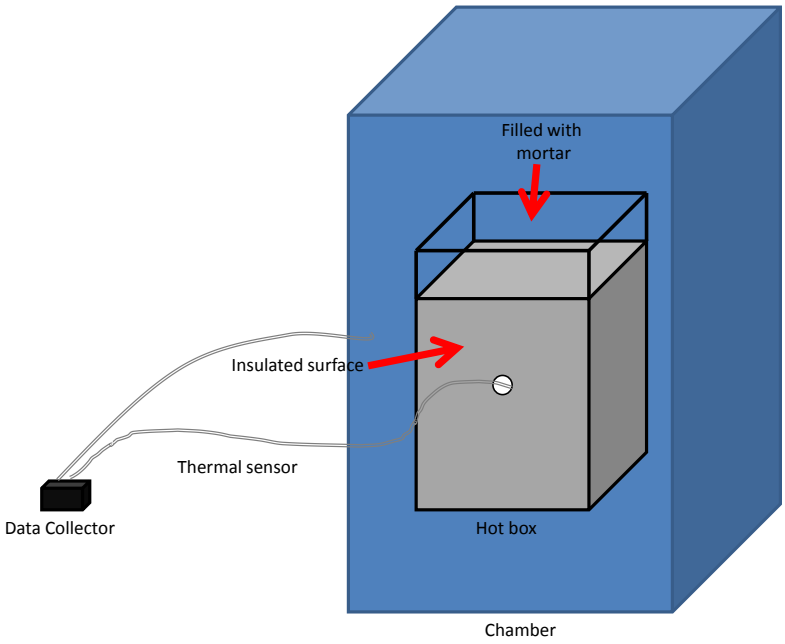

Figure 8.1: Schematic of the hot box test setup.

The other five faces of the box were covered with heavy duty insulation materials which include one layer of plastic foam and another layer of insulation tape. This was to make sure that the heat exchange will be done through the top surface covered by mortar. Figure 8.2 shows the environmental chamber and the hot box test setup.

The temperature profile was programmed for the chamber. The heating process started from room temperature to 55 °C with the heating rate of 1 °C/min. When the chamber temperature reached 55 °C, it was held for 2-3 hours. Then the cooling process started with the cooling rate of 1 °C/min till the temperature of the chamber reached room temperature. This temperature profile was used for all boxes. Figure 8.3 shows the temperature profile for this test.

Figure 8.2: The environmental chamber and the hot box test setup.

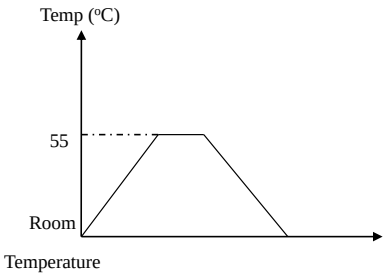

Figure 8.3: Temperature profile for the hot box test.

The testing process is as follows:

(1) The mortar is cast on the top surface of the box.

(2) The box is placed in the curing room for 28 days.

(3) The box is removed from the curing room and placed in the environmental chamber.

(4) Two temperature sensors are installed to measure the temperature in the box and in the chamber.

(5) The temperature profiles in the box and in the chamber are recorded.

8.4 Tests results and discussions

Figure 8.4 through Figure 8.7 show the hot box test results for the specimens. Figure 8.8 shows the temperature differences between the chamber and the box. A large temperature difference in the heating process means high insulation efficiency of the mortar.

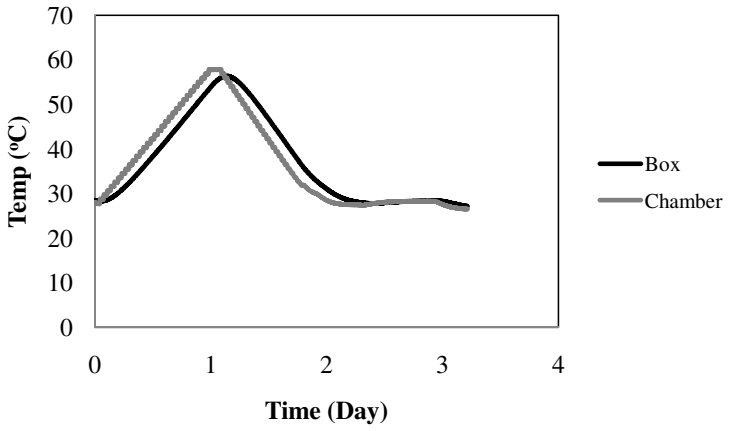

Figure 8.4: Hot box test result for normal mortar.

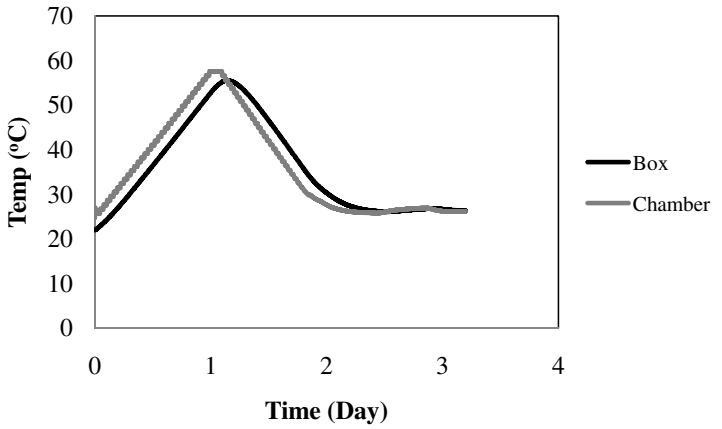

Figure 8.5: Hot box test result for rubberized-mortar (large rubber particles).

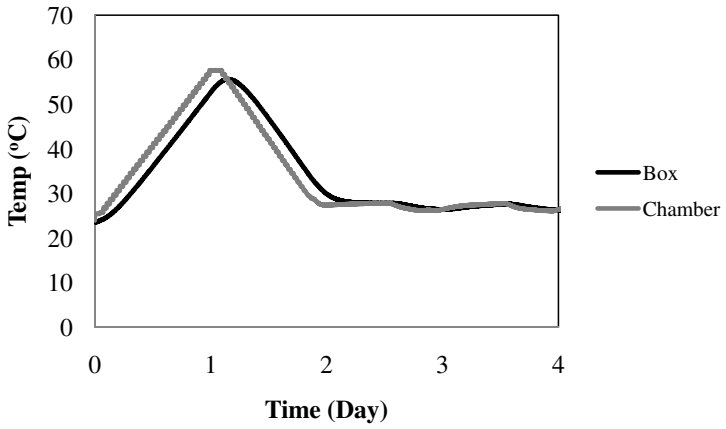

Figure 8.6: Hot box test result for rubberized-mortar (rubber powders).

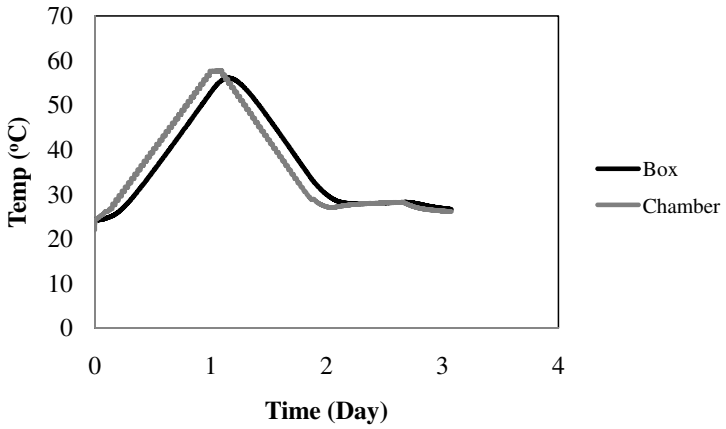

Figure 8.7: Hot box test result for PCM-mortar.

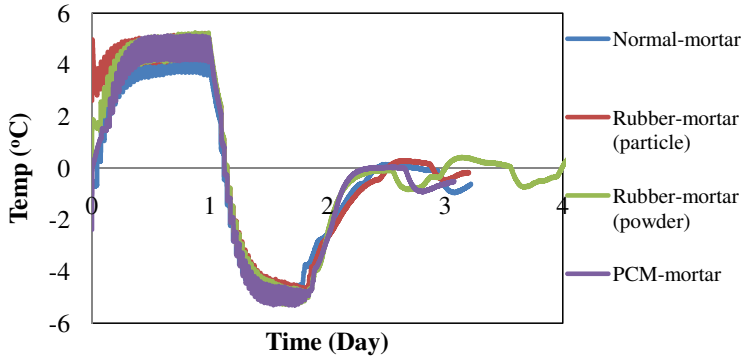

Figure 8.8: The temperature differences between the chamber and the box.

In order to eliminate noise in the test results shown in Figure 8.8, sixth-degree polynomial was used to curve-fitting the actual test data. Figure 8.9 shows the results of curve fitting.

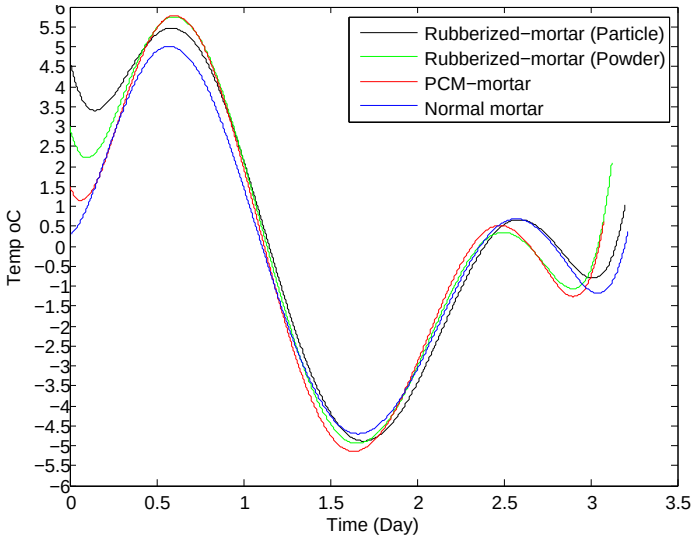

Figure 8.9: Comparison of the performance of each group using their polynomial functions.

Figure 8.9 Comparison of the performance of each group using their polynomial functions. The difference between each of these specimens is small, due to the small size of the specimens being used in this test (the size of the boxes is limited by the inner space of the chamber). However, it can be seen from the last two figures that the rubberized-mortar with rubber powders and PCM-mortar (red and green curves) have the largest temperature difference at the peak of the heating period, which means they perform best in the hot box test.

8.5 Conclusions

The hot box test results indicate that the rubberized-mortar with rubber powders and PCM-mortar have high insulation efficiency. From the view point of using waste tires, the mortar with rubber powders is the most efficient method in terms of thermal insulation.

Chapter 9

EFFECTIVE THERMAL DIFFUSIVITY OF COMPOSITE MATERIALS WITH HIGH ORDER STATISTICS OF MICROSTRUCTURE

9.1 Introduction

As reviewed in Chatpers 4 and 6, the effective properties of a composite material can be characterized by some composite models in terms of the properties and volume fractions of the constituent phases of the composite. In the models, many assumptions were made to simplify the spatial patterns of the microstructure, such as series coupling and parallel coupling. One of the common features of the models is that only volume fractions of the phases are taken into account, which, as discussed earlier, is the mean value (the first order statistics) of the random field. Higher order statistics of random microstructure were not incorporated in the models, and higher order statistics are important. As shown in Chapter 5 for testing thermal conductivity of PCM and rubber mortars, the conductivity depends not only on the volume fraction of the rubber particles but also on the average size of the particles, and the smaller the average size of the distributed insulator (rubber particles), the lower the conductivity of the mortar. In Chapter 2, it was shown that particle size can be characterized by coarseness of grain structure, which is a key parameter in the expression for autocorrelation function of the mosaic patterns.

The purpose of this chapter is to establish a theoretical model for effective thermal conductivity of composite materials that incorporate the first and the higher order statistical information of the microstructure. Specifically, the second order information, i.e. autocorrelation function of mosaic patterns will be used in the model due to their Thermal conductivity was selected as the

effective property to investigate because it represents in general a class of transport properties of composite materials, such as diffusivity of chemical species, water permeability, and electric conductivity.

In the following sections, mosaic patterns will be introduced first. Autocorrelation functions of mosaic patterns will be briefly derived (more details were provided in Chapter 2). A general model for effective properties of composite materials will be described in great detail. The general model takes into account higher order statistics of microstructure of composite, called n-point correlation function (when n = 2, the function is the autocorrelation function). Then, as a special case, the autocorrelation function of mosaic patterns will be used in the general model, providing more insight on the effect of volume fractions and particle sizes on the effective thermal conductivity of composite materials.

9.2 Mosaic patterns and autocorrelation functions

There exists two mosaic patterns, one is a random set mosaic and the other is a random line mosaic. The random set mosaic pattern is called S-mosaic and the random line mosaic is called L-mosaic. Beside these two patterns, Masao [48] proposed another mosaic pattern named covering mosaic pattern, which can be called C-mosaic. Therefore, the main mosaic patterns are as follows:

(a) Random line mosaic (L-mosaic).

(b) Random set mosaic (S-mosaic).

(c) Random covering mosaic (C-mosaic).

Figure 9.1 shows these different mosaic patterns.

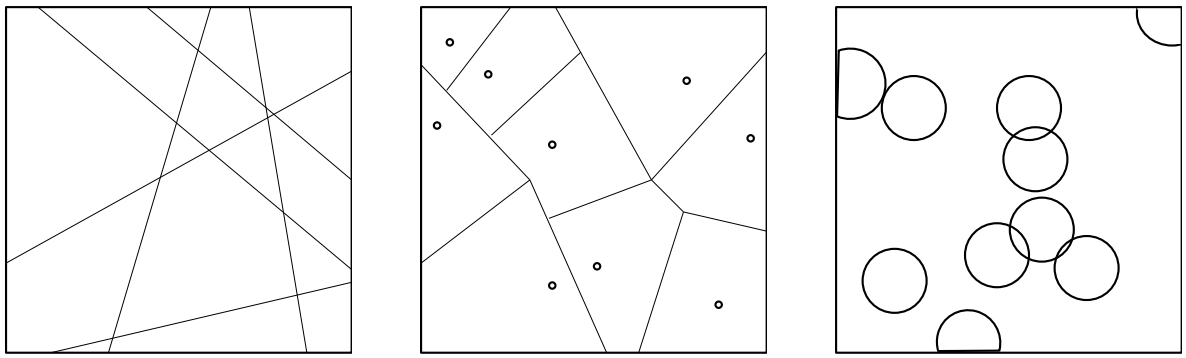

(a) L-mosaic (b) S-mosaic (c) C-mosaic

Figure 9.1: Random mosaic pattern. (Random set mosaic, Random line mosaic, Random covering mosaic)

There are various methods of constructing random mosaic. However, it is not possible to define a mosaic as random without specifying the exact definition of randomness [58]. Therefore, the following sections are explaining different approaches of constructing a random mosaic pattern.

9.2.1 L-mosaic

Generally, in the map of a mosaic pattern, the patch-phase (where things occur) should be colored black and the gap-phase (where it is absent) should be left white.

L-mosaic is one of the ways of constructing a random mosaic, which is based on drawing random lines, which subdivide an area into a network of convex polygons or cells. Then, each cell can be assigned its color with fixed probabilities. b for a black cell and w for a white cell with $b+w=1$.

When contiguous cells are assigned black color, they form a many-celled patch and if they are assigned white color, they form a many-celled gap. It should be noted that it is quite important to distinguish the differences between a cell, a patch and a gap. More specifically, the cells are defined as the small area formed when the random lines are drawn across the area. The cells are the units composed of patches and gaps. Patches consist of any number of contiguous cells which are assigned to be colored as black and gaps consist of any number of contiguous cells which are

assigned to be colored as white.

In order to draw random lines, the following method can be used. It can be assumed that the desired area in which the lines are to be drawn is circumscribed by a circle of radius r. The center of the circle can be considered as the pole of a polar coordinate frame and then an initial line can be drawn through it. Now, taking pairs of random polar coordinates (p,θ), a line can be drawn which passes through the point with the specific coordinate such as (p_1,θ_1) and it is perpendicular to the line connecting (p_1,θ_1) and the pole of the polar coordinate. This is a random line and therefore the method is called random line mosaic method [58].

Figure 9.2 shows a random line mosaic developed based on this method.

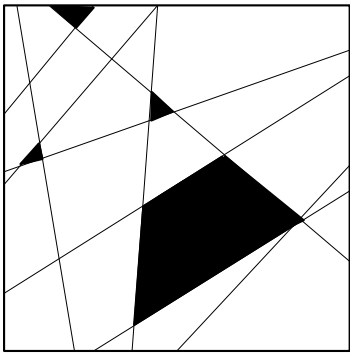

Figure 9.2: Random Line mosaic (L-mosaic).

9.2.2 S-mosaic

As it has been mentioned another type of mosaic pattern is called S-mosaic, which can be constructed as follows: a pattern of random dots should be drawn in the map area. Then each dot can be associated with a cell. Each segment of a cell boundary is the locus of points which are equidistant from the two nearest dots. Now, each cell can be colored independently as black or white with probability of b and w, respectively [58]. Figure 9.3 shows a random set mosaic pattern.

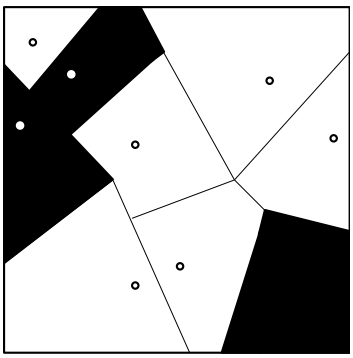

Figure 9.3: Random set mosaic (S-mosaic).

9.2.3 Mathematical modeling

There exists different ways of comparing various kinds of mosaic such as: means and variances of random variables including the number of sides per cell, cell perimeter, cell area, and angular and edge length distribution or comparing the theoretical autocorrelation functions.

To construct the mathematical model, it is more convenient to simplify a 3D model to a 2D model. This can be done by cutting the 3D mosaic with a 2D plane. Then the 2D mosaic pattern can be further simplified by cutting it with a transect and the result would be a 1D mosaic pattern. The line passing through the 2D mosaic pattern is degenerated to the points on the transect and between these points are the cut lengths of the cell which are called cell lengths. Figure 9.4 shows a 1D mosaic pattern.

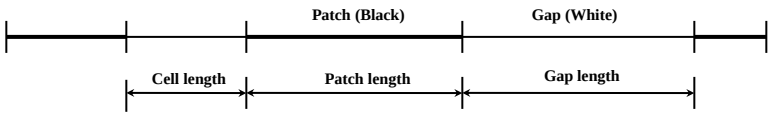

Figure 9.4: Transect through mosaic pattern.

Moreover, assuming that an L-mosaic is sampled at equidistant points along a line transect and recording the color of each point either black or white, the observation will be a sequence of Bs and Ws, for black and white respectively. Therefore, this sequence looks like a simple two-state Markov chain. Since the Markov chain states that the probability distribution of any system at the next time step depends only on the current state of the system and totally independent of the state of the system at previous time steps, it must be shown the probability distribution of L-mosaic follows this rule.

Let's assume $P(B_i, B_{i+1})$ is the probability of ith point and $i+1$th point to be black (B). Moreover, defining the $\pi_{i,i+1}$ as the probability of both points lying in the same cell of the random lines network, would lead to:

$$P(B_i, B_{i+1}) = \pi_{i,i+1} b + (1 - \pi_{i,i+1}) b^2 \tag{9.1}$$

This indicates the $P(B_i, B_{i+1})$ is the summation of two terms. The first term indicates that both points are located in the same cell which is assigned to be black. The second term, is the probability of these two points being in different cells which are assigned to be black as well. As one can see, the probability $P(B_i, B_{i+1})$ is just a function of $\pi_{i,i+1}$ and the color of the cell. Further investigation shows that $\pi_{i,i+1} = \pi$, which is a constant for all is. In other words, $P(B_i, B_{i+1})$ does not depend on i and it can be simply said:

$$P(B_i, B_{i+1}) \equiv b P_{BB} \tag{9.2}$$

This equation easily represents Markov chain process, because P_{BB} is the conditional probability which indicates any point will be a black (B), if the preceding point was a black (B).

However, since the sequence of states along the transect represents a continuous Markov process, instead of observing each phase at separate points and treating the observed sequence as a discrete Markov chain, it would be more convenient to measure the lengths cut off on the transect by patches and gaps. As a result, these would lead to a continuous two-state Markov process [58].

9.2.4 Comparison of L-mosaic and S-mosaic

As it has been mentioned, one way of comparing different mosaic patterns is the theoretical autocorrelation functions. Unfortunately, for S-mosaics this function can only be expressed in the one-dimensional case [58].

Pielou [58] has shown the probability of two points being in the same cell is π which is a function of the distance ν between two points and is equal to the correlation between the phases at two points which are apart by distance ν. In another word, the probability distribution only depends on the size of the cells in the network and not the colors assigned to the cells. This results are quite general for both L-mosaic and S-mosaic, regardless their dimensions.

Additionally, it can be said, if the cells are small, the correlation will be low and the mosaic pattern can be described as "fine-grained" and if the cells are large, the correlation will be high and the mosaic pattern can be described as "coarse-grained".

9.2.5 Autocorrelation function for L-mosaic pattern

As it was mentioned earlier, any 3D mosaic pattern can be simplified to a 2D or 1D. A one dimensional L-mosaic consists of contiguous non-overlapping linear cells, which satisfy the required conditions for the Poisson's probability distribution. These conditions are as following:

(a) The number of successes in any two disjoint time intervals are independent.

(b) The probability of success during a small time interval is proportional to the entire length of the time interval [28].

Thus, the Poisson's probability distribution can be applied to a L-mosaic pattern. This means that the number of the points in length interval ν, $N(x, x+\nu)$, is governed by the Poisson point process. Therefore, for an event $A_k = N(x, x+\nu) = k$, in which the interval ν is k, the homogenous Poisson process with density λ can be defined as:

$$P(A_k) = \frac{(\lambda \mid \nu \mid)^k e^{(-\lambda|\nu|)}}{k!} \tag{9.3}$$

Since π has been defined as the probability of both x and $x+\nu$ being in the same cell, which is equivalent to the probability of no intersection point in ν. In another word when k =0. Therefore, the equation 9.3 can be simplified as:

$$\pi = P(A_0) = e^{-\lambda\nu} \tag{9.4}$$

9.3 Theoretical model incorporating higher order statistics

9.3.1 Characteristic function in the heterogeneous media

Each realization ω of the n-phase random medium occupies the region of space $\nu \in \Re^d$ of volume V which is partitioned into n disjoint random phases, such as: phase one with region $\nu_1(\omega)$ and volume fraction ϕ_1, and phase two with region $\nu_2(\omega)$ and volume fraction ϕ_2 and so on. It should be noted that the sum of the regions of all the phases should add up to the total region of the space, which means:

$$\nu_1(\omega)\bigcup\nu_2(\omega)\bigcup..... = \nu \tag{9.5}$$

Also there is no common areas between any two of the phases, which means:

$$\begin{aligned} \nu_1(\omega)\bigcap\nu_2(\omega) &= \emptyset \\ \nu_1(\omega)\bigcap\nu_3(\omega) &= \emptyset \\ \nu_1(\omega)\bigcap\nu_4(\omega) &= \emptyset \\ &\vdots \end{aligned} \tag{9.6}$$

Moreover, the surface or the interface between any two phases is denoted by $\partial d(\omega)$. For the simplicity, a two-phase random medium can be considered.

Figure 9.5 shows a portion of a realization of a two-phase random medium.

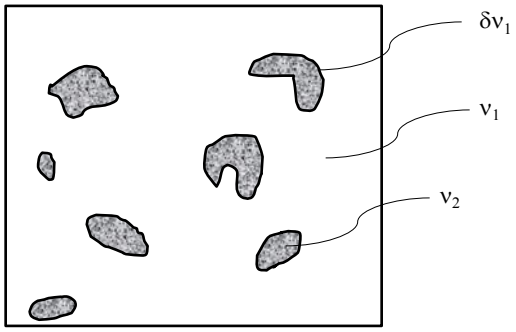

Figure 9.5: A portion of a realization of a two-phase random medium [73].

9.3.2 Indicator function

An indicator function or a characteristic function is a familiar term in mathematics. This function is defined on a set X, which indicates membership of an element in a subset A of X, which can have the value 1 for all the elements of A and the value of 0 for all the elements of X which do not belong to A. In a simple mathematics form, it can be defined as:

$$\mathcal{I}_A(x) = \begin{cases} 1 & \text{if} \quad x \in A \\ 0 & \text{if} \quad x \notin A \end{cases} \tag{9.7}$$

This function can be expanded to be used in a n-phase random medium as following:

$$\mathcal{I}^{(i)}(x;\omega) = \begin{cases} 1 & \text{if} \quad x \in \nu_i(\omega) \\ 0 & \text{if} \quad otherwise \end{cases} \tag{9.8}$$

For 2-phase random medium, i=1,2:

$$\mathcal{I}^{(1)}(x;\omega) + \mathcal{I}^{(2)}(x;\omega) = 1 \tag{9.9}$$

It should be noted that the indicator function for the interface can be defined as:

$$\mathcal{M}(x;\omega) = \mid \nabla \mathcal{I}^{(1)}(x;\omega) \mid = \mid \nabla \mathcal{I}^{(2)}(x;\omega) \mid \tag{9.10}$$

where x is a point on the interface. This is a generalized function which is non-zero when x is on the interface.

9.3.3 n-probability function

A probability distribution identifies the probability of each value of an unidentified random variable in the case of the discrete variable or the probability of the value falling within a specific interval in the case of continuous variable [24]. Moreover, the probability distribution describes the range of possible values, which a random variable can attain and the probability that the value of the random variable is within any subset of that specific range.

However, since the indicator function does not have a probability function, the probabilistic description of $\mathcal{I}^{(i)}$ is the probability that $\mathcal{I}^{(i)}$ equal to 1, which can be written as:

$$\mathcal{P}\{\mathcal{I}^{(i)}(x) = 1\} \tag{9.11}$$

And also,

$$\mathcal{P}\{\mathcal{I}^{(i)}(x) = 0\} = 1 - \mathcal{P}\{\mathcal{I}^{(i)}(x) = 1\} \tag{9.12}$$

The cumulative distribution function of discrete random variable X can be defined as:

$$F(x) = \mathcal{P}\{X \leq x\} \tag{9.13}$$

Additionally, the expectation of any function $f[\mathcal{I}^{(i)}(x)]$ can be defined as:

$$\langle f[\mathcal{I}^{(i)}(x)]\rangle = \mathcal{P}\{\mathcal{I}^{(i)}(x) = 1\}f(1) + \mathcal{P}\{\mathcal{I}^{(i)}(x) = 0\}f(0) \tag{9.14}$$

the brackets denote an average. When, $f[\mathcal{I}^{(i)}(x)] = \mathcal{I}^{(i)}(x)$, the above equation can be simplified as:

$$\langle \mathcal{I}^{(i)}(x)\rangle = \mathcal{P}\{\mathcal{I}^{(i)}(x) = 1\} \tag{9.15}$$

The above expression is referred to $\mathcal{S}_1^{(i)}(x)$ and it is called the one point probability function of phase i at position x. It should be noted that it is sometimes referred to as the one point correlation function for the phase indicator function.

The above equation can be expanded for n-point probability function in phase i at positions $x_1, x_2, ..., x_n$

$$\begin{aligned} S_n^{(i)}(x_1, x_2, ..., x_n) &\equiv \langle \mathcal{I}^{(i)}(x_1)\mathcal{I}^{(i)}(x_2)...\mathcal{I}^{(i)}(x_n)\rangle \\ &= \mathcal{P}\{\mathcal{I}^{(i)}(x_1) = 1, \mathcal{I}^{(i)}(x_2) = 1, ..., \{\mathcal{I}^{(i)}(x_n) = 1\} \end{aligned} \tag{9.16}$$

The n-point probability function is quite useful in rigorous expressions for the effective transport and mechanical properties of random heterogeneous media such as:

(a) Effective conductivity, diffusion coefficient, dielectric constant...

(b) Effective elastic moduli.

(c) Fluid permeability, etc [73].

9.3.4 Surface correlation function

Surface correlation functions contain information about the random interface $\partial\nu$ and they are so important in the case of flow problems. The simplest surface correlation function is the specific surface function $s(x)$ at point x, which is a one point correlation function for statistically inhomogeneous media. It should be noted that the specific surface is referred to an interface area per unit volume.

Moreover, if phase 1 denotes the fluid or void and phase 2 denotes the solid phase, the following equation can be written:

$$s(x) = \langle \mathcal{M}(x) \rangle \tag{9.17}$$

Two point surface correlation functions for statistically inhomogeneous media can be defined as:

$$\begin{aligned} F_{\nu\nu}(x_1, x_2) &= \langle \mathcal{I}(x_1)\mathcal{I}(x_2) \rangle \\ F_{s\nu}(x_1, x_2) &= \langle \mathcal{M}(x_1)\mathcal{I}(x_2) \rangle \\ F_{ss}(x_1, x_2) &= \langle \mathcal{M}(x_1)\mathcal{M}(x_2) \rangle \end{aligned} \tag{9.18}$$

where $F_{\nu\nu}$, $F_{s\nu}$ and F_{ss} are the void-void, surface-void and surface-surface correlation functions, respectively. Figure 9.6 shows a schematic of these functions.

9.3.5 Effective thermal conductivity

Consider a finite-sized large ellipsodial macroscopically anisotropic composite specimen in arbitrary space with d dimension. This arbitrary space is composed of two isotropic phases with

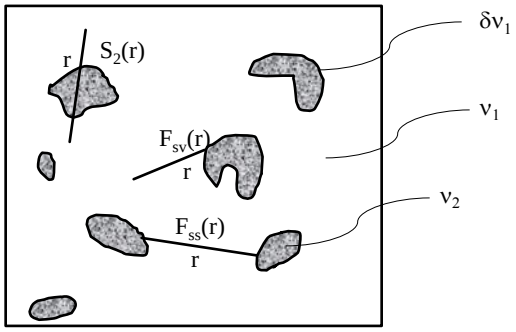

Figure 9.6: A schematic of surface-surface and surface-void functions in a random medium [73].

different thermal conductivities σ_1 and σ_2. The shape of the composite is quite arbitrary because the effective thermal conductivity tensor must ultimately be independent of the shape of the composite in the infinite volume limit. It should be noted that the microstructure is perfectly general and possesses a characteristic microscopic length scale which is much smaller than the semiaxes of the elliposid, therefore the specimen can be called statistically homogeneous. Figure 9.7 shows a schematic of a large d-dimensional ellipsodial.

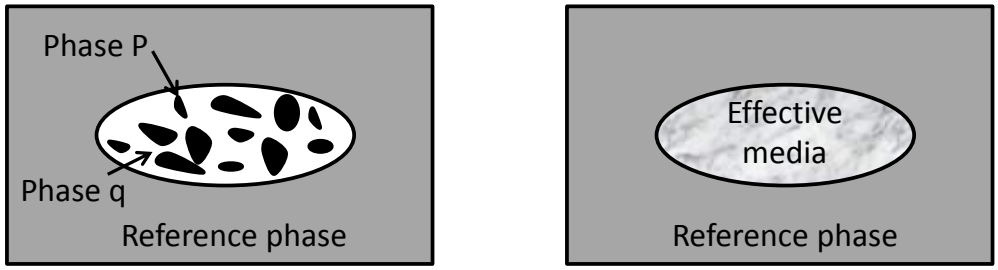

Figure 9.7: A schematic of a large d-dimensional ellipsodial.

The local thermal conductivity can be explained based on the indicator function for phases as following:

$$\sigma(x) = \sigma_1 I^{(1)}(x) + \sigma_2 I^{(2)}(x) \tag{9.19}$$

where

$$I^{(p)}(x) = \begin{cases} 1 & \text{if} \quad x \in phase \quad p \\ 0 & \text{if} \quad otherwise \end{cases} \tag{9.20}$$

As it can be seen from figure above, Torquato derived the effective thermal conductivity tensor based on a reference phase. In another word, he assumed the d-dimensional ellipsoidal composite specimen is embedded in an infinite reference phase which can be chosen to be arbitrary, however for the simplicity it can be one of the two phases within the composite. Assuming reference phase is phase q, which is subjected to an applied temperature field T(x) at infinity, therefore, the polarization field can be defined by:

$$\mathbf{P(x)} = [\sigma(x) - \sigma_q]\mathbf{T(x)} \tag{9.21}$$

Thus, the flux J can be reexpressed as:

$$\mathbf{J(x)} = \sigma_q \mathbf{T(x)} + \mathbf{P(x)} \tag{9.22}$$

The vector $\mathbf{P(x)}$ is called the induced flux polarization field relative to the medium, when the phase p is absent. Therefore, its value is zero in the reference phase q and it is nonzero in the polarized phase p.

Under steady state conditions without any sources, the flux is a divergence free and thus with the help of the above equation, it can be said:

$$\sigma_q \Delta\hat{\varphi}(x) = \nabla.\mathbf{P(x)} \tag{9.23}$$

Where $\hat{\varphi}(x) = \varphi(x) - \varphi_0(x)$ and $\varphi_0(x)$ is the potential at infinity. Therefore, it can easily be concluded that

$$\hat{\varphi}(x) \to 0, \quad \text{when} \quad |x| \to 0 \ . \tag{9.24}$$

On the other hand, the infinite-space Green's function can be defined to satisfy the equation below:

$$\begin{aligned} \sigma_p \Delta g^{(q)}(x,x') &= -\delta(x-x') \\ \Delta g^{(q)}(x,x') &\to 0, \quad \text{when} \quad |x| \to 0 \ . \end{aligned} \tag{9.25}$$

Multiplying both sides of equation 9.23 by the Green's function, replacing the $\hat{\varphi}(x)$ and integrating by part would result as:

$$\varphi(x) = \varphi_0(x) - \int \Delta g^{(q)}(x,x').\mathbf{P(x')}dx' \tag{9.26}$$

It should be noted that the integral is just over the finite-sized composite specimen and that is just because of the presence of polarization **P**. However, the integral is improper because the Green's function will hold singularity at x=x'. Excluding the region which causes the singularity is the only approach to differentiate under the integral. Therefore, in order to obtain the temperature field **T(x)**, this method can be adopted and the result would be as following:

$$\mathbf{T(x)} = \mathbf{T}_0\mathbf{(x)} + \int \mathbf{G}^{(q)}(r)\mathbf{P(x')}dx' \tag{9.27}$$

where:

$$\mathbf{G}^{(q)}(r) = -\mathbf{D}^{(q)}\delta(r) + \mathbf{H}^{(q)}(r) \tag{9.28}$$

In this equation, the D and H are defined based on the following equations:

$$\begin{aligned} \mathbf{D}^{(q)} &= \frac{1}{d\sigma_q}\mathbf{I} \\ \mathbf{H}^{(q)}(r) &= \frac{1}{\Omega\sigma_q}\frac{d\mathbf{nn}-I}{r^d} \end{aligned} \tag{9.29}$$

Additionally, it can be easily seen that the $\mathbf{H}^{(q)}(r)$ is the double gradient $\nabla\nabla g^{(q)}(r)$. Moreover, since the integral will be carried over the areas excluding at x=x', the integral of $\mathbf{H}^{(q)}(r)$ over the surface of a sphere of radius R¿0 should be equal to zero, i.e:

$$\int_{r=R} \mathbf{H}^{(q)}(r)d\Omega = 0 \tag{9.30}$$

Now replacing equation 9.28 into equation 9.27 would lead to the following equation:

$$\mathbf{T(x)} = \mathbf{T}_0\mathbf{(x)} + \int [-\mathbf{D}^{(q)}\delta(r) + \mathbf{H}^{(q)}(r)]\mathbf{P(x')}dx' \Rightarrow \mathbf{F(x)} = \mathbf{T}_0\mathbf{(x)} + \int \mathbf{H}^{(q)}(r)\mathbf{P(x')}dx' \tag{9.31}$$

The term $\mathbf{F(x)}$ is called cavity intensity field, which can be defined as:

$$\mathbf{F(x)} = \mathbf{I} + \mathbf{D}^{(q)}[\sigma(x) - \sigma_q].\mathbf{E(x)} \tag{9.32}$$

Comparing equation 9.21 and equation 9.32 would lead to:

$$\mathbf{P}(x) = \mathbf{L}^{(q)}(x)\mathbf{F}(x) \tag{9.33}$$

where $\mathbf{L}^{(q)}(x)$ can be defined as:

$$\mathbf{L}^{(q)}(x) = [\sigma(x) - \sigma_q]\{\mathbf{I} + \mathbf{D}^{(q)}[\sigma(x) - \sigma_q]\}^{-1} \tag{9.34}$$

As it can be seen from this equation, $\mathbf{L}^{(q)}(x)$ is fractional linear transformation of the local conductivity tensor ($\sigma(x) = \sigma(x)\mathbf{I}$) and since it is an isotropic tensor, it can be said:

$$\mathbf{L}^{(q)}(x) = L^{(q)}(x)\mathbf{I} \tag{9.35}$$

Thus a new notation can be introduced as:

$$\begin{aligned} L^{(q)}(x) &= \sigma_q d\beta_{pq} I^{(p)}(x) \\ \beta_{pq} &= \frac{\sigma_p - \sigma_q}{\sigma_p + (d-1)\sigma_q} \end{aligned} \tag{9.36}$$

It should be noted by using the $I^{(p)}(x)$ in the equation, the β_{pq} is linked to both the polarized and reference phases p and q, respectively and also the $I^{(q)}(x)$ would make the β_{pq} equal to zero.

With this background information, Torquato showed that the effective thermal conductivity can be expressed as following:

$$\beta_{pq}^2\phi_p^2[\sigma_e - \sigma_q\mathbf{I}]^{-1}.[\sigma_e + (d-1)\sigma_q\mathbf{I}] = \phi_p\beta_{pq}\mathbf{I} - \sum_{n=2}^{\infty}\mathbf{A}_n^{(p)}\beta_{pq}^n, p \neq q \tag{9.37}$$

where:

$$\begin{aligned} \beta_{pq} &= \frac{\sigma_p - \sigma_q}{\sigma_p + (d-1)\sigma_q} \\ \mathbf{A}_2^{(p)} &= \frac{d}{\Omega}\int d2\mathbf{t}(1,2)[S_2^{(p)}(1,2) - \phi_p^2] \\ \Omega(d) &= \frac{2\pi^{d/2}}{\Gamma(d/2)} \\ \mathbf{t}(r) &= \Omega\sigma_q\mathbf{H}(r) = \frac{d\mathbf{nn} - \mathbf{I}}{r^d} \\ \mathbf{n} &= \frac{r}{\mid r \mid} \end{aligned} \tag{9.38}$$

Explicitly, β_{pq} is called polarizability which is a scalar parameter. As it can be seen from the above equation, this term depends on the conductivities of the polarized and reference phases p and q, respectively. $\mathbf{A}_2^{(p)}$ is the n-point tensor coefficients and based on the above equation, it can be easily concluded that is a certain integral over the $S_2^{(p)}$ associated with phase p (polarized phase).

Since throughout the derivation, the fact that the $dr = \Omega(d)r^(d-1)dr$ has been used in a d-dimensional spherical coordinate system, thus the $\Omega(d)$ has to be defined as above equation. $\Omega(d)$ is the total solid angel contained in a d-dimensional sphere. Moreover, the term $\mathbf{t}(r)$ is the property independent tensor which is trivially related to $\mathbf{H}(r)$ tensor. $\mathbf{H}(r)$ is the double gradient $\nabla\nabla g^{(q)}(r)$ which is linked to the second order identity tensor I and the radial unit vector $\mathbf{n}$.

Considering micro-structures for which the n-point tensor coefficients $\mathbf{A}_n^{(p)}$=0 for $n \succeq 3$ would reduce the equation to:

$$\phi_p^2[\sigma_e - \sigma_q\mathbf{I}]^{-1}.[\sigma_e + (d-1)\sigma_q\mathbf{I}] = \phi_p\beta_{pq}^{-1}\mathbf{I} - \mathbf{A}_2^{(p)}, p \neq q \tag{9.39}$$

It is more convenient to use the expansion of the thermal conductivity tensor based on the difference in the phase conductivities for some subsequent calculations. Therefore, the following equation will be used in the calculation.

$$\sigma_e = \sigma_q\mathbf{I} + \sigma_q\sum_{n=1}^{\infty}\mathbf{a}_n^{(p)}(\frac{\sigma_p - \sigma_q}{\sigma_q})^n, p \neq q \tag{9.40}$$

where $\mathbf{a}$s are some coefficients which are defined based on the volume fractions of the polarized and reference phases as well as the n-point tensor coefficients in the following format:

$$\begin{aligned}\mathbf{a}_1^{(p)} &= \phi_p\mathbf{I} \\ \mathbf{a}_2^{(p)} &= \frac{1}{d}[\mathbf{A}_2^{(p)} - \phi_p\phi_q\mathbf{I}]\end{aligned} \tag{9.41}$$

Expanding the summation term in the above equation would lead to:

$$\sigma_e = \sigma_q\mathbf{I} + \sigma_q\mathbf{a}_1^{(p)}(\frac{\sigma_p - \sigma_q}{\sigma_q}) + \sigma_q\mathbf{a}_2^{(p)}(\frac{\sigma_p - \sigma_q}{\sigma_q})^2, p \neq q \tag{9.42}$$

Replacing the $\mathbf{a}$ values would result as:

$$\sigma_e = \sigma_q\mathbf{I} + \phi_p(\sigma_p - \sigma_q) + \frac{1}{2}(\mathbf{A}_2^{(p)} - \phi_p\phi_q)\frac{(\sigma_p - \sigma_q)^2}{\sigma_q}, p \neq q \tag{9.43}$$

Since the $\mathbf{A}_2^{(p)}$ which is called 2-point correlation, i.e. autocorrelation function. So, Equation 9.43 is a theoretical model that takes into account higher order statistical information of the internal structure of composite materials.

9.4 Application of mosaic pattern in the general model for effective thermal conductivity

9.4.1 Application of the autocorrelation function of L-mosaic pattern

$\mathbf{A}_2^{(p)}$ in Equation 9.43 can be replaced based on the L-mosaic 2-point correlation function, thus:

$$\mathbf{A}_2^{(p)} = \frac{d}{\Omega}\int_0^{\infty} d\nu \mathbf{t}(\nu)[\phi_p^2 + (\phi_p - \phi_p^2)exp^{-\lambda\nu} - \phi_p^2] \tag{9.44}$$

By some simple math operations, the above equation would become:

$$\mathbf{A}_2^{(p)} = \frac{1}{\pi}(\phi_p - \phi_p^2)\int_0^{\infty} \ln\frac{1}{\nu} exp^{-\lambda\nu} d\nu \tag{9.45}$$

The integral term can be simplified as:

$$\mathbf{A}_2^{(p)} = \frac{1}{\pi}(\phi_p - \phi_p^2)[\frac{0.5772}{\lambda}] + HOT \tag{9.46}$$

Substituting the Equation 9.46 into Equation 9.43 would assist to calculate the effective thermal diffusivity (thermal conductivity) of a two-phase composite.

9.4.2 Numerical results and discussions

Figures 9.8 through 9.10 show the effect of each of the parameters on the effective thermal diffusivity of a two-phase composite.

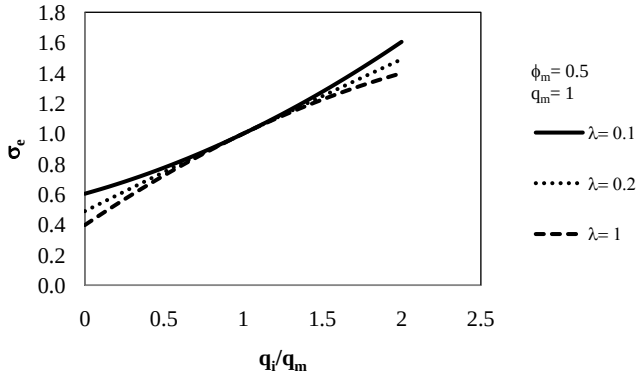

Figure 9.8: The effect of fixed volume fraction on effective thermal diffusivity.

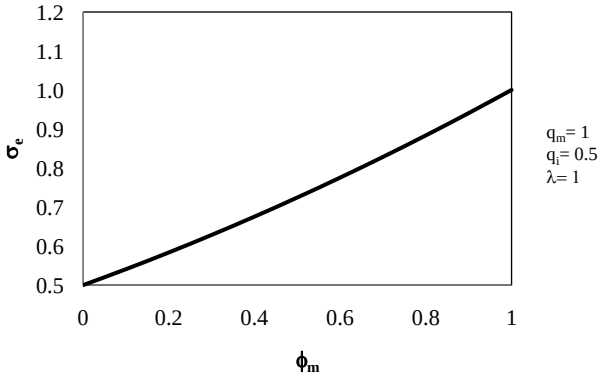

Figure 9.9: The effect of fixed coarseness on effective diffusivity.

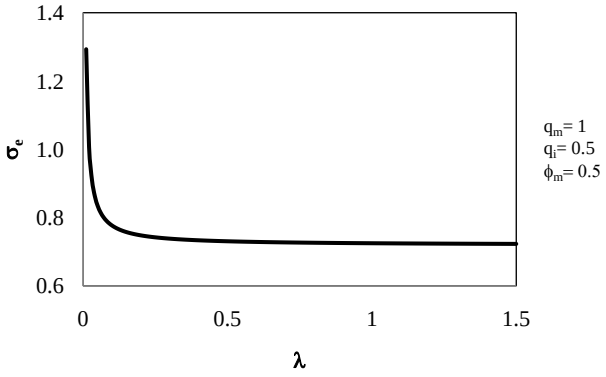

Figure 9.10: The effect of fixed volume fraction on effective diffusivity.

As it can be seen, for equal matrix and inclusion volume fraction, by increasing the thermal diffusivity of the inclusion phase, the effective thermal diffusivity is increasing as well, which indicates the key role of thermal diffusivity of the inclusions in the whole composite. However, if the thermal diffusivity of the matrix is higher than the thermal diffusivity of the inclusions, any increase in the volume fraction of the matrix would lead to higher effective thermal diffusivity. The effect of the coarseness on effective thermal diffusivity is another important factor. From Figure **??** it can be seen that for equal matrix and inclusion volume fractions, when the matrix has the dominant thermal diffusivity, the larger the coarseness are, the larger the decrease of effective thermal diffusivity of the composite. This decrease in the value of the thermal diffusivity continues until the coarseness no longer affects this value. The same result was observed in the case of the increase in the coarseness.

Rubberized-mortar can be considered as a three-phase composite, with sand as phase one, rubber particles as phase two and cement paste as phase three. Multi-phase analysis method based on generalized self-consistent model (see chapter 4) can be used in order to get the effective thermal diffusivity based on higher order autocorrelation developed in this chapter. Figure 9.11 shows the multi-scale modeling of rubberized-mortar.

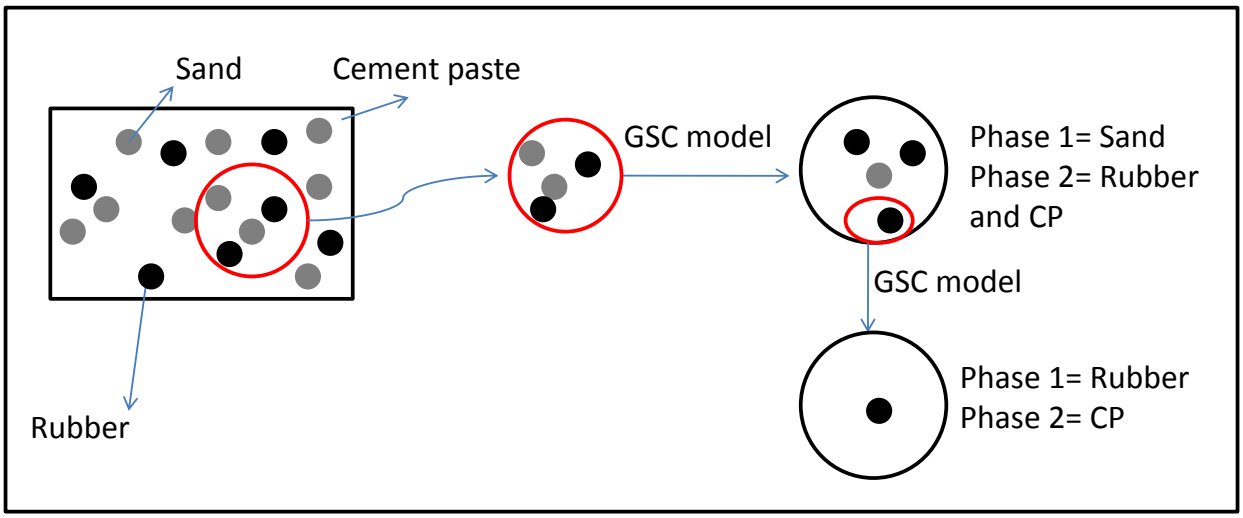

Figure 9.11: Multi-scale modeling of rubberized-mortar.

Figures 9.12 and 9.13 show the effect of change in the volume fraction of rubber and change in the coarseness of rubberized-mortar.

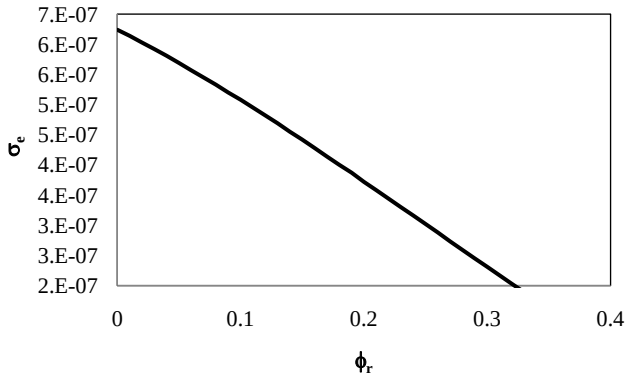

Figure 9.12: The effect of change in the volume fraction of rubber on effective thermal diffusivity of rubberized-mortar.

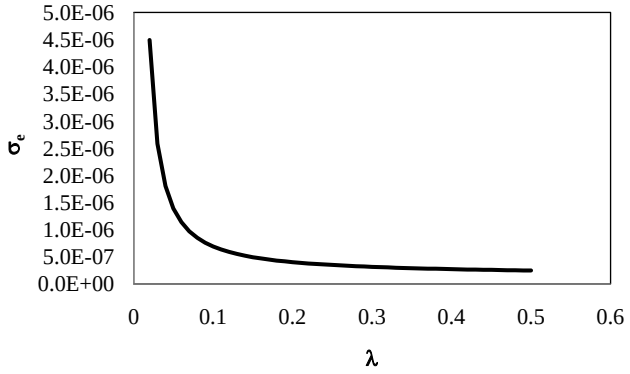

Figure 9.13: The effect of change in the coarseness on effective thermal diffusivity of rubberized-mortar.

As one can see, any increase in the rubber volume fraction would decrease the effective thermal diffusivity. The same results can be observed by increasing the coarseness and thus decreasing the particle sizes of rubberized-mortar as shown in Chapter 5.

9.5 Conclusions

A general theoretical model was introduced to characterize the effective thermal diffusivity of multi-phase composite considering higher order statistics of the microstructure of the composite. The autocorrelation function of L-mosaic pattern was used in the general model that can show not only the effect of volume fraction of the constituent phases but also the coarseness of the phases. Numerical results have revealed that:

(1) Any increase in the volume fraction of the inclusions which have a higher thermal diffusivity than the matrix would increase the effective thermal diffusivity.

(2) Any increase in the coarseness would decrease the effective thermal diffusivity. The model predictions were verified by the conductivity test data of rubberized-mortar.

The model was verified by using the rubberized-mortar as an application to a multi-phase composite.

Chapter 10

RECOMMENDATIONS FOR FUTURE WORK

The main goals of this dissertation were

(1) Characterization of heterogeneous microstructure of multi-phase cementitious materials and the effect of microstructural features on transport properties of the material.

(2) Utilization of phase change materials and recycled rubber particles from waste tires to improve thermal properties of insulation materials used in building envelopes.

To do so, several experimental and analytical studies were performed. Each chapter's focus is different from the other.

Since this dissertation focused on both analytical and experimental studies, the future works would be divided into two sections as well.

10.1 Analytical study

(1) Analytical study on moisture effect on thermal conductivity of multi-phase composite.

(2) Developing GSC model in terms of moisture and temperature to predict the thermal conductivity of multi-phase material.

(3) Developing GSC model in terms of moisture and temperature to predict the drying shrinkage of multi-phase material.

(4) Developing GSC model in terms of moisture and temperature to predict the chloride penetration into cementitious material.

(5) Developing an analytical model based on higher order autocorrelation functions for ion transport properties.

10.2 Experimental study

(1) (1) Studying damage development of concrete under high temperature based on different aggregate size, shape and volume fraction and comparing the results with the analytical model developed in this dissertation.

(2) The effect of different PCMs with different melting points, different physical appearances such as wet cake and dry powder on thermal conductivity of PCM-concrete and PCM-mortar.

(3) The effect of different PCMs with different melting points, different physical appearances such as wet cake and dry powder on drying shrinkage of PCM-mortar.

(4) The study of chloride penetration into PCM-concrete.

(5) The study of chloride penetration into rubberized-concrete with different rubber size particles.

It should be noted that since numerical studies with the use of finite element is a great help in various fields, it would be interesting to do some finite element analysis for different materials. The numerical study can be done considering the materials microstructure and predicting their effective transport properties, long term behavior as well as the crack propagation.

Bibliography

[1]

[2] B. L. Adams, G. R. Canova, and A. Molinari. A statistical formulation of viscoplastic behavior in heterogeneous polycrystals. Textures Microstruct, 11:57–71, 1989.

[3] C. Albanoa, N. Camachoa, J. Reyesa, J.L. Feliua, and M. Hernndezc. Rubber particles from recycled tires in cementitious composite materials. Composite Structures, 71(3-4):439–446, 2005.

[4] M. M. Balaha, A. A. M. Badawy, and M. Hashish. Effect of using ground waste tire rubber as fine aggregate on the behaviour of concrete mixes. Indian Journal of Engineering and Materials Science, 14(6):427–435, 2007.

[5] A. Bejan and A.D. Kraus. Heat Transfer Handbook. Hoboken: John Wiley & Sons, 2003.

[6] A. Benazzouk, O. Douzane, K. Mezreb, B. Laidoudi, and M. Queneudec. Thermal conductivity of cement composites containing rubber waste particles: experimental study and modelling. Construction and Building Materials, 22(4):573–579, 2008.

[7] D. P. Bentz and R. Turpin. Potential applications of phase change materials in concrete technology. Cement and Concrete Composites, 29:527–532, 2007.

[8] M. J. Beran. Statistical Continuum Theories. New York : Interscience Publishers, 1968.

[9] L. F. Cabeza, C. Castellon, M. Nogues, M. Medrano, R. Leppers, and O. Zubillaga. Use of microencapsulated pcm in concrete walls for energy savings. Energy and Buildings, 39:113–119, 2007.

[10] C. Castellon, M. Medrano, J. Roca, G. Fontanals, and L.F. Cabeza. Improve thermal comfort in concrete buildings by using phase change material. Energy Sustainability Conference, page 457463, 2007.

[11] C. Chen, H. Guo, Y. Liu, H. Yue, and C. Wang. A new kind of phase change material (PCM) for energy-storing wallboard. Energy and Buildings, 40(5):882–890, 2008.

[12] R. M. Christensen. Mechanics of composite materials. New York : John Wiley and Sons, 1979.

[13] P. B. Corson. Correlation functions for predicting properties of heterogeneous materials. II. empirical construction of spatial correlation functions for two phase solids. Journal of Applied Physics, 45:3165–3170, 1976.

[14] J. A. Epps. Uses of Recycled Rubber Tires in Highways. Transportation Research Board, National Research Council, 1994.

[15] E. Gneyisi, M. G. lu, and T. zturan. Properties of rubberized concretes containing silica fume. Cement and Concrete Research, 34(12):2309–2317, 2004.

[16] D. P. H. Hasselman and L. F. Johnson. Effective thermal conductivity of composites with interfacial thermal barrier resistance. Journal of Composite Materials, 21(6):508–515, 1987.

[17] D. W. Hawes, D. Banu, and D. Feldman. Latent heat storage in concrete. Solar Energy Materials, 19:335–348, 1989.

[18] D. W. Hawes, D. Banu, and D. Feldman. Latent heat storage in concrete. ii. Solar Energy Materials and Solar Cells, 21:61–80, 1992.

[19] D. W. Hawes and D. Feldman. Absorption of phase change materials in concrete. Solar Energy Materials and Solar Cells, 27:91–101, 1992.

[20] D.W. Hawes, D. Feldman, and D. Banu. Latent heat storage in building materials. Energy and Buildings, 20:77–86, 1993.

[21] J. P. Holman. Heat Transfer. New York: McGraw Hill College, 2001.

[22] http://en.wikipedia.org/wiki/Methyl-cellulose.

[23] http://en.wikipedia.org/wiki/Phase_change_material.

[24] http://en.wikipedia.org/wiki/Probability-distribution.

[25] http://www.celanese.com/.

[26] http://www.cff.de/us/.

[27] http://www.dow.com/.

[28] http://www.intmath.com/Counting-probability/13_Poisson-probability-distribution.php.

[29] http://www.microteklabs.com/.

[30] http://www.mineralstech.com/.

[31] B. Huang, G. Li, S. Pang, and J. Eggers. Investigation into waste tire rubber-filled concrete. Journal of Materials in Civil Engineering, 16(3):187–194, 2004.

[32] M. Hunger, A.G. Entrop, I. Mandilaras, H.J.H. Brouwers, and M. Founti. Enschede. The behavior of self-compacting concrete containing micro-encapsulated phase change materials. Cement and Concrete Composites, 31:731–743, 2009.

[33] H. Huynh, D. Raghavan, and Ferraris C.F. Rubber particles from recycled tires in cementitious composite materials. National Institute of Standards and Technology Internal Report 5850 R, pages 1745–1752.

[34] G. Jefferson, H. Garmestani, R. Tannenbaum, A. Gokhale, and E. Tadd. Two-point probability distribution function analysis of co-polymer nano-composites. International Journal of Plasticity, 21:185–198, 2005.

[35] Y. Jiao, F. H. Stillinger, and S. Torquato. A superior descriptor of random textures and its predictive capacity. Proceedings of the National Academy of Sciences(PNSA), 106(42):17634–17639, 2009.

[36] J. Kang and Y. Jiang. Improvement of cracking-resistance and flexural behavior of cement-based materials by addition of rubber particles. Journal of Wuhan University of Technology-Materials Science Edition, 23(4):579–583, 2008.

[37] J. H. Kim, R. E. Robertson, and A. E. Naaman. Structure and properties of poly(vinyl alcohol)-modified mortar and concrete. Cement and Concrete Research, 29(3):407–415, 1999.

[38] E. Kroner. Elastic moduli of perfectly disordered composite materials. Journal of the Mechanics and Physics of Solids, 15:319–329, 1967.

[39] E. Kroner. Statistical Continuum Mechanics. Springer, 1972.

[40] E. Kroner. Bounds for effective elastic moduli of disordered materials. Journal of the Mechanics and Physics of Solids, 25:137–155, 1977.

[41] F. Kuznik and J. Virgone. Experimental assessment of a phase change material for wall building use. Applied Energy, 86:2038–2046, 2009.

[42] D. Lencer, M. Salinga, B. Grabowski, T. Hickel, and J.O R.G Neugebauer. A map for phase-change materials. Energy and Buildings, 7:972–977, 2008.

[43] G. Li, M. A. Stubblefield, G. Garrick, J. Eggers, C. Abadie, and B. Huang. Development of waste tire modified concrete. Cement and Concrete Research, 34(12):2283–2289, 2004.

[44] Y. Li, M. Wang, L. Zhang, Z. Han, Y. Wu, and Z. Zheng. Influence of superplacticister and redispersible polymer powder on the strength of crumb rubber mortar. Journal of Beijing University of Technology, 35(9):1215–1219, 2009.

[45] Z. Li and X. Li. Advances in Construction Materials, chapter Development of thermal insulation materials with granular phase change composite, pages 741–748. Springer Berlin Heidelberg, 2007.

[46] S. Lin and H. Garmestani. Statistical continuum mechanics analysis of an elastic two-isotropic-phase composite material. Composites: Part B Engineering, 31:39–46, 2000.

[47] J. Luo and R. Stevens. Micromechanics of randomly oriented ellipsoidal inclusion composites. part I: Stress, strain and thermal expansion. Journal of Applied Physics, 79(12):9047–9056, 1996.

[48] F. Masao. Application of L-mosaic map to spatial analysis of urban map. Science and Technology, 25:113–134, 1976.

[49] P. Meshgin and Y. Xi. Effect of phase change materials on thermal and mechanical properties of concrete. ACI Journal of Material, 2010. Peer-review.

[50] P. Meshgin and Y. Xi. Utilization of phase change materials and rubber particles to improve thermal and mechanical propertiesof mortar. Construction and Building Materials, 2010. Peer-review.

[51] R. E. Miles. Random polygons determined by random lines in a plane. National Academy of Sciences-Proceedings, 52:901–907, 1964.

[52] G. W. Milton. The coherent potential approximation is a realizable effective medium scheme. Communications in Mathematical Physics, 99:463–500, 1985.

[53] O. Na and Y. Xi. Durability of insulation mortar with rubber powder.

[54] K.M. Nemati. Preserving microstructure of concrete under load using the wood's metal technique. International Journal of Rock Mechanics and Mining Sciences, 37(1-2):133–142, 2000.

[55] N. Oikonomou and S. Mavridou. Rubber particles from recycled tires in cementitious composite materials. Cement and Concrete Composites, 31(6):403–407, 2009.

[56] M. Ortiz and A. Molinari. Microstructural thermal stresses in ceramic materials. Journal of the Mechanics and Physics of Solids, 36(4).

[57] R. Osiroff and D. P.H. Hasselman. Effect of interfacial thermal barrier on the thermal stresses near spherical inclusion in matrix subjected to linear heat flow. Journal of Composite Materials, 25(12):1588–1598, 1991.

[58] E. C. Pielou. An Introduction to Mathematical Ecology. Wiley & Sons, 1969.

[59] R. Pyrz. Quantitative description of the microstructure of composites. part I: Morphology of unidirectional composite systems. Composites Science and Technology, 50:197–208, 1994.

[60] D. Raghavan, H. Huynh, and C.F. Ferraris. Workability, mechanical properties, and chemical stability of a recycled tyre rubber-filled cementitious composite. Journal of Materials Science, 33(7):1745–1752, 1998.

[61] M. J. Richardson. Compendium of thermophysical property measurement methods, chapter The application of differential scanning calorimetry to the measurement of specific heat, page 519. Plenum Press, New York, 1992.

[62] M. J. Richardson and A. W. Woods. An analysis of phase change material as thermal mass. The Royal Society, 464:1029–1056, 2008.

[63] K. Roth, D. Westphalen, and J. Brodrick. PCM technology for building materials. ASHRAE Journal, 49(7):129–131, 2007.

[64] A. Sharma, V. V. Tyagi, C. R. Chen, and D. Buddhi. Review on thermal energy storage with phase change materials and applications. Renewable and Sustainable Energy, 13(2):318–345, 2009.

[65] R. Siddique and T.R. Naik. Properties of concrete containing scrap-tire rubber-an overview. Waste Management, 24(6):563–569, 2004.

[66] N. B. Singh and S. Rai. Effect of polyvinyl alcohol on the hydration of cement with rice husk ash. Cement and Concrete Research, 31(2):239–243, 2001.

[67] ASTM Standards. ASTM Standards, chapter Standard test method for sieve analysis of fine and coarse aggregates. Number DOI: 10.1520/C0136-06. West Conshohocken : ASTM International, 2003.

[68] ASTM Standards. ASTM Standards, chapter Standard Test Method for compressive strength of concrete cylinders cast in place in cylindrical molds. Number 10.1520/C0873-C0873M-04E01. West Conshohocken : ASTM International, 2003.

[69] ASTM Standards. ASTM Standards, chapter Standard test method for flexural strength of concrete (using simple beam with center-point loading). Number DOI: 10.1520/C0293-08. West Conshohocken : ASTM International, 2003.

[70] ASTM Standards. ASTM Standards, chapter Standard test method for pull-off strength of coatings using portable adhesion testers. Number DOI: 10.1520/D4541-09. West Conshohocken : ASTM International, 2003.

[71] ASTM Standards. ASTM Standards, chapter Standard test method for length change of hardened hydraulic-cement mortar and concrete. Number DOI: 10.1520/C0157-C0157M-08. West Conshohocken : ASTM International, 2008.

[72] M. W. Tantala, J. A. Lepore, and I. Zandi. Quasi-elastic behavior of rubber included concrete (RIC) using waste rubber tires. 1997.

[73] S. Tarquato. Random Hetrogeneous Materials. Springer, 2002.

[74] I. B. Topcu and N. Avcular. Analysis of rubberized concrete as a composite material. Cement and Concrete Research, 27(8):1135–1139, 1997.

[75] I. B. Topcu and A. Demir. Durability of rubberized mortar and concrete. Journal of Materials in Civil Engineering, 19(2):173–178, 2007.

[76] I. B. Topcu and M. Sandemir. Prediction of rubberized mortar properties using artificial neural network and fuzzy logic. Journal of Materials Processing Tech, 199(1-3):108–18, 2008.

[77] S. Torquato and G. Stell. Microstructure of two-phase random media. I the n-point probability functions. The Journal of Chemical Physics, 77:2071–2077, 1982.

[78] Y. Xi. Representative volume of composite materials. Journal of Engineering Mechanics, 122(12).

[79] Y. Xi. Analysis of internal structures of composite materials by second order property of mosaic patterns. Materials Characterization, 36:11–25, 1996.

[80] Y. Xi and H. M. Jennings. Shrinkage of cement paste and concrete modelled by a multiscale effective homogeneous theory. Materials and Structures, 30:329–339, 1997.

[81] Y. Xi, Y. Li, Z. Xie, and J. S. Lee. Utilization of solid wastes (waste glass or rubber particles) as aggregate in concrete. Proceedings of the International Workshop on Sustainable Development and Concrete Technology, pages 45–54, 2004.

[82] B. Zalba, J. M. Marin, L. F. Cabeza, and H. Mehling. Free-cooling of buildings with phase change materials. International Journal of Refrigeration, 27:839–849, 2004.

[83] Y. Zhang and X. Zhang. Phase change material effect on heat property of mortar. ASHRAE Journal, 35(7):965–969, 2007.

[84] L. Zheng, X. S. Huo, and Y. Yuan. Experimental investigation on dynamic properties of rubberized concrete. Construction and Building Materials, 22(5):939–947, 2008.